Toughening of glassy amorphous polymers via chemically-induced phase separation

Document Version:
Publisher's PDF, also known as Version of Record (includes final page, issue and volume numbers)

Please check the document version of this publication:

• A submitted manuscript is the version of the article upon submission and before peer-review. There can be important differences between the submitted version and the official published version of record. People interested in the research are advised to contact the author for the final version of the publication, or visit the DOI to the publisher's website.
• The final author version and the galley proof are versions of the publication after peer review.
• The final published version features the final layout of the paper including the volume, issue and page numbers.

Link to publication

Toughening of Glassy Amorphous Polymers via Chemically-induced Phase Separation

B.J.P. Jansen

Toughening

of

Glassy Amorphous Polymers

via

Chemically-induced Phase Separation

Toughening

of

Glassy Amorphous Polymers

via

Chemically-induced Phase Separation

Dit proefschrift is goedgekeurd door de promotoren:

prof.dr.ir. H.E.H. Meijer
prof.dr. P.J. Lemstra

en de copromotor:

dr. S. Rastogi

Aan Linda & mijn ouders

Contents

Chapter 7   Conclusions and Recommendations

Summary

The brittleness of amorphous polymers such as polystyrene (PS) and poly(methyl methacrylate) (PMMA) is the result of a catastrophic strain localisation in the form of crazes. Considering the network density of these polymers, however, their intrinsic toughness is expected to be even higher than that of polycarbonate (PC), a well-known example of a ductile engineering thermoplastic which deforms via shear yielding. The reason for the occurrence of crazing or shear yielding, and thus brittle or tough macroscopic behaviour, can be found in the relative extent of intrinsic strain softening and strain hardening. The high network density of PC causes a more pronounced strain hardening behaviour which enhances delocalisation. In contrast, polystyrene suffers from strong strain softening in combination with limited strain hardening which gives rise to an extreme localisation during deformation in the form of crazes.

Hence, delocalisation of the deformation process can be used to toughen PS and PMMA since this will transfer their high intrinsic ductility to the macroscopic level. A possible route to enhance delocalisation is the modification by voids or rubber particles in order to transform the mode of microscopic deformation from crazing to shear yielding which, subsequently, will result in a toughness improvement. The combination of this desired effect with a minimum loss in modulus and strength can be achieved by the application of a sub-micron or even nano-sized morphology. In this case shear yielding can be obtained using a minimal amount of voids or rubber.

These morphologies, however, cannot be produced via conventional physical blending routes, e.g. using an extruder. An alternative chemical blending method has, therefore, been developed using epoxy resins as reactive solvent for thermoplastics. Curing the initially homogeneous solution, causes chemically-induced phase separation (CIPS) which results in a blend consisting of a thermoplastic matrix filled with crosslinked epoxy spheres. The final size of these particles can be tailored by controlling the viscosity of the reacting mixture during curing and phase separation of the epoxy resin. Coalescence will be suppressed by the application of a curing temperature equal to the glass transition temperature of the initially homogeneous solution. This curing strategy has been applied successfully to produce the sub-micron morphologies required for toughness.

By using an aliphatic epoxy resin as a reactive solvent in the chemical blending procedure described above, a sub-micron rubber morphology can be introduced in brittle amorphous polymers. Suppression of coalescence by enhancing the system viscosity during CIPS can also be used during the simultaneous polymerisation of methylmethacrylate and aliphatic epoxy resin. This route is successfully used to produce transparent rubber-toughened PMMA. Considering the poor mechanical properties of both the rubber and PMMA, a remarkable synergistic toughening effect is observed under both tensile and impact conditions. The maximum tensile toughness is found at a rubber content of 30-40 wt% which shifts towards 60-70 wt% if the deformation rate is enhanced to impact. The toughness improvement for blends containing less than 40 wt% rubber is completely lost upon this increase in strain rate. Using the sample with a rubber content of 20 wt%, however, it is shown that the impact toughness can be restored by predeforming (leading to precavitation) the test samples in slow speed uniaxial tension prior to impact testing.

Considering the mechanical behaviour described above, the deformation process on the microscopic level will be of crucial importance to reveal the relation between the morphology and the toughness of the PMMA/epoxy blends. Time-resolved small angle X-ray scattering (SAXS) using synchrotron radiation has proven to be a powerful technique to determine the mode and the development of microscopic deformation. Depending on the rubber content, deformation of the PMMA/epoxy blends in uniaxial tension is demonstrated to be accompanied by several different deformation mechanisms. Brittle systems tend to deform by crazing which can be identified by the typical cross-like shaped scattering pattern. Upon increasing the rubber content, shear yielding becomes the most important mode of microscopic deformation which explains the enhanced toughness found for the macroscopic tensile tests. The PMMA/epoxy 80/20 system, however, requires the occurrence of cavitation prior to shear yielding. The formation of voids appears to relieve the triaxial stress state which, subsequently, enhances shear yielding and thus the ductile behaviour of this blend. In contrast, blends with a higher rubber content deform via shear yielding without the occurrence of any dilatation processes (i.e. crazing or cavitation).

This 80/20 blend offers the possibility to study the influence of sub-micron voids on the mechanical performance of brittle amorphous polymers. During deformation in slow speed uniaxial tension, cavitation occurs which results in a ductile macroscopic behaviour. Since under impact condition a brittle mechanical response is observed, the influence of strain rate on the cavitation process during deformation of this blend is monitored by time-resolved SAXS measurements. Initially, the amount of cavitation appears to increase as the strain rate is enhanced. The mode of microscopic deformation, however, suddenly transforms from

cavitation induced shear yielding to crazing as the strain rate is increased even further. This explains the loss of the toughness improvement at impact conditions which can be restored by precaviting the test samples in uniaxial tension at low deformation rates prior to impact testing. For the PMMA/epoxy 80/20 blend, void formation is a prerequirement for shear yielding, and thus a ductile mechanical response, which apparently cannot occur under impact conditions.

Incomplete demixing may be the major drawback of using CIPS to prepare model blends to study the influence of sub-micron rubber morphologies on the mechanical performance of brittle amorphous polymers. The high viscosity applied to control morphology development will, in combination with the required compatibility of the constituents, result in a suppression of the degree of demixing between the PMMA and epoxy phase. An additional decrease in the demixing by crosslinking the PMMA or copolymerisation of both phases does not result in significant differences in the macroscopic toughness. Closer examination of the stress strain behaviour and monitoring the microscopic deformation by time-resolved SAXS measurements, however, clearly demonstrates that the deformation behaviour is affected by the degree of demixing. Nevertheless, interphase mixing alone cannot be responsible for the enhanced toughness of the PMMA/epoxy blends. The mechanical response depends on the mode of microscopic deformation which is clearly influenced by the morphology.

Summarising, chemically-induced phase separation can be used to prepare a tough heterogeneous system based on brittle amorphous polymers. The size of the rubber phase in the PMMA/epoxy model system has been decreased to sub-micron scale in order to combine the ductile mechanical behaviour with a minimum loss in modulus and strength. The observed toughness improvement is indeed the results of the anticipated transition in mode of microscopic deformation from crazing to shear yielding. It is, however, demonstrated that a detailed analysis of the deformation on microscopic level is of crucial importance in order to draw any firm conclusions concerning the relation between the macroscopic properties and aspects like rubber morphology, strain rate and the degree of interphase mixing.

Chapter 1

Introduction

1.1 Mechanical behaviour of amorphous polymers

1.1.1 Introduction

Construction materials should possess resistance against mechanical deformation and fracture. Mechanical performance in high loading conditions is, therefore, a general requirement for the successful application of polymeric materials and products. As a result, toughness enhancement has been the subject of many studies in the past in which great attention has been paid to reveal the fundamentals of different toughening mechanisms[1,2]. A vast amount of literature exists concerning rubber toughening and the relation between morphology and both, microscopic and macroscopic, properties. A general fundamental understanding is, however, still limited and solutions to toughening problems are often quite system specific. Concerning the toughness of amorphous polymers, more general theoretical approaches have been proposed recently[3,4], involving the introduction of sub-micron or even nano-sized voids or rubber particles. This thesis deals with the development of a route to prepare those heterogeneous polymer systems and the evaluation of the resulting mechanical properties on both microscopic and macroscopic level.
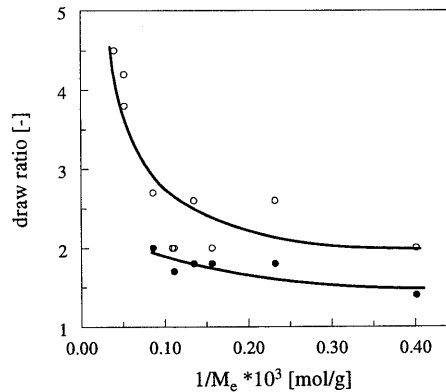
Figure 1.1: *Draw ratio in deformation zones (●) and craze fibrils (○) for various amorphous polymers versus their network density. Data from reference 6.*

1.1.2 Crazing versus shear yielding

Considering their mechanical behaviour, a distinction can be made between brittle and ductile amorphous polymers. An example of a ductile amorphous engineering thermoplastic is polycarbonate (PC) which deforms by shear yielding, via stress induced co-operative motion of polymer chain segments, which is comparable to the deformation of a thermoplastic network above its glass transition temperature, T_g. In unaxial tension, this results in macroscopic localisation of the deformation in the form of a neck which propagates through the sample till fracture occurs at a strain at break of approximately 80%.

Considering its limited network density, the strain at break of polystyrene (PS) is expected to exceed that of PC and indeed, as demonstrated by Kramer et al.[5], the draw ratio in deformation zones directly correlates with the polymer network density, see Figure 1.1. Nevertheless, PS is *the* example of an extremely brittle polymer with a macroscopic strain at break of only a few percent instead of the theoretically estimated value of 300%. This is caused by a *catastrophic* strain localisation in the form of crazes. Within these crazes, however, large draw ratios are obtained in the fibrils which span the craze surfaces[6]. On a local scale polystyrene deforms more ductile than polycarbonate which indicates that polystyrene is indeed an *intrinsically* ductile polymer.

1.1.3 Localisation of deformation

As demonstrated above, localisation phenomena on the microscopic level play an important role in the macroscopic mechanical performance of a polymer system. Therefore, understanding of the parameters which determine localisation is of crucial importance in developing successful toughening methods.
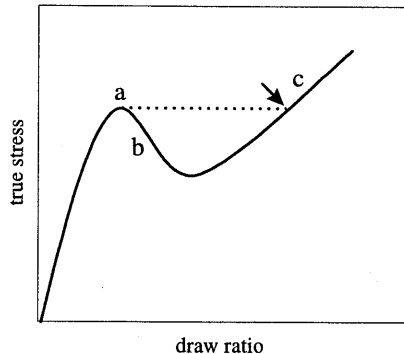
Figure 1.2: *General stress-strain behaviour of a homogeneously deforming zone of an amorphous polymer network: (a) yield stress, (b) strain softening and (c) strain hardening.*

Let us consider the stress-strain behaviour of a homogeneously deforming zone in an amorphous polymer network, somewhere in a test sample, see Figure 1.2. The initial elastic response transforms into plastic deformation as the yield stress (a) is approached. Upon further deformation, the stress decreases, and increases again, which is know as strain softening (b) and strain hardening (c), respectively. The occurrence and extent of strain localisation during deformation of a polymer network is mainly determined by the interplay and relative importance of these three parameters. As the stress in the homogeneously deforming local zone reaches the yield point (a), strain localisation occurs since the deformation process can proceed at a lower stress. The deformation can only be transferred to another zone, i.e. being *delocalized*, when the local strain hardening process results in a stress which exceeds the yield stress in the undeformed parts of the test sample, see the arrow in Figure 1.2. This should occur before the breaking strength of the locally stretched polymer network is reached.

The localisation via crazing or necking mainly occurs during loading in uniaxial tension but is suppressed in compression. Therefore, compression tests usually reflect much more the intrinsic deformation behaviour of the polymer network. Figure 1.3 clearly shows the differences in strain softening and hardening behaviour of polystyrene, poly(methyl methacrylate) and polycarbonate. As mentioned before, an important difference between polystyrene and polycarbonate is their network density which for polycarbonate results in less strain softening followed by a more pronounced strain hardening behaviour and a considerably lower intrinsic draw ratio than found for polystyrene. Hence, the tendency for delocalisation is stronger in polycarbonate and a tough behaviour results.
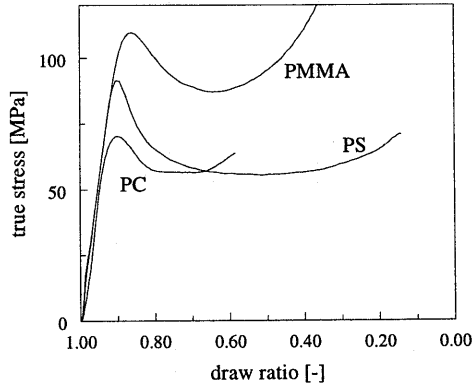
Figure 1.3: *Compressive behaviour of polystyrene (PS), poly(methyl methacrylate) (PMMA) and polycarbonate (PC)[7].*
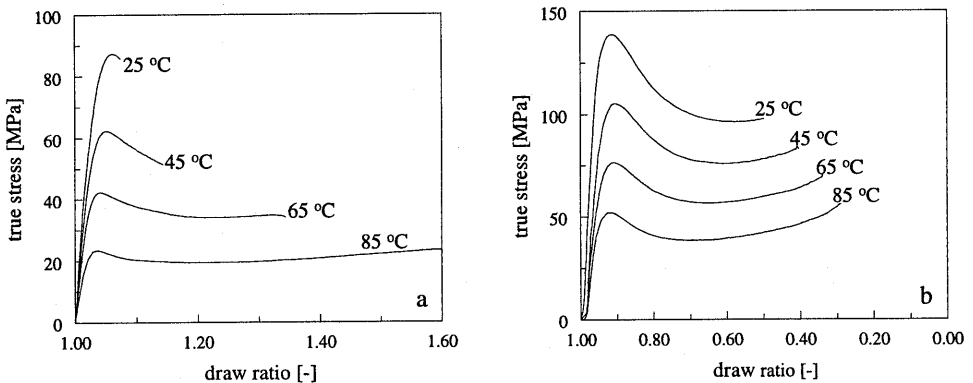
Figure 1.4: *Tensile (a) and compressive (b) behaviour of PMMA at various temperatures[7].*

Additional experimental evidence for this localisation approach can be obtained by performing both tensile and compression tests at different temperatures[7,8]. The macroscopic strain at break in tensile testing of e.g. poly(methyl methacrylate) appears to increase from ~10% to almost 100% with increasing temperature, see Figure 1.4a, which can be explained by the changes in intrinsic behaviour measured in the compression tests, see Figure 1.4b. The amount of strain softening clearly decreases with increasing temperature which enhances the occurrence of delocalisation and, subsequently, suppresses premature fracture due to craze formation. In contrast, polystyrene remains brittle during tensile testing, even at temperatures approaching the glass transition temperature, see Figure 1.5a. This is, however, expected considering the temperature independence of the intrinsic strain softening behaviour as

observed in the compression tests, see Figure 1.5b. Catastrophic localisation via crazing will cause brittle failure at limited macroscopic draw ratios also at higher test temperatures.

Understanding the intrinsic deformation behaviour of polymer networks is of extreme importance in the development of successful toughening procedures. The challenge will be to modify brittle amorphous polymers in order to avoid catastrophic localisation and transfer the intrinsic ductile behaviour to the macroscopic level. As described above this can be achieved by decreasing the strain softening behaviour, see I in Figure 1.6, and/or increasing the strain hardening, see II in Figure 1.6[4].
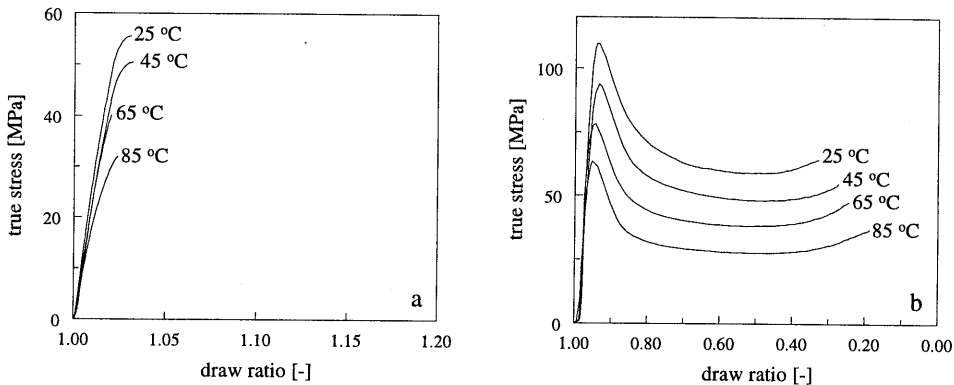
Figure 1.5: *Tensile (a) and compressive (b) behaviour of PS at various temperatures[7].*
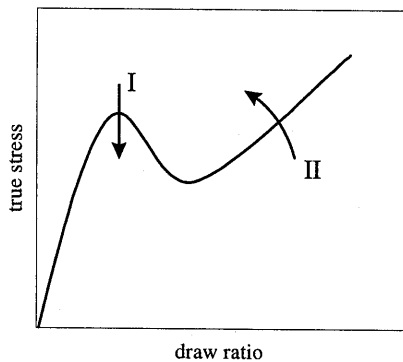
Figure 1.6: *Schematic representation of the possible routes to improve the toughness of amorphous polymers: (I) decreasing strain softening and (II) increasing strain hardening[4].*

Possible routes to enhance strain hardening are crosslinking or preorientation of the network. By crosslinking of polystyrene, Henkee et al.[9] showed that its mode of microscopic deformation can indeed be transformed from crazing to shear yielding. Apart from increasing

the test temperature as discussed above, toughness enhancement by lowering the strain softening behaviour can be obtained by the addition of a plasticiser[10] or the application of mechanical rejuvenation[11]. An example of the latter case is the reduction of the degree of strain softening in polystyrene by rolling the tensile bars at room temperature prior to testing. This causes an increase in strain at break of this originally brittle polymer to almost 40% without the occurrence of crazing. All these methods for the toughness improvement of *homogeneous* polymers have their apparent drawback. More practical routes imply the application of rubber inclusions as will be discussed in the following section.

1.1.4 Concept of critical thickness

In this thesis, the toughening of *heterogeneous* polymer systems based on brittle amorphous polymers is studied. The aim is to transfer the *intrinsic* ductile behaviour of this class of polymers to the macroscopic level by suppressing the tendency for localisation in the form of crazes. Hence, instead of the initiation of multiple-crazing as aimed for in classical rubber toughening, crazing should be transformed into shear yielding. Considering the high draw ratios in craze fibrils, it is anticipated that this can be realised by decreasing the local thickness in brittle amorphous polymers to the sub-micron level.

Van der Sanden et al.[12] demonstrated that the intrinsic ductility of polystyrene could indeed be completely transferred from the microscopic to the macroscopic level by creating sufficiently thin multi-layered tapes[13] or applying high volume fractions of small non-adhering core-shell rubber particles[14]. The observed toughness enhancement is accompanied by a transition in mode of microscopic deformation from crazing to shear yielding. In the latter case this occurs if the interparticle distance becomes smaller than a certain critical value. The drawback of this method is the large amount (60 wt%) of 200 nm sized particles required to obtain the sudden increase towards 200% strain at break on macroscopic level. This strain at break appears to be determined by that of the applied core-shell rubber particles. Additional experiments, however, demonstrated that the transition can be shifted to a lower rubber content by the application of smaller, 80 nm sized, core-shell rubbers, see Figure 1.7[15]. This once more stresses the existence of a certain critical matrix ligament thickness below which a shift in mode of microscopic deformation causes a sudden increase in toughness.

Apart from the transition in microscopic mode of deformation, also for these systems an enhanced delocalisation contributes to the observed toughness improvement. This may find its origin in a decreased glass transition temperature of the extremely thin ligaments[16-19] affecting the relative values of yield stress, strain softening and/or hardening. Smit[3,4] modeled the deformation of amorphous polymers by evaluating the influence of voids and rubber particles on the degree of localisation and the resulting macroscopic mechanical behaviour. It is claimed that the maximum improvement in toughness can be obtained by the introduction of a

sub-micron or even nano-sized dispersed phase. In order to circumvent the notch sensitivity of tough polymer systems like polycarbonate this dispersed phase may consist of voids while for brittle polymers like polystyrene easily cavitating rubber particles are preferred as the rubber inclusions will enhance the effective hardening modulus on a local scale.

In conclusion, the morphology of rubber modified brittle amorphous polymers should meet a few requirements in order to transfer their intrinsic ductile mechanical behaviour to macroscopic level. The rubber phase should possess a low resistance against cavitation while the interparticle distance should be smaller than a certain critical value in order to transform the mode of microscopic deformation from crazing to shear yielding. In order to combine the resulting toughening effect with a minimum loss in modulus and yield stress, the required rubber content should be decreased by decreasing the size of the rubber morphology to sub-micron or even nano-sized level.
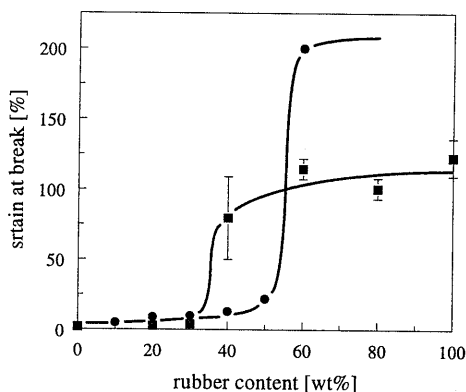
Figure 1.7: *Strain at break versus rubber content of core-shell rubber modified polystyrene using a particle size of 200 nm[12] (●) and 80 nm[15] (■).*

1.2   Rubber blending

1.2.1   Physical versus chemical blending

In this thesis, the results mentioned above will be considered as guidelines to develop new tough polymer systems based on rubber modification. The ultimate goal is the introduction of a sub-micron or even nano-sized rubber phase which requires a careful control over the morphology development during the blending process. In general, blending can roughly be subdivided in physical and chemical blending techniques. Physical blending, the most common technique, involves mixing of immiscible polymers using processing equipment such as extruders, rolling-mills or batch-kneaders. The final morphology is determined by the

processing conditions, compatibility, viscosity and viscosity ratio of the polymers involved. During chemical blending, at least one of the polymers involved is synthesised in the presence of the other polymer(s). The final morphology is the result of chemically-induced phase separation (CIPS) which occurs during polymerisation. Examples of this blending route are the production of rubber toughened thermoplastics such as high-impact polystyrene (HIPS), acrylonitrile-butadiene-styrene (ABS) and reactor modified polypropylene[1].

The sub-micron rubber morphologies required for the toughening of brittle amorphous polymers cannot be prepared via physical blending. Therefore, the alternative method using chemically-induced phase separation has to be explored somewhat further. Two optional routes are discussed below.

1.2.2 Reactive solvents

Venderbosch et al. introduced the concept of processing intractable polymers such as poly(2,6-dimethyl-1,4-phenylene ether) (PPE) using reactive solvents, as schematically represented in Figure 1.8[20-23]. The high processing temperature required for PPE is effectively decreased by applying epoxy resin as reactive solvent yielding a solution possessing a significantly decreased glass transition temperature and melt-viscosity. After processing, the homogeneous solution is cured which causes CIPS and phase inversion, resulting in a blend of epoxy spheres in a PPE matrix with its original high glass transition temperature, see Figure 1.8. Hence, in contrast to the application of polystyrene as processing aid (Noryl® of General Electric Plastics) the advantageous thermal and mechanical properties of PPE are recovered.
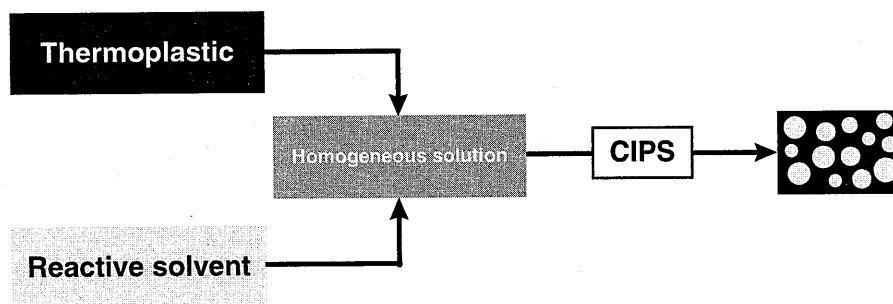
Figure 1.8: *Schematic representation of the concept of processing thermoplastic polymers using reactive solvents[20].*

Epoxy resins are reported to be effective solvents for many thermoplastics, for example polystyrene, poly(methyl methacrylate)[24], polyetherimide[25,26], polysulphone[27] and polyethersulphone[28,29]. The aim of most studies was to enhance the fracture toughness of the glassy epoxy resin. Hence, the cured epoxy was meant to be the continuous phase, in contrast to its application as a reactive solvent in which dispersed epoxy particles are locked up in thermoplastic matrix. As shown by Venderbosch at al., this offers the unique possibility to use this dispersed epoxy as a toughening agent by the application of an aliphatic epoxy resin which yields a rubber after curing. Therefore, this route can be considered as an alternative blending route to produce rubber toughened polymers. In all examples discussed by Venderbosch et al., the size of the dispersed phase proved to be one micrometer or larger. In this study, however, the intended toughening of brittle amorphous polymers requires a considerably smaller rubber morphology.

1.2.3 Interpenetrating polymer networks

The second example of using CIPS for rubber modification of polymers are so-called interpenetrating polymer networks (IPN)[30,31]. IPNs are defined as a combination of two or more polymer networks, with at least one of them polymerised and/or crosslinked in the immediate presence of the other(s)[32]. The size of the morphologies obtained are sometimes on the scale of only tens of nanometers which, in some cases, yields unique mechanical properties. Examples are the IPNs of polymethacrylates with polyurethane[33-37] or siloxanes[38], and poly(ethylene terephtalate) with castor oil[39]. However, hardly any attention is paid to the fundamental explanation of the improved toughness and the relation between morphology and microscopic deformation.

Generally, two types of IPNs can be distinguished: full-IPNs in which all networks are crosslinked and semi-IPNs in which at least one thermoplastic phase is present. For full-IPNs, simultaneous crosslinking of the networks involved will suppress the occurrence of coalescence after phase separation and thus the size of the final morphology. This approach can also be used to accomplish comparable morphologies in semi-IPNs in which the crosslinked phase forms the matrix. However, in the case that a thermoplastic matrix is desired, an alternative procedure should be developed to control the morphology since the coarsening process cannot be arrested by crosslinking. Examples of the latter semi-IPNs are in fact the thermoplastic - reactive solvent systems discussed above which possess a micron-sized particle morphology. Nevertheless, the application of the simultaneous polymerisation of separate polymer networks offers an additional option for the preparation of rubber modified polymers with an extremely small rubber phase.

1.3   Microscopic deformation studied by small angle X-ray scattering

As discussed in Section 1.1.3, the macroscopic mechanical properties are determined by the deformation and localisation on microscopic level. It has been demonstrated that one should understand the microscopic deformation in order to draw any solid conclusions concerning the relation between the morphology and the toughness of a blend. Synchrotron radiation is increasingly used to perform time-resolved small angle X-ray scattering (SAXS) experiments during mechanical testing, to monitor deformation development at a microscopic level. Several studies have been reported for both amorphous[40-46] and semi-crystalline[47-50] polymers. The advantage of using SAXS to characterise microscopic deformation is that the detailed analyses clearly yield more quantitative data in comparison with other techniques such as dilatometry and microscopy. For rubber modified amorphous polymers, the occurrence of dilatation processes such as debonding, cavitation and crazing can easily be distinguished from shear yielding. Crazing can be identified by SAXS as it results in typical cross-like scattering patterns consisting of two perpendicular streaks[51,52]. One is positioned along the tensile direction and the other perpendicular. The intense streak in the tensile direction, often indicated as "anomalous peak", is the result of scattering caused by the electron density difference between the polymer matrix and the craze-bulk. The less intense streak, which develops parallel to the craze plane, is attributed to the scattering of the craze fibrils and can be used to calculate the amount of crazing and the craze fibril diameter[40,41,53]. In several synchrotron studies this fibril scattering is used to determine the contribution of crazing to the total amount of strain in rubber modified thermoplastics[40,41]. Bubeck et al.[40] showed that during impact deformation of HIPS and ABS (acrylonitrile-butadiene-styrene), only half of the total strain can be ascribed to crazing. The remaining strain is accompanied by other dilatation processes and shear yielding. Recently, He et al.[42,43] showed that the craze density decreases as the toughness increases in commercial rubber toughened PMMA. The craze density was first found to increase and then to decrease with increasing rubber particle concentration or crosslink density. Besides crazing, Lovell et al.[44] also observed other dilatation processes for rubber modified PMMA which contained multi-layered core-shell rubber particles. The scattering patterns found are ascribed to the occurrence of rubber particle cavitation and debonding. Earlier, Ijichi et al. reported rubber cavitation and debonding as the most important mode of microscopic deformation in rubber modified blends of poly(phenylene ether) (PPE) and Nylon-6[45,46].

Also in this thesis, time-resolved SAXS measurements during deformation of rubber blends are used to identify and monitor the development of microscopic deformation.

1.4   Scope of the thesis

The aim of this thesis is the development of a ductile heterogeneous polymer system based on originally brittle amorphous polymers via the modification with a dispersed rubber phase. First, a new blending method has been developed since the ultimate toughness is expected exclusively for morphologies in the order of tens of nanometers which cannot be produced via conventional physical blending techniques.

In Chapter 2 the application of reactive solvents is studied. The relative influence of both the reaction rate and the system viscosity on the morphology coarsening process after chemically-induced phase separation is evaluated. It is demonstrated that the viscosity can be used to control the size of the final morphology. In Chapter 3 this approach is applied for the rubber modification of polystyrene and poly(methyl methacrylate) using an aliphatic epoxy resin as reactive solvent. Moreover, a simultaneous polymerisation technique for methylmethacrylate and epoxy has been developed. Also in this case, the morphology is tailored by controlling the viscosity of the reacting mixture yielding transparent epoxy-rubber modified PMMA.

In the subsequent chapters the mode of microscopic deformation of these PMMA/epoxy blends is studied by means of time-resolved small angle X-ray scattering experiments during tensile deformation. Slow speed uniaxial tension is discussed in Chapter 4 while in Chapter 5 the effect of strain rate on the occurrence of rubber cavitation is evaluated. The aim is to gain additional information concerning the toughening mechanisms in order to draw final, and more fundamental, conclusions on the relation between the morphologies, the mode of microscopic deformation and the resulting macroscopic mechanical properties.

In order to determine whether or not the enhanced toughness is caused by the morphology, in Chapter 6 the influence of the degree of demixing on the mechanical behaviour is studied on both macroscopic and microscopic level. A limited degree of demixing can be expected in these systems, considering the phase separation during blending and the large amount of interface between the phases involved as result of the small morphology.

Finally, this thesis ends with some general conclusions and recommendations in Chapter 7.

This thesis is based on a number of papers[8,54-58]. Moreover, the author also contributed to some other papers that are not part of the thesis. This includes the characterisation of the rubber modified poly(methyl methacrylate) discussed in this thesis by means of solid state NMR[59] and dielectric spectroscopy[60] and the development of a new type of preformed crosslinked rubber particles which were successfully applied as toughening agents in glassy epoxy resin[61].

1.5 References

(1) Bucknall, C.B. *Toughened Plastics*, Applied Science Publishers LTD: London, **1977**.

(2) Riew, C.K.; Kinloch A.J. *Advances in Chemistry Series*; American Chemical Society: Washington DC, **1993**, *233*.

(3) Smit, R.J.M.; Meijer, H.E.H.; Brekelmans, W.A.M.; Govaert, L.E. *J. Mater. Sci.* **1998**, submitted.

(4) Smit, R.J.M. *Ph.D. thesis*, Eindhoven University of Technology, **1998**.

(5) Kramer, E.J.; Berger, L.L. *Adv. Polym. Sci.* **1990**, *91/92*, 1.

(6) Donald, A.M.; Kramer, E.J. *J. Polym. Sci., Polym. Phys. Edn.* **1982**, *20*, 899.

(7) Casteren van, I.A. *Masters thesis*, Eindhoven University of Technology, **1998**.

(8) Casteren van, I.A.; Melick van, H.G.H.; Jansen, B.J.P.; Govaert, L.E.; Meijer, H.E.H. in preparation.

(9) Henkee, C.S.; Kramer, E.J. *J. Polym. Sci., Polym. Chem. Edn.* **1984**, *22*, 721.

(10) Ritchie, P.D.; Critchley, S.W.; Hill, A. *Plasticisers, Stabilisers and Fillers*, Lliffe Books: London, **1972**.

(11) Tervoort, T.A. *Ph.D. thesis*, Eindhoven University of Technology, **1996**.

(12) Sanden van der, M.C.M. *Ph.D. thesis*, Eindhoven University of Technology, **1993**.

(13) Sanden van der, M.C.M.; Meijer, H.E.H.; Lemstra, P.J. *Polymer* **1993**, *34*, 10, 2148.

(14) Sanden van der, M.C.M.; Buijs, L.G.C.; Bie de, F.O.; Meijer, H.E.H. *Polymer* **1994**, *35*, 13, 2783.

(15) Pauwels, H.J.M.P. *Masters thesis*, Eindhoven University of Technology, **1995**.

(16) Wallace, W.E.; Zanten van, J.H.; Wu, W.L. *Phys. Rev. E* **1995**, 52, 52.

(17) Forrest, J.A.; Dalnoki-Veress, K.; Dutcher, J.R.; Rowat, A.C.; Stevens, J.R. *Mat. Res. Soc. Symp. Proc.* **1996**, 407, 131.

(18) Forrest, J.A.; Dalnoki-Veress, K.; Stevens, J.R.; Dutcher, J.R. *Phys Rev. Lett.* **1996**, 77, 2002.

(19) Keddie, J.L.; Jones, R.A.L.; Cory, R.A. *Europhys. Lett.* **1994**, 27, 59.

(20) Venderbosch, R.W. *Ph.D. thesis*, Eindhoven University of Technology, **1995**.

(21) Goossens J.G.P. *Ph.D. thesis*, Eindhoven University of Technology, **1998**.

(22) Venderbosch, R.W.; Meijer, H.E.H.; Lemstra, P.J. *Polymer* **1994**, *33*, 20, 4349.

(23) Venderbosch, R.W.; Meijer, H.E.H.; Lemstra, P.J. *Polymer* **1995**, *36*, 15, 2903.

(24) Gomez, C.M.; Bucknall, C.B. *Polymer* **1993**, 34, 2111.

(25) Park, J.W.; Kim, S.C. *IPNs around the world*, John Wiley & Sons, Chichester, **1997**, 27.

(26) Chean, C.S.; Eamor, M.W. *Polymer* **1995**, 36, 2883.

(27) Min, B.G.; Hodgkin, J.H.; Stachurski, Z.H. *J. Appl. Polym. Sci.* **1993**, 50, 1065.

(28) Akay, M.; Cracknell, J.G. *J. Appl. Polym. Sci.* **1994**, 52, 663.

(29) Yamanaka, K.; Inoue, T. *Polymer* **1989**, 30, 662.

(30) Klempner, D.; Sperling, L.H.; Utracki, L.A. *Advanced Chemistry Series*, American Chemical Society: Washington DC, **1994**, *239*.

(31) Kim, S.C.; Sperling, L.H. *IPNs around the world*; John Wiley & Sons: Chichester, **1997**.

(32) Sperling, L.H.; Mishra, V. In *IPNs around the world*; Kim, S.C., Sperling, L.H.; John Wiley & Sons: Chichester, **1997**, 1.

(33) Akay, M.; Rollins, S.N. *Polymer* **1993**, *34*, 9, 1865.

(34) Akay, M.; Rollins, S.N.; Riordan, E. *Polymer* **1988**, *29*, 37.

(35) Chou, Y.C.; Lee, L.J. *Polym. Eng. Sci.* **1995**, *35*, 12, 976.

(36) Han, X.; Chen, B.; Guo, F. In *IPNs around the world*; Kim, S.C., Sperling, L.H.; John Wiley & Sons: Chichester, **1997**, 241.

(37) Hourston, D.J.; Schäffer, F.U. *Polymer* **1996**, *37*, 16, 3521.

(38) Gilmer, T.C.; Hall, P.K.; Ehrenfeld, H.; Wilson, K.; Bivens, T.; Clay, D.; Emdreszl, C. *J. Polym. Sci., Polym. Chem. Ed.* **1996**, *34*, 1026.

(39) Barret, L.W.; Sperling, L.H.; Gilmer, J.W.; Mylonakis, S.G. In *Advances in Chemistry Series*; Klempner, D., Sperling, L.H., Utracki, L.A.; American Chemical Society: Washington DC, **1994**, *239*, 489.

(40) Bubeck, R.A.; Buckley, D.J.; Kramer; Brown, H.R. *J. Mater. Sci.* **1991**, *26*, 6249.

(41) Buckley, D.J., Jr. *Ph.D. thesis*, Cornell University, **1993**.

(42) He, C.; Donald, A.M.; Butler, M.F.; Diat, O. *Polymer* **1998**, *39*, 659.

(43) He, C.; Donald, A.M.; Butler, M.F. *Macromolecules* **1998**, *31*, 158.

(44) Lovell, P.A.; Ryan, A.J.; Sherratt, M.N.; Young, R.J. *Polym. Mat. Sc. Eng.* **1994**, *70*, 155.

(45) Ijichi, Y.; Kojima, T.; Suzuki, Y.; Nishio, T.; Kakugo, M. *Macromolecules* **1993**, *26*, 4, 829.

(46) Okamoto, Y.; Miyagi, H.; Uno, T.; Amemiya, Y. *Polym. Engin. Sci.* **1993**, *33*, 1608.

(47) Butler, M.F.; Donald, A.M.; Ryan, A.J. *Polymer* **1997**, *38*, 5521.

(48) Butler, M.F.; Donald, A.M.; Ryan, A.J. *Polymer* **1997**, *39*, 781.

(49) Butler, M.F.; Donald, A.M.; Bras W.; Mant, G.R.; Derbyshire, G.E.; Ryan, A.J. *Macromolecules* **1995**, *28*, 6383.

(50) Hughes, D.J.; Mahendrasinngam, A.; Oatway, W.B.; Heeley, E.L.; Martin, C.; Fuller, W. *Polymer* **1997**, *38*, 6427.

(51) Paredes, E.; Fischer, E.W. *Macromol. Chem.* **1979**, *180*, 2707.

(52) Brown, H.R.; Kramer, E.J. *J. Macromol. Sci. - Phys.* **1981**, *B19*, 487.

(53) Magalhaes, A.M.L.; Borggreve, R.J.M. *Macromolecules*, **1995**, *28*, 5841.

(54) Jansen, B.J.P.; Meijer, H.E.H.; Lemstra, P.J. *Polymer* **1998**, accepted, chapter 2.

(55) Jansen, B.J.P.; Meijer, H.E.H.; Lemstra, P.J. *Macromolecules* **1998**, submitted, part 1, chapter 3.

(56) Jansen, B.J.P.; Rastogi, S.; Meijer, H.E.H.; Lemstra, P.J. *Macromolecules* **1998**, submitted, part 2, chapter 4.

(57) Jansen, B.J.P.; Rastogi, S.; Meijer, H.E.H.; Lemstra, P.J. *Macromolecules* **1998**, submitted, part 3, chapter 5.

(58) Jansen, B.J.P.; Rastogi, S.; Meijer, H.E.H.; Lemstra, P.J. *Macromolecules* **1998**, submitted, part 4, chapter 6.

(59) Mulder, F.M.; Jansen, B.J.P.; Lemstra, P.J.; Meijer, H.E.H.; Groot de, H.J.M. *Phys. Rev. Lett.*, submitted.

(60) Williams, G. et al., in preparation.

(61) Jansen, B.J.P.; Tamminga, K.Y.; Meijer, H.E.H.; Lemstra, P.J. *Polymer* **1998**, submitted.

Chapter 2

Morphology control during chemically-induced phase separation of reactive solvents

2.1 Introduction

As outlined in Chapter 1, the aim of this thesis is the development of a procedure to prepare tough heterogeneous polymer systems based on brittle amorphous polymers. The toughness enhancement should be the result of a transition in the mode of microscopic deformation from crazing to shear yielding. In order to combine this with a minimum loss in yield strength and modulus, the size of the dispersed phase should be reduced to sub-micron or even nano-scale. These morphology sizes, however, cannot be produced via physical blending techniques. Therefore in this chapter, the application of reactive solvents as an alternative blending route is studied. In this case, the morphology is the result of chemically-induced phase separation (CIPS) which must be controlled in order to achieve the desired morphologies.

Venderbosch et al.[1-4] used epoxy resin as reactive solvent to process the intractable thermoplastic poly(2,6-dimethyl-1,4-phenylene ether) (PPE). Upon curing the initially homogeneous epoxy - thermoplastic solution, phase separation is induced resulting in micron-sized epoxy spheres in a thermoplastic matrix. According to Venderbosch et al. the size of the morphology is not influenced by the curing temperature within the temperature range studied. According to other studies[5-12], however, the morphology will depend on the applied reaction temperature. Generally, it is expected that the size of the final morphology is determined by the competition between the reaction kinetics and the rate of phase separation.

In this chapter, the morphology control during chemically-induced phase separation is investigated using PPE-PS/epoxy as a model system. The advantage of this system is that the

viscosity of the thermoplastic phase can be varied at a constant curing temperature by changing the ratio of the compatible PPE-PS blend. The objective is to obtain more understanding of those kinetic factors that determine the size of the final morphology. The final interest is the development of a route to produce the sub-micron morphologies required for the described toughening purposes.

2.2   Experimental

2.2.1   Sample preparation

Poly(2,6-dimethyl-1,4-phenylene ether) (PPE), PPO 803 possessing a molar mass of 32 kg/mol (M_w), was supplied by General Electric Plastics (Bergen op Zoom, The Netherlands) and polystyrene (PS), SHELL N5000 possessing a M_w of 260 kg/mol, was supplied by BPM (Bredase Polystyreen Maatschappij, Breda, The Netherlands). As a reactive solvent for these polymers, a diglycidyl ether of bisphenol-A epoxy resin (SHELL Epikote 828 EL) was used. Two different aromatic curing agents, supplied by Lonza Ltd (Breda, The Netherlands), were used; 4,4'-methylenebis(3-chloro-2,6-diethylaniline) (M-CDEA) and 4,4'-methylenebis(2,6-diethylaniline) (M-DEA).
The PPE-PS blends and PPE-PS/epoxy solutions were prepared using either a Brabender Plasticorder batch kneader (60 cm^3) or a miniature co-rotating recirculating twin-screw extruder (5 cm^3)[1]. Depending on the relative amounts of the three constituents, a processing temperature of 150 °C to 230 °C was used. Blending and dissolution was continued until a homogeneous, optically transparent, solution was obtained. High epoxy content solutions (>60 wt%) of PS/epoxy were prepared by stirring a mixture of PS and epoxy in a glass beaker at ±120 °C.
After a homogeneous solution was obtained, the curing agent, if any, was added (51 phr for M-CDEA, 43.3 phr for M-DEA), and mixing was continued for several minutes. The solutions obtained were compression moulded and, subsequently, cured at various temperatures. The exact curing temperatures and times are indicated below.

2.2.2   Solution behaviour

The phase behaviour of the binary PS/epoxy and the ternary PPE-PS/epoxy system, was studied using a light scattering set-up. Compression moulded films were heated between two glass slides in a Linkham Hot Stage until a homogeneous solution was obtained. The intensity of a laser beam, which was directed through the sample, was recorded using a light detector. The reported cloud-point temperatures correspond with the onset of the measured decrease in light transmission, caused by phase separation of the samples upon cooling (2 °C/min). All solutions showed an upper critical solution temperature (UCST) behaviour.
The dynamic mechanical behaviour (DMTA) of both, blends and solutions, was determined using a Polymer Laboratories MkII. The measurements were performed in a double cantilever bending mode using a frequency of 1 Hz and heating rate of 2 °C/min. The maximum of the loss peak tan δ was taken as the glass transition temperature, T_g.

A Rheometrics RDSII spectrometer operated at a frequency of 10 rad/s was used to measure the viscosity of the PPE-PS/epoxy solutions, by cooling (5 °C/min) homogeneous samples from a starting temperature of 225 °C.

2.2.3 Morphology

Scanning electron microscopy (SEM, Cambridge Stereoscan 200) was used to visualize the morphology. Sample preparation occurred by cryogenic fracture of the PPE-PS/epoxy blends. Additionally, for blends possessing a sub-micron morphology transmission electron microscopy (TEM, Jeol TEM 2000 FX) was performed. Samples were ultramicrotomed (Reichert Ultracut E) at room temperature and, subsequently, vapour stained using rutheniumtetraoxide (RuO_4).

If possible, an even better estimate of the epoxy particle size in the blends was obtained by extracting the particles from the PPE-PS matrix. An ultracentrifuge was used to separate the non-soluble thermosetting epoxy particles from the soluble PPE-PS matrix. After each of the three ultracentrifuge steps, the solvent was replaced. Chloroform was used in the first step, toluene during the remaining two steps. An aluminum strip was immersed in the final solution and, subsequently, dried at 100 °C for 20 hours, before studying the particles size by using SEM.
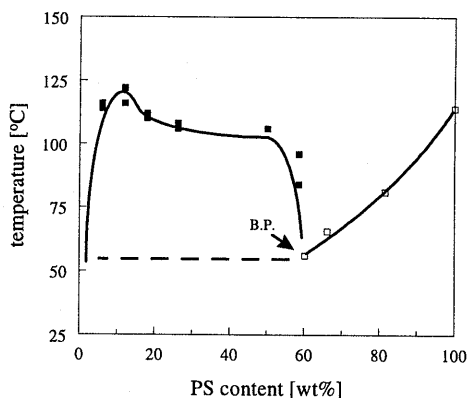
Figure 2.1: *Binary phase diagram of PS/epoxy, (■) cloud-point data, (□) glass transition temperatures, dashed line represents the T_g of the phase separated solutions.*

2.3 Results and discussion

2.3.1 Phase behaviour of binary epoxy solutions

First the phase behaviour of both, the binary PS/epoxy and the ternary PPE-PS/epoxy system, will be presented and discussed. PPE-PS is known as one of the few combinations of polymers that are miscible over the whole composition range[13,14]. The phase behaviour of PPE/epoxy has been reported earlier by Venderbosch et al.[1] for three PPE molecular weights.

The cloud-point and vitrification curve of the PS/epoxy system, determined by respectively light scattering and DMTA, are presented in Figure 2.1. Solutions with a PS content not exceeding 60 wt% are homogeneous at elevated temperatures but phase separate upon cooling. The curve of the cloud-point temperatures shows a rather unexpected concentration independent behaviour in the composition range of 20 - 50 wt% PS. The maximum cloud-point temperature is measured at approximately 125 °C, which is low compared to the 180 °C as was found for PPE/epoxy[1]. Upon cooling solutions containing more than 60 wt% polystyrene, vitrification occurs prior to thermally-induced phase separation. Visually, homogeneous solidified solutions are obtained, possessing a T_g in accordance with the Fox relationship[15]. The intersection point of this vitrification curve and the cloud-point curve is called the Berghmans-point[16] (B.P.) and is found at approximately 60 wt% polymer for both PS/epoxy and PPE/epoxy. To a good approximation, the phase separated solutions all possess a T_g equal to that of the Berghmans-point, as is represented by the dashed line.
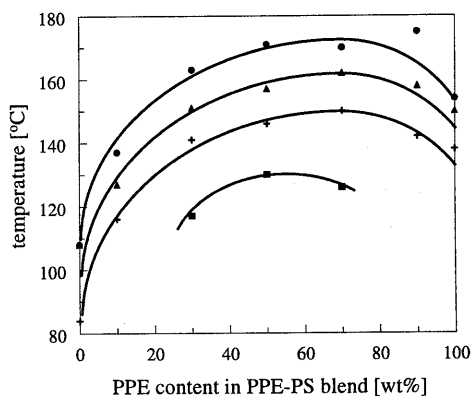
Figure 2.2: *Cloud point curves of some ternary PPE/PS-epoxy solutions for four fixed epoxy concentrations, 30 wt% (■), 40 wt% (+), 50 wt% (▲), 60 wt% (●).*

2.3.2 Phase behaviour of ternary PPE-PS/epoxy solutions

The phase behaviour of ternary PPE-PS/epoxy solutions has been studied. In Figure 2.2 the cloud-point temperatures of four solutions with varying PPE-PS ratios are presented at constant epoxy concentrations of respectively 30, 40, 50 and 60 wt%. Cloud point curves are found over the whole PPE-PS composition range at epoxy concentrations of 60, 50 and 40 wt%, indicating that thermally-induced phase separation occurs prior to vitrification. Higher temperatures are required to obtain homogeneous solutions when the epoxy concentration in the ternary system is increased. Moreover, the cloud-point temperatures for the PS rich solutions (left hand side in Figure 2.2) are lower compared to those for the PPE rich solutions (right hand side). In the 30 wt% epoxy solutions, thermally-induced phase separation occurs

only if both PPE and PS are present in considerable amounts whereas the binary solutions, PPE/epoxy and PS/epoxy, vitrify prior to demixing. In contrast, all ternary solutions with an epoxy content of 20 wt% or less are miscible over the whole PPE-PS composition range.
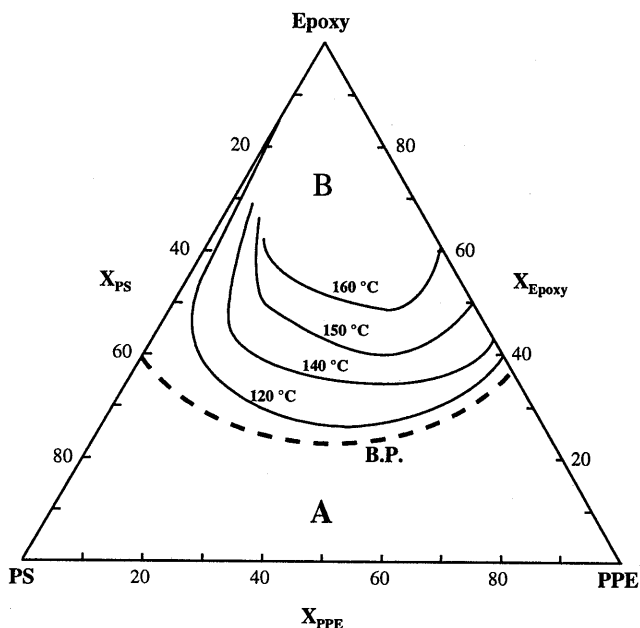
Figure 2.3: *Ternary cloud-point diagram of the PPE/PS-epoxy solution. The drawn lines represent the isothermals of measured cloud-points at the indicated temperatures, the dashed line (B.P.) represents the collection of Berghmans points which separates: (A) direct vitrification from homogeneous solution and (B) thermally-induced phase separation prior to vitrification.*

The cloud-point data depicted in Figure 2.2 are used to construct the ternary cloud-point diagram as presented in Figure 2.3. The base line of the diagram represents the homogeneous PPE-PS blend while the two remaining axis cover the cloud-point curves of the PS/epoxy system, see Figure 2.1, and the PPE/epoxy system, see ref. 1. The collection of Berghmans points is represented by the dashed line, B.P., the Berghmans curve. PPE and/or PS rich solutions possessing compositions underneath this line (region A) will all vitrify upon cooling and, therefore, remain homogeneous. In contrast, if the epoxy concentration exceeds those given by the Berghmans curve (region B), phase separation will occur upon cooling. The thermoplast concentration at the Berghmans points appears to increase from approximately 60 wt% for the binary systems, PS/epoxy and PPE/epoxy, to almost 80 wt% for a PPE-PS 50-50 blend. The cloud-point data presented in Figure 2.2 are used to construct the four isothermal

cloud-point curves for 120, 140, 150 and 160 °C in Figure 2.3. A rather similar concentration dependence is observed as for the Berghmans curve. The strong curved shape of the isotherms as the PS/epoxy axis is approached is the result of the relatively lower cloud-point temperatures of the binary PS/epoxy system in comparison to PPE/epoxy.

2.3.3 Curing of PPE-PS/epoxy solutions

In order to cure the epoxy resin, a curing agent has to be added to the PPE-PS/epoxy solutions. Since this changes the ternary solution into a quaternary system, the phase behaviour as presented in Figure 2.3 can only be used as a first indication for the miscibility at a certain composition. Most probably, the curing agents applied in this study do not decrease the compatibility since an improved miscibility has been reported once a curing agent such as M-CDEA is introduced into the PPE/epoxy system[17,18].
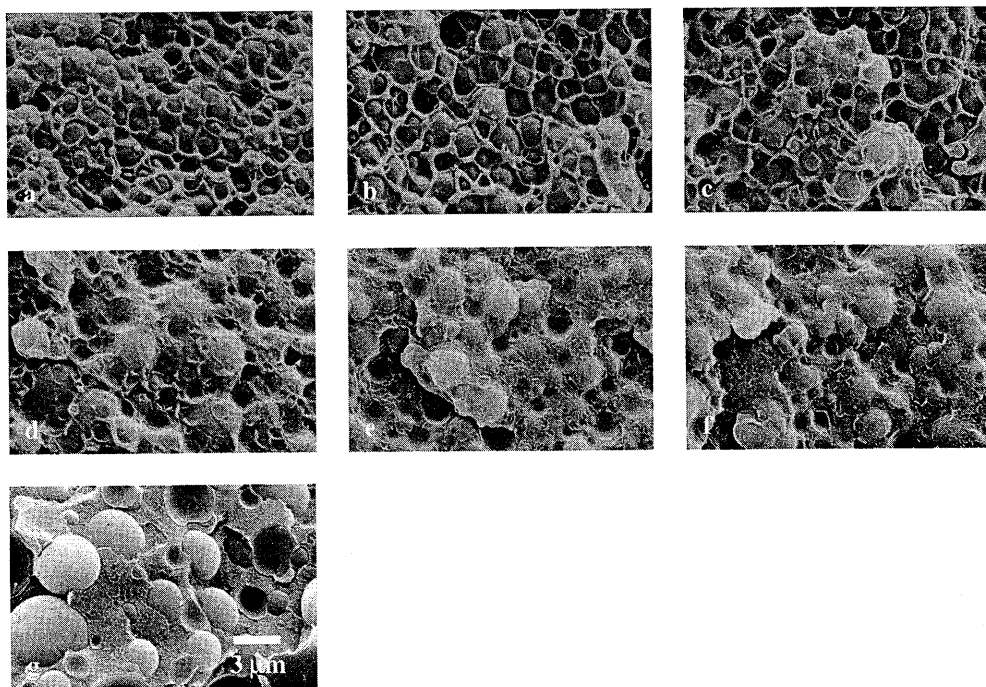
Figure 2.4:   *Morphology of PPE-PS/epoxy blends containing 50 wt% epoxy, cured at 225 °C (M-CDEA), PPE-PS (a) 100-0, (b) 90-10, (c) 70-30, (d) 50-50, (e) 30-70, (f) 10-90, (g) 0-100.*

Upon curing of the homogeneous solutions, chemically-induced phase separation is expected to occur since the epoxy resin is transformed into a non-solvent. In the case of PPE/epoxy, the concomitant phase inversion leads to a final morphology consisting of dispersed epoxy

particles in a PPE matrix as can be observed in Figure 2.4a. The epoxy spheres appear to be partially covered with PPE. As can be observed in Figure 2.4g, a similar morphology is obtained upon curing a PS/epoxy solution, however, the epoxy particles appear to possess a much smoother surface. Figure 2.4 shows that the amount of matrix, covering the epoxy particles, gradually changes with the PPE-PS ratio which is, most probably, the result of the reactivity of the PPE component. The hydroxyl end-groups of the PPE polymer can react with the epoxy resin, giving rise to an improved interfacial bonding compared to PS/epoxy. The formation of this "co-polymer" will most probably also act as compatibiliser and, therefore, will somewhat reduce the final epoxy particle size in the blend. This is confirmed by the particle sizes depicted from Figure 2.4, which decrease from approximately 3 μm for PS/epoxy to 2 μm for PPE/epoxy.
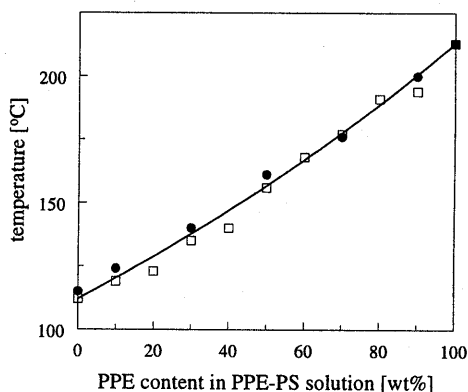
Figure 2.5: *Glass transition temperatures of the compatible PPE-PS blends (□) and the PPE-PS phase of the cured PPE-PS/epoxy system containing 50 wt% epoxy (●). The draw line represents the Fox equation.*

In the case of curing the binary solutions, PPE/epoxy and PS/epoxy, a two phase system is obtained. Apparently, in the present case of the ternary PPE-PS/epoxy system also a two phase system results, see Figure 2.4. More direct evidence on the heterogeneity can be obtained from monitoring the glass transition temperatures of the resulting blends by using dynamic mechanical analysis. The results are presented in Figure 2.5 which shows the T_g's of the PPE-PS phase in the cured systems compared to those of neat PPE-PS blends. The T_g of the cured blends follows the trend of the pure PPE-PS, confirming that a two phase system results. The T_g of the PPE-PS phase roughly follows the Fox equation[14]. Some care in the interpretation of these results is required since the T_g of the epoxy phase formed will be found in the same range as the intermediate PPE-PS blend compositions. The absence of separate PPE and/or PS

transitions confirms that the PPE-PS phase can be considered as one single phase during chemically-induced phase separation in the ternary solutions.

2.3.4 Influence of curing temperature on the morphology

One-step curing at T$_g$. Mechanical properties of blends are determined by the properties of the constituent phases and by their morphology. Venderbosch et al.[1,4] did not observe any relevant changes in morphology of PPE/epoxy systems upon varying the curing temperature, the curing agent and its amount over a relatively broad range. Nevertheless, it could be expected that extreme curing conditions should yield different results. As an example Figures 2.6b and c show the resulting morphology of PPE/epoxy (70/30) cured at a very low curing temperature of 105 °C, which is indeed considerably lower than the temperature range used by Venderbosch et al., see Figure 2.6a. The size of the epoxy particles is decreased by one order of magnitude, from approximately 1.5 μm to 200 nm, (compare Figures 2.6a and b). This substantial difference in the resulting particle size can be attributed to the large influence of the curing temperature on the coalescence rate versus reaction rate[6-8]. The final morphology size in processes involving chemically-induced phase separation (CIPS) will depend on the rate of coarsening after phase separation and the available time which is determined by gelation or vitrification of the epoxy phase. At high reaction rates gelation and, consequently, morphology fixation occurs at an early stage of the coarsening process,[11] while on the contrary a low curing temperature yields a high viscosity that slows down the coalescence rate. The lower limit of the second route is, obviously, curing at the T$_g$ of the initial solution. This was already partially recognised by Yamanaka et al.[7]. A clear disadvantage of curing at T$_g$ is that the curing cycles will be long (in the order of hours). This is a result of the solution preparation which requires high processing temperatures (see the phase diagram in Figure 2.3) and, consequently, slowly reacting curing agents or, alternatively, extremely short mixing times.
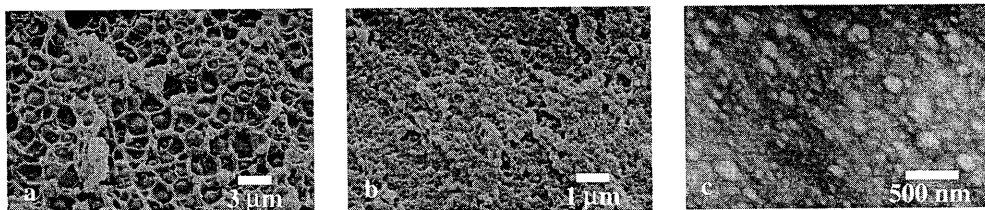
Figure 2.6: *Morphology of PPE/epoxy 70/30 blends, (a) SEM, T$_{cure}$= 225 °C, (b) SEM, T$_{cure}$= 105 °C, (c) TEM, T$_{cure}$= 105 °C.*

Moreover, the T_g-curing approach can only be applied for systems which remain homogeneous and can, therefore, only successfully be performed for the PPE-PS/epoxy solutions that vitrify upon cooling. For example, solutions with 30 wt% epoxy can be cured at T_g provided that the content of PPE or PS content is high (e.g. PPE-PS/epoxy 90-10/30 or 10-90/30), see Figure 2.7a and 2.9 for 90-10/30. Systems with more symmetric PPE-PS compositions, e.g. 50-50/30 in Figure 2.7b, possess a micron-sized morphology rather than the 200 nm sized dispersions found earlier. The morphology of this blend (Figure 2.7b) is the result of thermally-induced phase separation prior to curing, which occurs upon cooling to the T_g, i.e. 90 °C (which would have been the solution T_g if thermally-induced phase separation would not have occurred). The obtained particle size is only slightly smaller compared to the same system cured at 225 °C for which the morphology is the result of chemically-induced phase separation only.
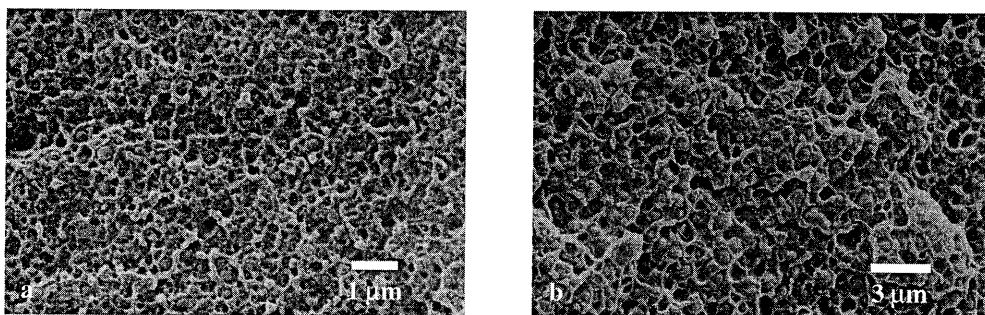
Figure 2.7: *SEM micrographs of PPE-PS/epoxy blends, (a) 90-10/30, $T_{cure}= 105$ °C, (b) 50-50/30, $T_{cure}= 90$ °C.*

Thus far, all examples presented on morphology control by adapting the T_g-curing schedule were taken from systems with a relatively low epoxy fraction. The reason is the requirement of obtaining an initially vitrified solution, which is, for the PPE-PS system, only possible for a solvent content of 30 wt% or less (see Figure 2.3). The general applicability of the new processing route described here, is confirmed by polyetherimide (PEI)/epoxy for which vitrified solutions can be obtained up to an epoxy content of 70 wt%[19]. In Figure 2.8, two final morphologies of a 50/50 solution are presented which are the result of curing at the T_g of the initial solution (90 °C) and at a high temperature (225 °C) respectively. This example clearly illustrates the previous conclusion that morphology development can be controlled by affecting the coarsening process after phase separation and that this procedure is not restricted to systems with relatively low solvent contents.
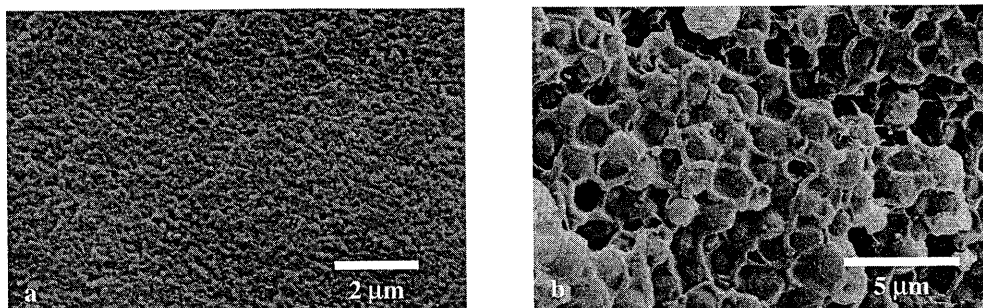
Figure 2.8: *Morphology of PEI/epoxy 50/50 blend cured at (a) 90 °C, (b) 225 °C.*
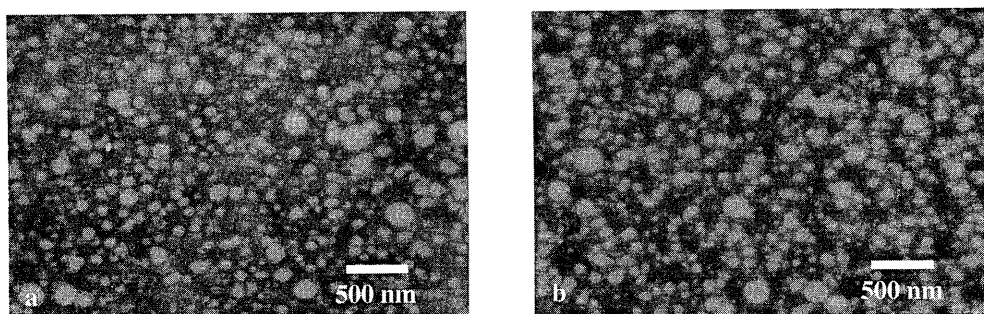
Figure 2.9: *Transmission electron micrographs of PPE-PS/epoxy 90-10/30 cured at (a) 105 °C (b) cured at 105 °C, initially post-cured at 150 °C and, subsequently, at 180 and 200 °C.*

Multi-step curing at T_g. Another drawback of curing at relatively low temperatures is that no full epoxy conversion and phase separation can be obtained as a result of vitrification of either the epoxy-rich or the PPE-PS-rich phase. This causes a conflict in the curing schedule; a low curing temperature is desired to establish the sub-micron morphologies while higher curing temperatures are needed to reach full conversion. This conflict can be partially reconciled by adapting a stepwise curing procedure increasing the conversion while keeping the control over the morphology. The optimum curing schedule is realised by making the curing temperature equal to the increasing glass transition temperature of the reacting and phase separating system: $T_{cure}(t) = T_g(t)$.

The morphology of a PPE-PS/epoxy 90-10/30 blend cured at the T_g of the initial solution (105 °C) is shown in Figure 2.9a. For comparison, Figure 2.9b shows that of the same system, also cured at T_g, but subsequently post-cured at 150, 180 and 200 °C. Obviously, the particles size does not increase during post-curing. In Figure 2.10 the dynamic mechanical behaviour of these blends before and after curing and post-curing is depicted. Although the morphology is fixed after the first curing step at 105 °C, the DMTA results clearly show a continuing reaction with increasing curing temperature. Even though the exact interpretation of these

DMTA data is somewhat obscured by the ongoing reaction during the measurements (especially at the lower conversions, curves *i* and *ii*), still some useful information is obtained. As observed in Figure 2.10a, the modulus of the uncured system (curve *i*) falls at a significantly lower temperature than for the cured systems (curves *ii-v*). Post-curing clearly shifts the T_g of the system to higher temperatures, from approximately 140 °C after the first curing step, to almost 200 °C, see also the tan δ measurements in Figure 2.10b. As the curing temperature approaches 200 °C (curves *iii-v*), the maximum in tan δ can indeed be related to the T_g 's of the blend. Two phases are distinguished: an epoxy-rich phase with a T_g of ~160 °C and a PPE-PS-rich phase with a T_g of ~190 °C. Only a minor increase in the T_g of the latter phase is observed as a result of additional post-curing at 180 °C and 200 °C (curves *iv* and *v*). Remarkably, the peaks broaden and partially merge and finally the epoxy peak has become a shoulder of the PPE-PS transition. These phenomena are known from the formation of interpenetrating polymer network structures in which peak broadening and shifts are ascribed to incomplete demixing or interphase mixing of the crosslinked components[20].
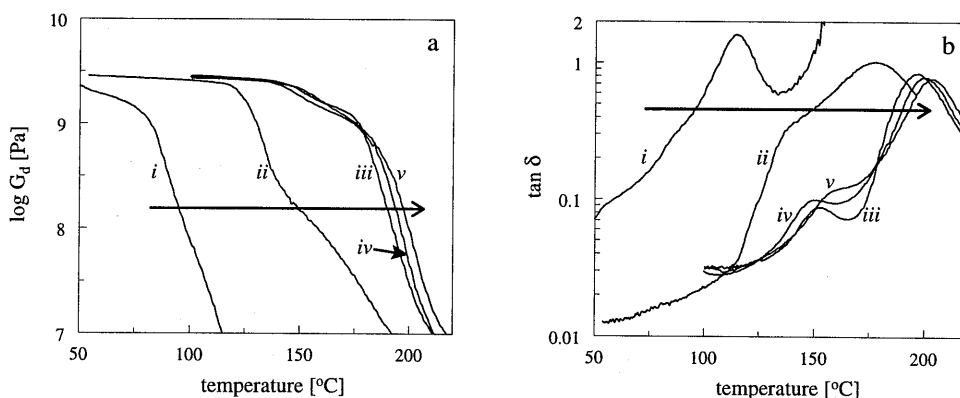
Figure 2.10: *(a) Dynamic modulus (G_d) and (b) loss angle (tan δ) versus temperature, of a PPE-PS/epoxy 90-10/30 solution prior to curing (i), after the first curing step at 105 °C (ii), after the additional post-curing steps at 150 °C (iii), 180 °C (iv), 200 °C (v).*

2.3.5 Influence of viscosity on the morphology

Generally, it will be difficult to separate the influence of the viscosity and reaction rate on the resulting morphology. This is due to the fact that both parameters are a function of temperature and, therefore, cannot be varied independently. However, the PPE-PS system offers the unique possibility to study the influence of the viscosity at a fixed curing temperature by varying the T_g of the initial solution via changing the PPE-PS ratio. One has to keep in mind, however, that the overall reaction rate always consists of a chemical reaction

rate combined with a diffusion rate[21]. The reaction rate does not change during curing at a fixed temperature while the diffusion rate still does, given its dependence on the viscosity and thus on the PPE-PS ratio. However, this last effect could be of minor importance, considering all complex processes involved during chemically-induced phase separation.
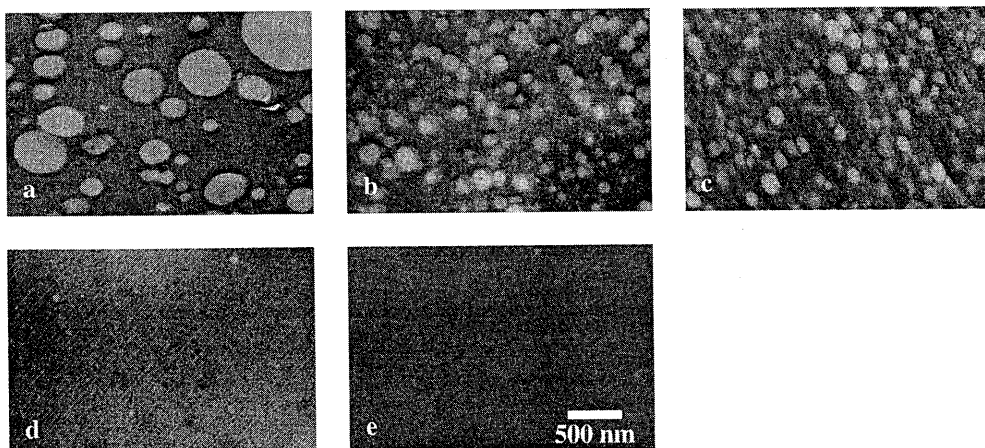
Figure 2.11: *Transmission electron micrographs of PPE-PS/epoxy blends cured at 90 °C, (a) 10-90/20, (b) 30-70/20, (c) 50-50/20, (d) 70-30/20, (e) 90-10/20.*

A 20 wt% epoxy system is chosen, since higher solvent concentrations result in thermally-induced phase separation as explained above (Figure 2.3). The curing temperature is chosen equal to the T_g of the PPE-PS/epoxy 50-50/20 solution (i.e. approximately 90 °C). Consequently, systems with more than 50 wt% PPE (relatively to PS) are initially cured *below* and those with less than 50 wt% PPE are cured *above* their T_g. The morphology of the blends is visualised by using transmission electron microscopy, see Figure 2.11. For the sample with the highest amount of PS (PPE-PS 10-90), a rather coarse morphology is observed, see Figure 2.11a. The difference between T_g of the initial solution and the curing temperature is apparently too large. Upon increasing the PPE content, from PPE-PS 10-90 to 30-70, the particle size decreases, as expected, see Figure 2.11b. This difference is ascribed to the enhanced viscosity, preventing coalescence. Figure 2.12 shows this more clearly for the extracted epoxy particles of PPE-PS/epoxy 30-70/30 after curing at an elevated temperature of 225 °C (Figure 2.12a) and close to the initial T_g of the solution (90 °C, Figure 2.12b). Upon increasing the PPE content, no further decrease in particle size is found, see Figure 2.11c. Remarkably, the obtained blend can no longer be dissolved but only swells upon the addition of solvent which suggests the formation of a phase inverted or bicontinuous morphology or, alternatively, a semi-interpenetrating polymer network[20,22]. This trend is confirmed by the samples possessing the highest PPE contents (PPE-PS 70-30 and 90-10) that cannot be

dissolved either. They are cured below the T_g of the initial solution, which appears to prevent the development of a real particle morphology, see Figures 2.11d and e.
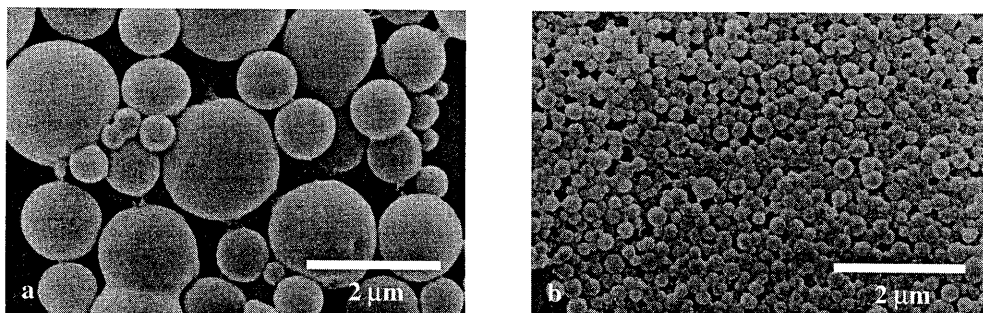
Figure 2.12: *SEM micrographs of extracted epoxy particles of PPE-PS/epoxy 30-70/30 blends cured at (a) 225 °C, (b) 90 °C.*
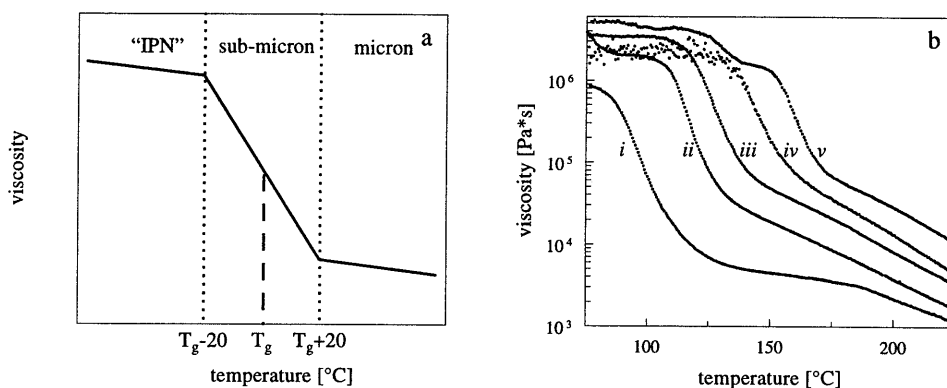
Figure 2.13: *(a) Schematic representation of the morphology sizes obtained after curing at different temperatures, (b) viscosity vs temperature for PPE-PS/epoxy solution with 20 wt% (no curing agent) for five PPE-PS ratios, i) 10-90, ii) 30-70, iii) 50-50, iv) 70-30, v) 90-10.*

In conclusion, roughly three morphology types can be distinguished related to the viscosity of the system or the curing temperature, as schematically presented in Figure 2.13a. Curing above the T_g of the initial solution yields micron-sized epoxy particles which are one order larger compared to the sub-micron particles for solutions cured near T_g. From Figure 2.13b it is concluded that the sub-micron morphology can only be obtained within a temperature window of approximately 40 °C. Curing at temperatures lower than T_g, thus in an almost vitrified system, results in an interpenetrating polymer network where hardly any dispersed

phase is formed. This set of experiments clearly shows that the actual viscosity during curing is the morphology determining parameter.

Of course, the problem of the viscosity dependent diffusion and its influence on the reaction rate remains. However, the statement that this effect is negligible for the systems studied, is confirmed by the conclusion that for a decreasing reaction rate, the time for the morphology to coarsen after phase separation increases while the final morphology size only decreases upon lowering the curing temperature. Apparently, the increase in viscosity overrules the influence of the reaction rate.

2.4 Conclusions

The aim of this chapter was to study morphology development in blending routes involving chemically-induced phase separation. It was tried to independently vary the different influences on the processes involved, i.e. reaction rate and the rate of morphology coarsening. Therefore, the system PPE-PS/epoxy was studied allowing for an independent change of viscosity and curing temperature.

First, the phase behaviour of binary PS/epoxy and ternary PPE-PS/epoxy systems was studied. For the PPE-PS/epoxy system, thermally-induced phase separation upon cooling occurs for solutions with 30 wt% epoxy or more while those with a relatively low epoxy content are compatible over the whole PPE-PS composition range. This compatibility is less in comparison to both binary PPE/epoxy and PS/epoxy systems which is reflected by the higher cloud-point temperatures.

Upon curing of PPE-PS/epoxy solutions, phase separation occurs which results in a two phase morphology consisting of dispersed epoxy particles in a PPE-PS matrix.

An extremely fine, sub-micron, morphology can be obtained by controlling the morphology coarsening process after phase separation. For solutions that vitrify upon cooling prior to the occurrence of thermally-induced phase separation, this can be achieved by applying a protocol of curing at the glass transition temperature of the initial solution. In this case, phase separation occurs in a highly viscous medium which restricts the coarsening process and, in the end, results in a sub-micron morphology. This morphology can be sustained during additional post-curing steps, necessary to reach a maximum conversion of the epoxy.

By changing the PPE-PS ratio, the PPE-PS/epoxy system offers the unique possibility to vary the viscosity independently of the curing temperature. Generally, three types of morphologies are identified. If the PS content in the initial solution is high (e.g. PPE-PS/epoxy 10-90/20), a micron-sized morphology is obtained. In contrast, a real sub-micron one is obtained as the PPE content is increased (PPE-PS/epoxy 30-70/20, 50-50/20). This remarkable decrease in the

size of the dispersed phase can only be explained in terms of the increasing viscosity, when the PPE content is raised, restricting the morphology to coarsen after phase separation. As the PPE content is increased even further (PPE-PS/epoxy 70-30/20, 90-10/20), transmission electron microscopy does no longer show any evidence of a second phase and those blends can no longer be dissolved. This either indicates the formation of a semi-interpenetrating polymer network or the occurrence of a (partial) phase inversion.

In conclusion, blending routes which use chemically-induced phase separation of reactive solvents can possibly be applied to produce the required sub-micron rubber morphologies to toughen brittle amorphous polymers.

2.5 References

(1) Venderbosch, R.W. *Ph.D. thesis*, Eindhoven University of Technology, **1995**.

(2) Venderbosch, R.W.; Meijer, H.E.H.; Lemstra, P.J. *Polymer* **1994**, *33*, 20, 4349.

(3) Venderbosch, R.W.; Meijer, H.E.H.; Lemstra, P.J. *Polymer* **1995**, *36*, 6, 1167.

(4) Venderbosch, R.W.; Meijer, H.E.H.; Lemstra, P.J. *Polymer* **1995**, *36*, 15, 2903.

(5) Chean, C.S.; Eamor, M.W. *Polymer* **1995**, *36*, 15, 2883.

(6) Min, B.G.; Hodgkin, J.H.; Stachurski, Z.H. *J. Appl. Polym. Sci.* **1993**, *50*, 1065.

(7) Yamanaka, K.; Inoue, T. *Polymer* **1989**, *30*, 662.

(8) Inoue, T. *Prog. Polym. Sci.* **1995**, *20*, 119.

(9) Brown, J.M.; Srinivasan, S.; Rau, A.; Ward, T.C.; McGrath, J.E.; Loos, A.C.; Hood, D.; Kranbeuhl, D.E. *Polymer* **1996**, *37*, 9, 1691.

(10) Kim, S.C.; Ko, M.B.; Won, H.J. *Polymer* **1995**, *36*, 11, 2189.

(11) Yamanaka, K.; Takagi, Y.; Inoue, T. *Polymer* **1989**, *60*, 1839.

(12) Verchere, D., Pascault, J.P., Sautereau, H., Moschiar, S.M., Riccardi, C.C. and Williams, R.J.J. *J. Appl. Polym. Sci.* **1991**, *42*, 701.

(13) Gallagher, R.K. *J. Chem. Phys.* **1964**, *41*, 3061.

(14) Prest, W.M.; Porter R.S. *J. Polym. Sci. Phys. Ed.* **1972**, *10*, 1639.

(15) Fox, T.G. *Bull. Amer. Phys. Soc.* **1956**, *1*, 123.

(16) Vandeweerdt, P.; Berghmans, H.; Tervoort, Y. *Macromolecules* **1991**, *24*, 3547.

(17) Riccardi, C.C.; Borrajo, J.; Williams, R.J.J.; Girard-Reydet, E.; Sautereau, H.; Pascault J.P. *J. Polym. Sci. Phys. Ed.*, to be published.

(18) Pascault, J.P. *Macromol. Symp.* **1995**, *93*, 43.

(19) Park, J.W. and Kim, S.C. *IPNs around the world*, John Wiley & Sons, Chichester, **1997**, 27.

(20) Klempner, D.; Sperling, L.H.; Utracki, L.A. *Interpenetrating Polymer Networks*, Advanced Chemistry Series, ACS, Washington DC, **1994.**

(21) Girard-Reydet, E.; Riccardi, C.C.; Sautereau, H.; Pascault, J.P. *Macromolecules* **1995**, *28*, 7599.

(22) Kim, S.C.; Sperling, L.H. *IPNs around the world*, John Wiley & Sons, Chichester, **1997**.

Chapter 3

Rubber modification of brittle amorphous polymers using chemically-induced phase separation: Morphology and mechanical properties

3.1 Introduction

The toughness of brittle amorphous polymers can be considerably enhanced by delocalization of deformation which is accompanied by a transition in mode of microscopic deformation from crazing to shear yielding[1-4]. As explained in Chapter 1, this requires the introduction of a sub-micron dispersed phase in the form of rubber particles or voids. In Chapter 2, it has been demonstrated that reactive solvents can be used to prepare blends consisting of sub-micron epoxy spheres in a thermoplastic matrix. The size of the morphology, which is the result of chemically-induced phase separation, was suppressed by controlling the coarsening process via an enhanced system viscosity. The aromatic epoxy resin used in the PPE-PS/epoxy model system results, however, in glassy epoxy particles with a high glass transition temperature which thus cannot be utilised as a toughening agent[5,6]. Therefore in this chapter, an aliphatic epoxy is used as reactive solvent for the brittle amorphous polymers polystyrene and poly(methyl methacrylate). After curing, the aliphatic epoxy resin results in a dispersed thermosetting rubber phase.

An alternative method is investigated for the PMMA/epoxy system based on the simultaneous polymerisation of the thermoplastic glassy matrix and the thermosetting dispersed rubber phase. The polymerisation procedure is rather similar to the classical routes used in the synthesis of interpenetrating polymer networks (IPNs)[7,8].

The ultimate objective of both chemical blending routes is the preparation of rubber modified polystyrene or poly(methyl methacrylate) which possess the required sub-micron or nano-sized morphologies. The influence of these morphologies on the resulting macroscopic mechanical properties are determined, under both tensile and impact conditions.

3.2 Experimental

3.2.1 Materials

Two amorphous polymers were used, polystyrene (PS, SHELL N5000, M_w=260 kg/mol), supplied by BPM (Bredase Polystyreen Maatschappij, Breda, The Netherlands), and poly(methyl methacrylate) (PMMA, Atohaas VO52, M_w=110 kg/mol). The epoxy resin used is a diglycidyl ether of polypropylene oxide (DGEPPO, SHELL Epikote 877) supplied by Chemische Fabriek Zaltbommel (CFZ, Zaltbommel, The Netherlands). The curing agent, Jeffamine D230 supplied by Huntsman (Zaventem, Belgium), is a diamine which is also based on a polypropylene oxide (PPO) backbone.

The free-radical polymerisation of methylmethacrylate (MMA, Aldrich, purified prior to use) was performed over a broad temperature range which requires the application of three initiators with different reactivity: 2,2'-azobis(4-methoxy-2,4-dimethylvaleronitrile) (V-70 initiator supplied by WAKO Chemicals, Neuss, Germany), 2,2-azobis(isobutyronitrile) (Perkadox AIBN, AKZO-NOBEL) and *tert*-butyl-peroxybenzoate (Aldrich). The 10 hour half-life time decomposition temperature in toluene of these initiators increases, respectively, from 30, 64 to 103 °C.

3.2.2 Blend preparation

Blends of PS or PMMA with epoxy resin were prepared by using a Brabender Plasticorder kneader. First two homogeneous solutions of the thermoplastic with, respectively, epoxy resin and curing agent were prepared. Next both solutions were mixed in correct relative amounts to obtain a stoichiometric mixture of epoxy and amine curing agent. The reactive homogeneous solution was prepared at elevated temperatures but the processing time was minimised to prevent premature polymerisation and phase separation. The solutions obtained were subsequently compression-moulded and cured at various temperatures.

Comparable PMMA/epoxy blends were prepared by the simultaneous polymerisation of MMA and epoxy. Homogeneous solutions of MMA, epoxy, curing agent and all three mentioned free-radical initiators were prepared at room temperature for several MMA-epoxy weight ratios. The solutions were poured into cast moulds which were closed after being purged with nitrogen gas for several minutes. The solutions were left at room temperature for 24 hours during which the free-radical MMA polymerisation was initiated by the most reactive initiator, V-70. Accordingly, the moulds were placed in an oven with a programmed temperature profile: 20 hours at, subsequently, 30 °C, 50 °C, 70 °C and 90 °C, followed by two post curing steps at 110 °C for 3 hours and 120 °C for 2 hours. The three free-radical initiators with different half-life time were applied in order to ensure the continuation of the MMA polymerisation over the entire temperature range. After completion of the

polymerisation, the moulds were kept in the oven which was allowed to slowly cool to room temperature.

3.2.3 Analysis

Dynamic mechanical thermal analysis (DMTA) was performed for all blends prepared. A Polymer Laboratories (now: Rheometrics Scientific) Dynamic Mechanical Thermal Analyser MkII was used in the bending mode with a frequency of 1 Hz, a strain of 40 μm and a heating rate of 2 °C/min.

The morphology of the blends was studied using both scanning (SEM, Cambridge Strereoscan 200) and transmission (TEM, Jeol 2000 FX) electron microscopy. The surfaces of the SEM samples were microtomed at liquid nitrogen temperature and, subsequently, etched with oxygen plasma and coated with gold-palladium layer. The TEM coupes were microtomed on a Reichert-Jung Ultracut E ultratome and stained with RuO_4 vapour for 10 min.

Raman measurements were performed to study the kinetics of the MMA polymerisation at 90 °C in the presence of epoxy resin. Spectra were collected using a Dilor XY-800 spectrograph coupled with a liquid nitrogen cooled Princeton CCD array detector. The 488 nm laser line was used to monitor the polymerisation reactions which were performed in sealed glass capillaries heated in a Linkham THMS 600 hot-stage.

3.2.4 Mechanical properties

Tensile tests were performed at room temperature using a Zwick 1445 tensile machine. Dog-bone shaped tensile bars with a gauge length of 38 mm were machined from the polymerised plaques and tested at a strain rate of $1.3*10^{-3}$ s^{-1}. An Instron Extensometer 2630-107 was used to collect accurate displacement data to measure the blend moduli.

Two types of impact tests were performed using test specimens prepared according to the ASTM D-256 protocol. The first test involved the standard Izod impact pendulum test. Alternatively, a fast tensile test (1 m/s) was performed using a Zwick Rel SB 3122 tensile machine. In the latter test, the machined notches were sharpened prior to testing using a fresh razor blade. The impact energy was calculated by integration of the measured force-displacement curve divided by the fracture surface area.

3.3 Results and Discussion

3.3.1 Thermoplastic/epoxy blends

PS/epoxy blends. The chemical blending route involving reactive solvents as presented in Chapter 2, can be applied to prepare rubber modified amorphous polymers. The SEM micrographs of the PS/epoxy blends in Figure 3.1 show that chemically-induced phase separation (CIPS) can be used to produce a dispersed rubber-epoxy phase in a PS matrix. As expected, the particle size decreases with decreasing epoxy content and curing temperature. The effect of curing temperature can be explained by a suppressed coalescence due to the

enhanced viscosity of the initial solution at reduced temperatures, see Chapter 2. The disadvantage of trying to obtain small particles by lowering the curing temperature is the incomplete degree of demixing. In Figure 3.2 the resulting glass transition temperature, T_g, of the PS matrix is plotted as function of the curing temperature. For the 90/10 blend the T_g depression of the solution cured at 60 °C is clearly larger compared to the other blends. The relatively low T_g is attributed to a suppressed phase separation due to the high viscosity during morphology development. However, this T_g depression is not observed for the 70/30 and 50/50 solutions cured at 60 °C. For these blends the morphology is the result of a thermally-induced phase separation process (TIPS) occurring during cooling of the solutions prior to reaching the curing temperature of 60 °C. Apparently, TIPS results in higher T_g's for the PS matrix in comparison to CIPS.
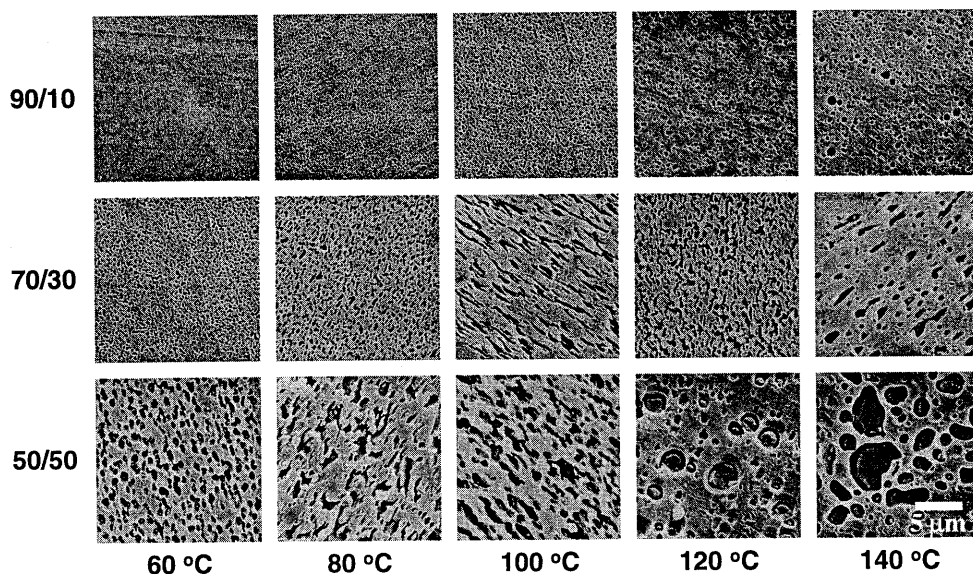
Figure 3.1: *Morphology of PS/epoxy blends for three compositions cured at different temperatures.*

PMMA/epoxy blends. In contrast to PS/epoxy systems, PMMA/epoxy solutions are homogeneous over the whole composition range. Consequently, all the produced morphologies are the result of a chemically-induced phase separation process. Moreover, all solutions can be cured at the T_g of the initial solution which is a requirement to produce the sub-micron or nano-sized morphology, see Chapter 2. In Figure 3.3, the morphologies of PMMA/epoxy 70/30 and 50/50 blends are shown as function of curing temperature. For the 70/30 blend, the viscosity during phase separation appears again to be the morphology determining parameter since the size of the dispersed phase decreases with the curing

temperature. This eventually results in a transparent blend after curing at 60 °C which corresponds to the T_g of the initial homogeneous solution. Despite its transparent appearance, the DMTA measurement in Figure 3.4a clearly proves the existence of a two phase morphology. Apparently the size of the dispersed phase has become too small to induce light scattering[9].
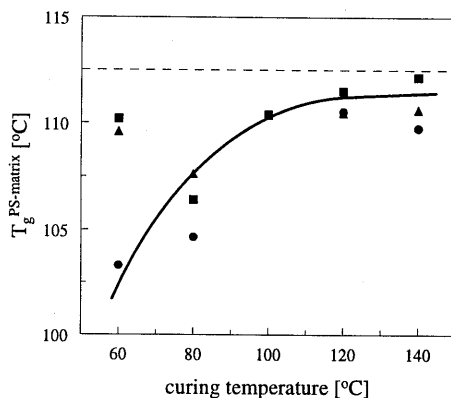
Figure 3.2: *Glass transition temperature of the PS matrix in PS/epoxy blends prepared by chemically-induced phase separation versus the curing temperature; 90/10 (●), 70/30 (▲) and 50/50 (■). The dashed line represents the T_g of neat PS.*
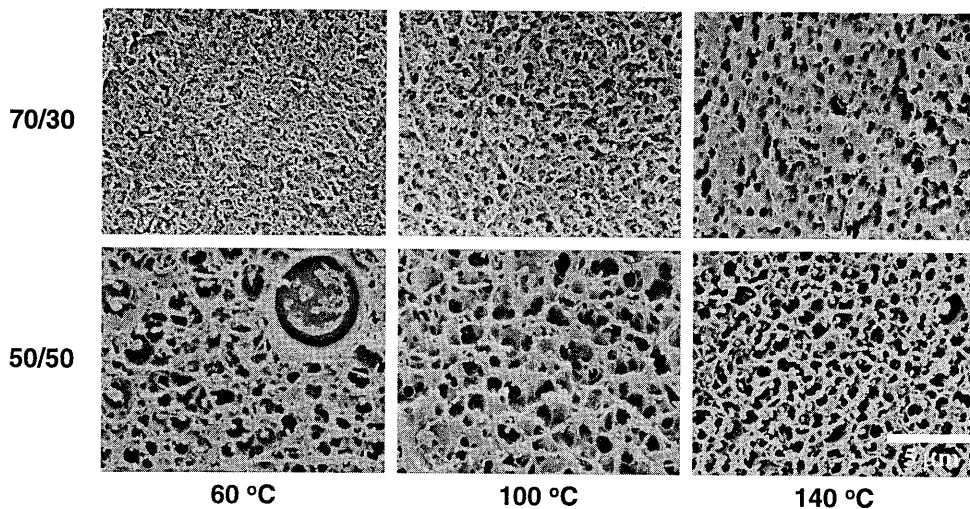
Figure 3.3: *Morphology of several PMMA/epoxy blends prepared by chemically-induced phase separation for a composition of 70/30 and 50/50, cured at 60 °C, 100 °C and 140 °C.*

In contrast to the 70/30 system, the PMMA/epoxy 50/50 system does not coarsen with increasing curing temperature. An explanation can be found in the competition between the time scales involved in accomplishing phase separation and reaction. Considering the low solution viscosity for this composition, the final morphology is mainly determined by the effect of an enhanced reaction rate[10]. After phase separation, the morphology coarsening process due to coalescence is arrested by gelation and/or vitrification of one of the involved phases. Consequently, the particle size decreases as the reaction rate is enhanced by using an elevated curing temperature. Considering this phenomenon, a maximum is expected for the relation between particle size and curing temperature, as schematically depicted in Figure 3.5a. The largest particle size will be found for an intermediate curing temperature for which the coarsening process is not restricted by either an enhanced viscosity or an increased reaction rate. This is confirmed by the PMMA/epoxy 70/30 system which clearly exhibits smaller particles after curing at an elevated temperature of 220 °C, not shown in Figure 3.3.

An incomplete degree of demixing will again be the main drawback of the application of extreme curing conditions, both high and low temperatures. The optimum in the modulus versus curing temperature of a PMMA/epoxy 60/40 blends as shown in Figure 3.5b, can also be explained following this reasoning, since chemically-induced phase separation at intermediate temperatures is not, or less, restricted by a high system viscosity or too high reaction rate. This results in an enhanced phase separation and, consequently, a higher modulus since less plasticising epoxy remains in the PMMA matrix. Incomplete demixing is also observed in the DMTA measurement of a PMMA/epoxy 70/30 solution cured at 220 °C, see Figure 3.4b. The loss angle, tan δ, does no longer show the two distinct peaks for the epoxy and PMMA phase. Both transitions start to overlap and show peak broadening which indicates an increased amount of interphase mixing, i.e. incomplete demixing resulting in a broad interface in which the composition gradual changes from one phases to other[11-13]. For this same reason the dynamic modulus G_d slowly decreases over the broad temperature range between the T_g's of the neat polymers. Reason for the suppressed phase separation may, besides the high reaction rates, also be the possible reaction between PMMA and epoxy resin or curing agent. Both effects will have the same consequences for the resulting modulus and T_g.

For the PMMA/epoxy 70/30 and 50/50 blends prepared via these routes, promising results concerning rubber toughening were obtained. Table 3.1 demonstrates a distinct correlation between the particle size and the resulting strain at break. However, the blend preparation method and, consequently, the mechanical properties suffered from poor reproducibility. This is the result of the processing problems caused by the rather primitive and laborious preparation routes followed and the introduction of the reactive curing agents which are necessary given the extreme curing conditions (i.e. low or high temperatures and a low epoxy

content). Possible solutions to these processing problems can be found in using more advanced continuous mixing techniques as applied in the preparation of very similar fast reacting solutions (polysulphone (PSU)/epoxy) using a multi-step processing route in an optimised corotating twin-screw extruder (ZSK 25)[14]. However, in this project these processing routes were not further explored, since an interesting alternative route proved to be available to procedure similar rubber blends as will be discussed in the following section.
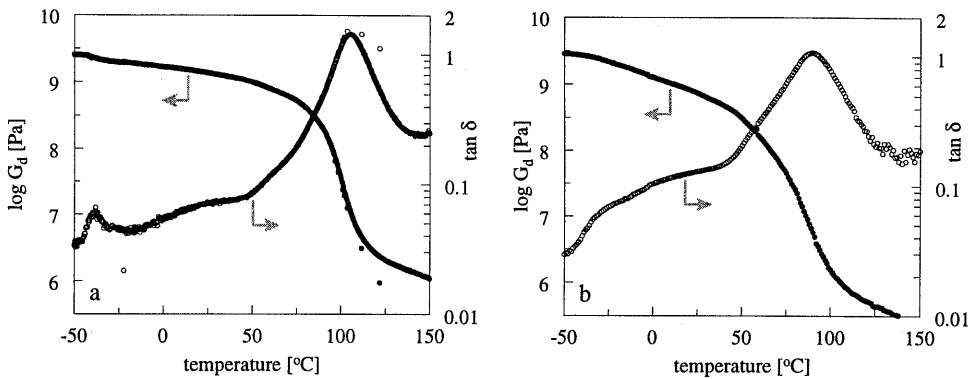

Figure 3.4: *DMTA measurements of transparent PMMA/epoxy 70/30 blends after curing at (a) 60 °C and (b) 220 °C.*
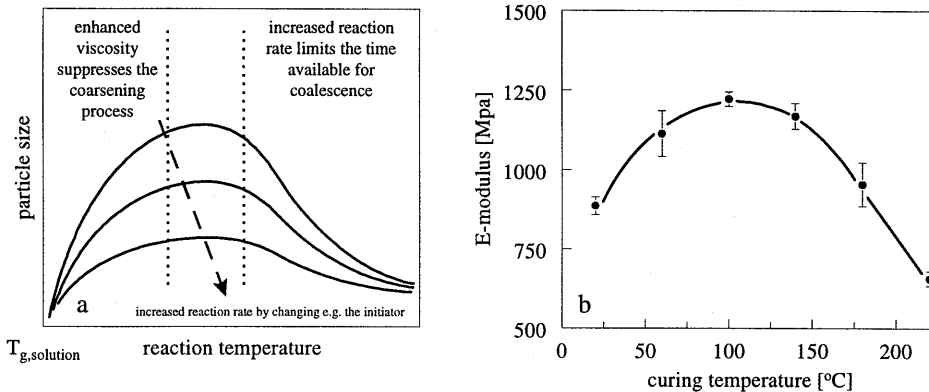

Figure 3.5: *(a) Schematic presentation of the relation between the particles size and the curing temperature. (b) E-modulus as function of the curing temperature for a PMMA/epoxy 60/40 system.*

Table 3.1: *The relation between the estimated particle size, d [μm], and the strain at break, ε_b [%], for several PMMA/epoxy blends cured at different temperatures.*

PMMA/epoxy	90/10		70/30		50/50	
T_{cure} [°C]	d [μm]	ε_b [%]	d [μm]	ε_b [%]	d [μm]	ε_b [%]
60	0*	2.9	~0.05	27.4	2	3.9
100	0*	2.4	0.5	6.5	1.5	8.0
140	0*	2.0	1	2.8	1	48.2

* No separate rubber phase, homogeneous blend

3.3.2 In-situ polymerisation of MMA/epoxy

Polymerisation strategies. To avoid the processing problems described above, an alternative route has been developed to prepare the desired PMMA/epoxy blends with sub-micron or nano-sized morphology. Instead of PMMA, MMA-monomer was used yielding a very low viscous solution consisting of MMA, epoxy resin, curing agent and selected radical initiators. The MMA and epoxy are polymerised in-situ by two non-interfering reactions; a free-radical and a step-growth polymerisation, respectively. This method is similar to the classical routes used in the synthesis of interpenetrating polymer networks (IPNs)[7,8].

Polymerisation of MMA is started at room temperature in order to prepare a highly viscous gel. Formation of the PMMA phase prior to the epoxy phase is beneficial for the development of a continuous PMMA matrix phase. Moreover, the viscosity will be enhanced which can again be used to control the morphology coarsening process. During polymerisation, the conversion of the MMA reaction and, subsequently, the viscosity of the solution is maximised by slowly increasing the reaction temperature. The continuation of the MMA radical polymerisation is accomplished by the application of the different radical initiators. In order to maximise the degree of phase separation and conversion of both polymerisation reactions, the temperature is finally increased up to 120 °C, the T_g of pure PMMA[15].

For a PMMA/epoxy 50/50 blend, the effect of two different polymerisation procedures on the resulting morphology is demonstrated in Figure 3.6. If the polymerisation of the solution is started at 60 °C, the viscosity during phase separation will be low which enhances the coarsening process and thus the final rubber particle size, see Figure 3.6b. This can be avoided by starting the polymerisation at room temperature which decreases the particle size by one order of magnitude, Figure 3.6a. The morphology obtained can be compared to standard IPNs[7,8,16]. The main difference is that for IPNs crosslinking is used to suppress the coarsening process during phase separation, see also Chapter 6. In this study, however, controlling the coarsening process via the viscosity is the preferred route since this results in the aimed thermoplastic PMMA matrix.
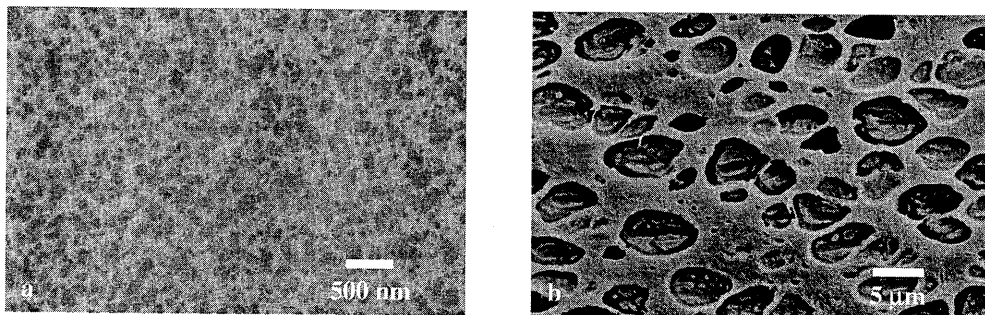
Figure 3.6: *Morphology of in-situ polymerised PMMA/epoxy 50/50 blends, start temperature of polymerisation profile (a) 20 °C (TEM), (b) 60 °C (SEM).*
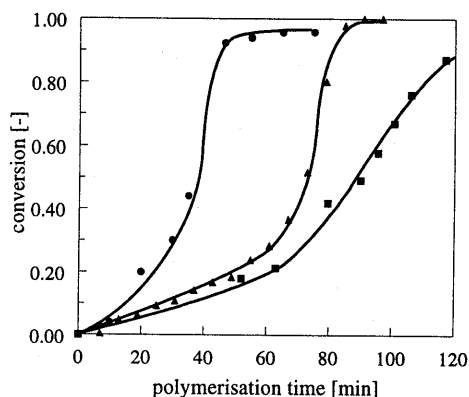
Figure 3.7: *MMA conversion at 90 °C (1 mg AIBN/g MMA) measured by Raman-spectroscopy versus the polymerisation time, using epoxy resin as diluent, 0 (●), 30 (▲) and 50 (■) wt% epoxy.*

A drawback of this morphology control strategy is that it is more difficult for solutions with a higher epoxy concentration as clearly demonstrated by the in-situ Raman conversion-time measurements in Figure 3.7. For pure MMA, a sudden stepwise increase in conversion is observed. This well-known Trommsdorf effect can be explained in terms of the enhanced viscosity during polymerisation since the termination reactions are more hindered by the viscosity increase than the propagation reaction[17]. Due to dilution, the Trommsdorf effect becomes less pronounced with increasing epoxy concentration, see Figure 3.7. For morphology control, especially the viscosity at the start of the chemically-induced phase separation process is of crucial importance. Therefore, it can be concluded that a carefully designed polymerisation schedule becomes more important as the epoxy concentration increases. For a real excess of epoxy resin it can be expected that the viscosity will always be insufficient to restrict the morphology coarsening. In contrast, for low epoxy contents the

resulting morphology will be less dependent on the polymerisation temperature, due to a sufficiently high viscosity caused by the excess of PMMA. Nevertheless, PMMA should always be polymerised first in order to obtain a dispersed epoxy phase.

Morphology. The morphology of the in-situ polymerised blends is studied by solid-state NMR and transmission electron microscopy (TEM). The 50/50 blend has a hazy appearance which is in accordance with the observed particle size of approximately 150 nm (see Figure 3.8d). Blends with a lower amount of epoxy resin are all transparent. In Table 3.2 the morphology sizes as determined via solid state NMR by Mulder et al.[18] are presented. According to these measurements the size of the dispersed phase of PMMA/epoxy 60/40 and 70/30 blend is receptively ~70 and ~30 nm which is in accordance with the TEM micrographs, Figure 3.8b and c. In the case of the 80/20 blend, the second phase is hardly visible which complicates the identification of the dispersed phase. According to the NMR study, phase separation has occurred in this system on a scale of approximately 20 nm. The PMMA/epoxy 90/10 blend is homogeneous and no evidence of phase separation is found using either of the techniques. Dielectric spectroscopy data obtained by Williams et al., however, indicated the presence of a separate epoxy phase for all PMMA/epoxy compositions[19].
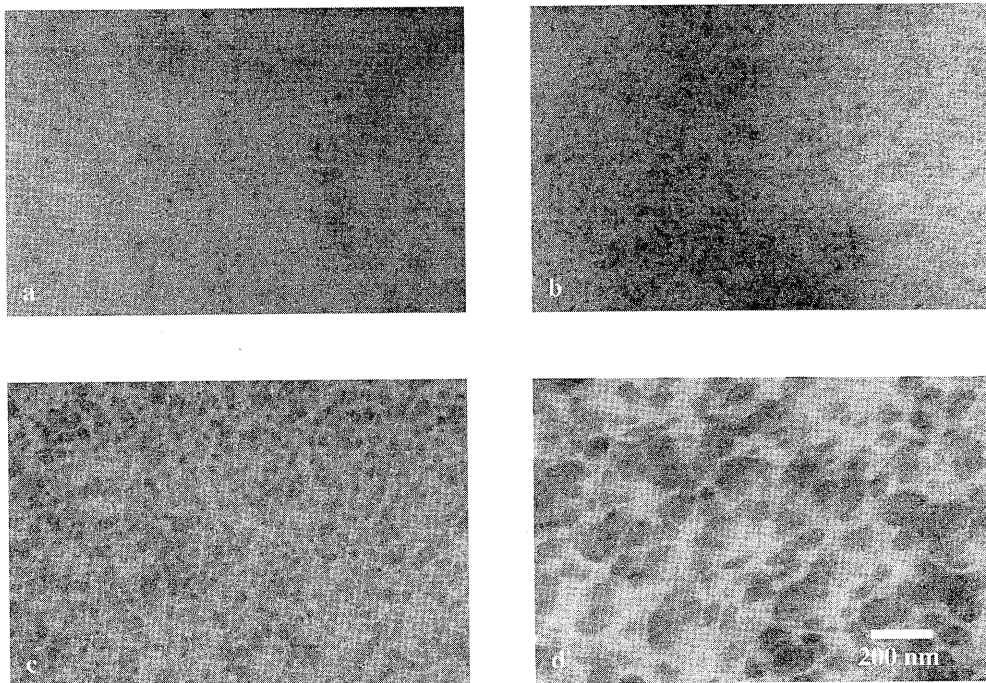
Figure 3.8: *Transmission electron micrographs of the in-situ polymerised PMMA/epoxy blends, (a) 80/20, (b) 70/30, (c) 60/40, (d) 50/50.*

Table 3.2: *Morphology size of the rubbery epoxy phase determined using solid state NMR[18].*

PMMA/epoxy	domain size [nm]
90/10	0 (homogeneous)
80/20	20
70/30	30
60/40	70
50/50	>100
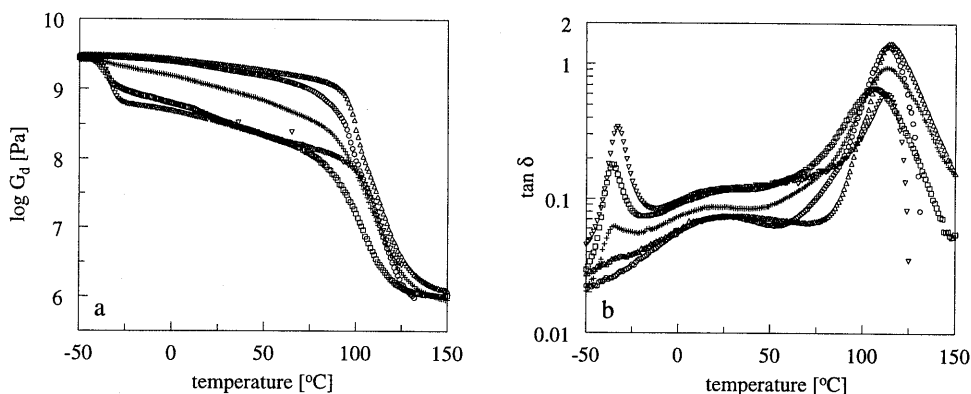
Figure 3.9: *DMTA measurements of in-situ polymerised PMMA/epoxy blends, (a) dynamic modulus (G_d), (b) loss angle (tan δ). ($\triangle$) 100/0, (○) 90/10, (+) 70/30, (□) 50/50, ($\triangledown$) 30/70.*

DMTA measurements. Besides the morphology size, also the composition of both phases will be of importance for the mechanical properties. The degree of demixing can be monitored by the dynamic mechanical behaviour as already discussed above for the two PMMA/epoxy 70/30 blends, see Figure 3.4. In comparison to these results, those of the in-situ polymerised 70/30 blend exhibit an intermediate behaviour, see Figure 3.9. Phase separation has occurred but seems to be partially incomplete as can be concluded from the peak broadening in the loss angle (tan δ), the shoulder-like rubber transition and the smoothly decreasing dynamic modulus (G_d) with increasing temperature. The differences in mechanical behaviour between the blends prepared via both preparation routes can be explained by the miscibility of the monomers and polymers involved. In both cases phase separation will only occur between the polymers, PMMA and cured epoxy, since the monomers are compatible with both polymer networks. Although in case of the in-situ polymerisation of MMA/epoxy the PMMA reaction is preceding the formation of the epoxy phase, the MMA conversion will not be complete until the final polymerisation temperature, notably the T_g of neat PMMA, is reached. As a result there will always be some MMA present at all stages of the polymerisation process.

Therefore, after phase separation, the dispersed cured epoxy phase will be partially swollen with MMA which may be polymerised within this thermosetting network in a later stage. This obviously cannot occur in the case of the PMMA/epoxy system due to the absence of MMA monomer. For this reason, a reduced degree of demixing and an enhanced formation of interphase[20] is observed for the in-situ polymerised MMA/epoxy blends.

Although also for other compositions some interphase mixing is found, demixing is enhanced as the epoxy content increases, see Figure 3.9. For the 50/50 and 30/70 blends clearly two tan δ peaks are observed, indicating the presence of a two phase morphology. The intermediate temperature range again suggests the presence of some interphase mixing. As expected, for the homogeneous 90/10 system only one tan δ peak is found. Compared to neat PMMA, the peak broadens and a slightly decreased modulus is found in the temperature range between the glass transition temperatures of pure epoxy and PMMA.

Tensile testing. The objective of the presented research is to study the relation between sub-micron rubber morphologies in originally brittle amorphous polymers and their mechanical properties. The limited degree of demixing causes, however, a contradiction in the blend preparation. A maximum, or even complete, phase separation is required to perform a unambiguous systematic study of the morphological influences on the final properties. On the other hand phase separation is suppressed since a certain compatibility between both polymers and a proper polymerisation route is required to produce the desired morphologies. Therefore, some care should be taken in the interpretation of the results concerning the mechanical properties.
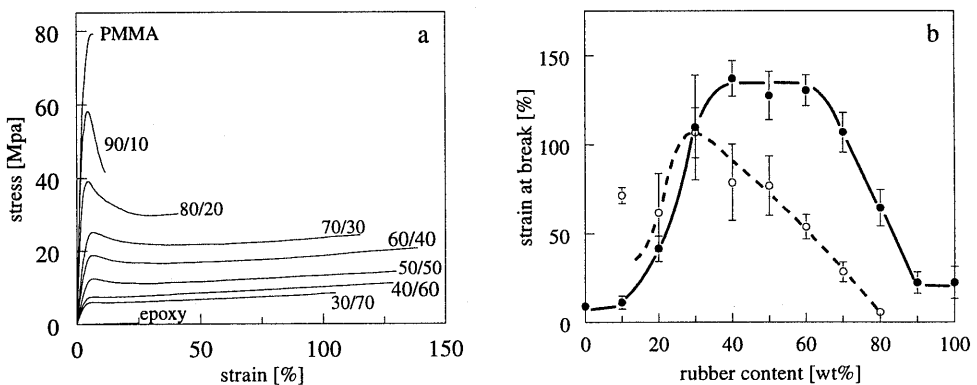

Figure 3.10: *Tensile properties of the in-situ polymerised PMMA/epoxy blends, (a) stress-strain behaviour, (b) macroscopic (●) and local (○) strain at break.*

In Figure 3.10 the tensile behaviour of the in-situ polymerised MMA/epoxy system is presented demonstrating a remarkable synergistic effect for the strain at break. A strain of almost 150 % is reached for the ductile blends of intermediate composition while both neat polymers are rather brittle. Like neat PMMA, the 90/10 blend suffers from brittle fracture upon deformation. For the ductile 80/20 blend stress-whitening is observed accompanied by strain localisation and neck formation. Blends containing 30 wt% up to 70 wt% epoxy resin are ductile and do not show any stress-whitening. Deformation occurs homogeneously without any macroscopic strain localisation. The microscopic deformation mechanisms in these blends have been studied by using in-situ small angle X-ray scattering during tensile deformation. As will be discussed in Chapter 4, very diverse modes of deformation are found for the different PMMA/epoxy blends.

The local strain at break in Figure 3.10b is determined by comparing the cross-sectional area of a test specimen before and after fracture, assuming the absence of dilatation processes, like crazing and rubber cavitation, during deformation. This local strain gives some insight in the amount of plastic deformation and, therefore, of the contribution of the PMMA network to the total macroscopic strain at break. The high strain at break of the blends containing more than 40 wt% epoxy seems to be a result of the enhanced influence of the elastic rubber phase, comparable to some PMMA based IPNs where an enhanced strain at break was attributed to the tendency of the rubber phase to become continuous[21-25]. In case of the PMMA/epoxy systems, however, the PMMA forms the continuous matrix up to a composition of 70 wt% epoxy which emphasis the peculiar behaviour of the 80/20, 70/30 and 60/40 blends. As discussed in the introduction, this can be the result of a decreased ligament thickness which transforms the microscopic mode of deformation from crazing to shear yielding. However, some synergy due to the presence of the rubber phase cannot be ignored since the macroscopic strain at break found for these blends exceeds the maximum drawability of a PMMA network (~75 %)[26]. A second explanation may be found in the incomplete demixing of the PMMA and epoxy phases. The resulting blends appear to possess a broad composition spectrum with intermediate glass transition temperatures, as monitored by the gradual modulus decrease in the DMTA measurements. This may cause strain delocalisation and, subsequently, an improvement of the tensile behaviour on the macroscopic scale[1,4]. However, since the two explanations for the improved mechanical properties do not exclude each other, a combination of both mechanisms is also possible.

Tensile versus impact toughness. Figure 3.11a shows the tensile toughness of the PMMA/epoxy blends which is defined as the absorbed energy till fracture, represented by the area under the stress-strain curve (see Figure 3.10a), divided by the surface fracture area. The maximum tensile toughness is obtained for 30 to 40 wt% epoxy as a result of the combination

of a large strain at break and a relatively high yield stress and modulus. As concluded from the local strain in Figure 3.10a, the influence of the rubber phase becomes more pronounced for blends with more than 40 wt% epoxy. Despite the high strain, the tensile toughness clearly decreases for these blends as a result of the decreasing yield stress and modulus.

Although a similar increase in toughness with rubber content can be expected for the impact tests, the maximum impact toughness is observed at a significantly higher epoxy content, see Figure 3.11b. In contrast to the tensile toughness, all blends with epoxy contents lower than 40 wt% are brittle in impact. Apparently, the difference in local deformation rates is responsible for the differences in mechanical response. This is confirmed by comparing the impact results of the Izod (dashed line in Figure 3.11b) and the notched fast tensile tests. The absolute values are a direct result of the type of test and should, therefore, not be compared. The most important difference is the epoxy content at which the first toughness improvement is observed. For the Izod tests this occurs at a rubber content of 30 wt%, while for the notch tensile tests this value is shifted to 40 wt%. In the latter case the notch was sharpened prior to testing using a razor blade which again suggests an extreme notch sensitivity and/or strain rate dependent toughness.
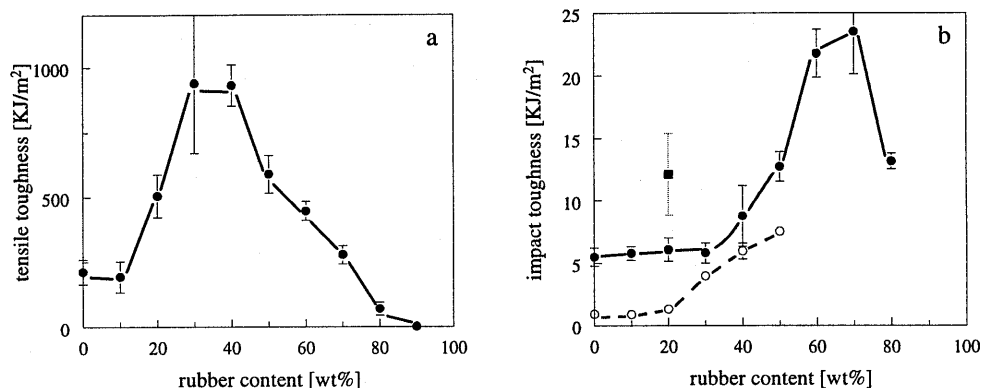
Figure 3.11: *(a) The tensile toughness of the in-situ polymerised PMMA/epoxy blends. (b) The impact toughness of the same blends, (○) Izod test, (●) notched fast tensile test, (■) notched fast tensile test after predeformation in tension.*

For the PMMA/epoxy 80/20 blend, time-resolved small angle X-ray scattering experiments during tensile testing revealed the occurrence of cavitation on a sub-micron level as will be discussed in the subsequent chapters. Cavitation relieves the triaxial stress state which enhances the occurrence of shear yielding and, consequently, results in an improved tensile toughness. At high deformation rates, however, void formation apparently cannot occur and, therefore, results in a brittle failure and a poor impact toughness equal to that of neat PMMA.

In order to support this statement, some samples of the 80/20 blend were predeformed in tensile at a relatively low deformation rate prior to notching and impact testing. This procedure resulted in a doubling of the impact toughness, see Figure 3.11b. During the predeformation, the triaxial stress state is already relieved by the introduction of voids which promotes shear yielding during the impact test and, consequently, increases the toughness. A possible explanation for the absence of the required cavitation during an impact test can be found in the strain rate dependence of the rubber modulus[1,4]. At high deformation rates the modulus of the rubber phase will approach that of a glass which prevents cavitation and the initiation of shear yielding.

3.4 Conclusions

Two different blending routes, using chemically-induced phase separation, were explored to prepare rubber modified PS and PMMA. In both cases, the morphology can be tailored by control over the coarsening process after phase separation via the system viscosity or the reaction rate. As a result, these blending procedures can be used to prepare the sub-micron or nano-sized rubber morphologies that are interesting for the toughening purposes of brittle amorphous polymers.

For the in-situ polymerised MMA/epoxy systems a remarkable synergism in the mechanical behaviour is found, especially for the macroscopic strain at break. The tensile toughness is improved at an epoxy content of 20 wt% which is, however, still higher than the preferred 5-15 wt%. This is most probably the result of the limited degree of demixing at low epoxy contents which, besides the morphology, also influences the mechanical properties as will be discussed in more detail in Chapter 6.

The toughness of the PMMA/epoxy blends demonstrate a strong strain rate dependence. In contrast to the impact toughness, the tensile toughness of the blends with a relatively low epoxy content, is already substantially improved. The poor impact toughness of these blends can, however, easily be enhanced by the introduction of voids via predeformation prior to testing as demonstrated for the 80/20 composition. Cavitation relieves the triaxial stress state which promotes shear yielding and, consequently, leads to an enhanced ductility. Apparently, cavitation is suppressed during impact, possibly as the result of an enhanced rubber modulus at higher deformation rates.

In conclusion the results show that the toughness of brittle amorphous polymers can be improved by the introduction of sub-micron rubber particles. However, the most effective toughening agents should possess a strong tendency for cavitation upon loading.

3.5 References

(1)   Sanden van der, M.C.M. *Ph.D. thesis*, Eindhoven University of Technology, **1993**.

(2)   Sanden van der, M.C.M.; Meijer, H.E.H.; Lemstra, P.J. *Polymer* **1993**, *34*, 10, 2148.

(3)   Smit, R.J.M.; Meijer, H.E.H.; Brekelmans, W.A.M.; Govaert, L.E. *J. Mater. Sci.* **1998**, submitted.

(4)   Smit, R.J.M. *Ph.D. thesis*, Eindhoven University of Technology, **1998**.

(5)   Venderbosch, R.W.; Meijer, H.E.H.; Lemstra, P.J.; *Polymer* **1994**, *33*, 20, 4349.

(6)   Venderbosch, R.W. *Ph.D. thesis*, Eindhoven University of Technology, **1995**.

(7)   Klempner, D.; Sperling, L.H.; Utracki, L.A. *Advanced Chemistry Series*, American Chamical Society: Washington DC, **1994**, *239*.

(8)   Kim, S.C.; Sperling, L.H. *IPNs around the world*; John Wiley & Sons: Chichester, **1997**.

(9)   Conaghan, B.F.; Rosen, S.L. *Polym. Eng. Sci.* **1972**, *12*, 2, 134.

(10)   Yamanaka, K.; Takagi, Y.; Inoue, T. *Polymer* **1989**, *60*, 1839.

(11)   Lipatov, Y.S. In *Advances in Chemistry Series*; Klempner, D., Sperling, L.H., Utracki, L.A.; American Chemical Society: Washington DC, **1994**, *239*, 125.

(12)   Hourston, D.J.; Schäfer, F.U. In *IPNs around the world*; Kim, S.C., Sperling, L.H.; John Wiley & Sons: Chichester, **1997**, 155.

(13)   Akay, M.; Rollins, S.N. *Polymer* **1993**, *34*, 5, 967.

(14)   Nelissen, H.; Pas, R. *European Patent*, EP-A1-0720901, and Kok de, J.M.M. *Internal Report*, Eindhoven University of Technology, **1997**.

(15)   Kim, S.; An, J.H. *J. Appl. Polym. Sci.* **1995**, *58*, 491.

(16)   Chen, Q.; Ge, H.; Chen, D.; He, X.; Yu, X. *J. Appl. Polym. Sci.* **1994**, *54*, 1191.

(17)   Trommsdorff, E. *Makromol. Chem.* **1970**, *1*, 169.

(18)   Mulder, F.M.; Jansen, B.J.P.; Lemstra, P.J.; Meijer, H.E.H.; Groot de, H.J.M. *Phys. Rev. Lett.*, submitted.

(19)   Williams G. et al., in preparation.

(20)   Mishra, V.; Du Prez, F.E.; Goethals, E.J.; Sperling, L.H. *J. Appl. Polym. Sci.* **1995**, *58*, 347

(21)   Akay, M.; Rollins, S.N. *Polymer* **1993**, *34*, 9, 1865

(22)   Akay, M.; Rollins, S.N.; Riordan, E. *Polymer* **1988**, *29*, 37

(23)   Han, X., Chen, B. and Guo, F. In *IPNs around the world*; Kim, S.C., Sperling, L.H.; John Wiley & Sons: Chichester, **1997**, 241.

(24)   Gilmer, T.C.; Hall, P.K.; Ehrenfeld, H.; Wilson, K.; Bivens, T.; Clay, D.; Endreszl C. *J. Polym. Sci., Polym. Phys.* **1996**, *34*, 1025.

(25)   Kojima, T.; Ohnaga, T.; Inoue, T. *Polymer* **1995**, *36*, 11, 2197.

(26)   Kramer, E.J.; Berger, L.L. *Adv. Polym. Sci.* **1990**, *91/92*, 1.

Chapter 4

The mode of microscopic deformation studied by in-situ small angle X-ray scattering during tensile deformation

4.1 Introduction

The previous chapters deal with the development of a new chemical blending route to prepare tough rubber blends based on originally brittle amorphous polymers. In general, an enhanced macroscopic mechanical behaviour is often directly ascribed to a specific rubber morphology on the microscopic level. This relation is, however, rather arbitrary since the attention should be focused on the mode of microscopic deformation. The toughness of high-impact-polystyrene, for example, is the result of the initiation of multiple crazes by the micron-sized rubber morphology[1]. The aim of this research is to accomplish the ultimate toughness which requires a transition in microscopic deformation from crazing to shear yielding. In order to optimise the mechanical performance of rubber modified polymers, it is, therefore, important to obtain additional understanding of those morphological parameters that can influence the type and extent of the microscopic deformation mechanisms. This is not a straightforward issue as has already been demonstrated in Chapter 3 for the tensile behaviour of the PMMA/epoxy blends. Several different modes of microscopic deformation may be responsible for the enhanced ductility of the blends with 20 wt% rubber, and more, as indicated by the optical observations during tensile testing. The PMMA/epoxy 80/20 blend clearly shows stress-whitening and necking while the 70/30 blend remains almost transparent and deforms homogeneously.

At present, synchrotron radiation is more and more used to study microscopic deformation by means of time-resolved small angle X-ray scattering (SAXS) [2-12]. The advantage of using synchrotron radiation is that the development of deformation can be followed during mechanical testing. Moreover, the analysis of SAXS data will yield more quantitative data in comparison to alternative techniques like dilatometry[13] and microscopy[14].

In this chapter the mode of microscopic deformation of the in-situ polymerised PMMA/epoxy blends of Chapter 3 is studied by time-resolved SAXS measurements during slow speed uniaxial tensile deformation.

4.2 Experimental

4.2.1 Materials

The preparation, morphology and properties of the PMMA/epoxy blends used in this studied are discussed in more detail in Chapter 3. All blends are prepared via chemically-induced phase separation during the simultaneous polymerisation of an initially homogeneous solution of methyl methacrylate (MMA) and an aliphatic epoxy resin. By a careful control over the system viscosity during phase separation, sub-micron morphologies were obtained, see Chapters 2 and 3. Here, the following materials were used: PMMA/epoxy blends with 10, 20, 30 and 50 wt% epoxy resin, cast-PMMA which was prepared via the same polymerisation route, and a commercial PMMA grade (Atohaas, VO52) which was used for comparison.

Table 4.1: *Overview of the experimental detail for the beam-lines used in this study.*

	ESRF (Grenoble, France)	CLRC (Daresbury, UK)
Beam-line	ID2-BL4	Station 2.1
Radiation wavelength [Å]	1	1.54
Sample-to-detector distance [m]	8	9
Beam-size [mm²]	0.5 x 0.5	3 x 1
Collection time [sec/frame]	30	20

4.2.2 Techniques

The mode of microscopic deformation of the blends was studied by performing time-resolved small angle X-ray scattering (SAXS) measurement during tensile testing using the synchrotron radiation sources available at the ESRF (European Synchrotron Radiation Facilities, Grenoble, France) and the CLRC (Daresbury Laboratories, Warrington, United Kingdom). The experimental details of the two different beam-lines used are summarised in Table 4.1. In both cases, scattering data were collected

using a gas-filled multiwire two-dimensional (2D) detector. The test samples, as shown in Figure 4.1a, were stretched using a Rheometrics Minimat miniature tensile machine at a strain rate of 0.05 or 0.1 mm/min.

For experiments performed at the CLRC, the beam-stop was positioned out of the centre of the 2D-detector which allowed for the measurement of a larger range of scattering angles. Since the beam was rectangular in shape, the set-up was equipped with a rectangular beam stop. In order to avoid experimental errors in measuring the scattered intensity, parallel and perpendicular to the tensile direction, the Minimat was tilted 45^0 from the vertical direction. In order to convert the data into absolute intensities, the background scattering and the scattering of a reference sample was measured. As a reference sample, polyurethane (PUR) was used with known absorption coefficients. Moreover, the total beam intensity in front of and behind the sample was recorded by ionisation chambers during the complete drawing process, see Figure 4.1b.
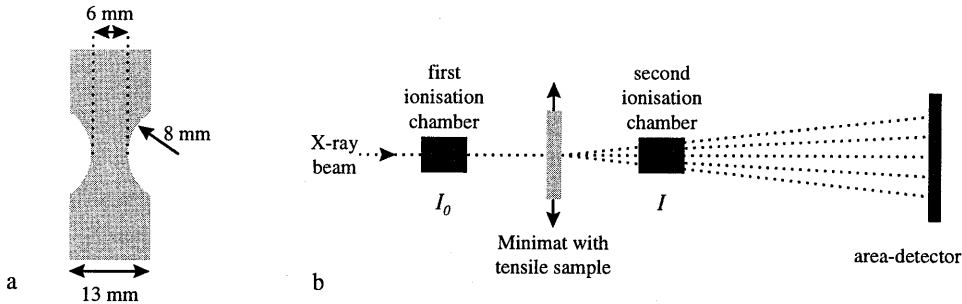
Figure 4.1: *Schematic representation of (a) test bars used in the simultaneous SAXS-tensile experiments (b) the experimental set-up at the CLRC.*

4.3 Analysis

4.3.1 Analysis of scattering data

The 2D X-ray scattering patterns presented in Figure 4.4 are measured using the ESRF facilities. The tensile direction is vertical. From the scattering patterns, three-dimensional azimuthal plots are constructed to visualise the development of orientation and dilatation during tensile deformation. Therefore, the 2D scattering patterns are first divided into 90 cake sections, of 4 degrees each which are, subsequently, integrated to determine the total intensity in each section, see Figure 4.2a. The distribution of the scattered intensity in the different directions relative to the tensile direction can be visualised by plotting the integrated intensity against the azimuthal angle, see Figure 4.2b. Intensities at 90^0 and 270^0 correspond to the tensile direction, whereas those at 180^0 are related to the perpendicular direction. A three-dimensional plot can be constructed by using the deformation time as third axis, as an example see Figure 4.5a.

Figure 4.2: *Schematic representation of data analyses as performed for the ESRF measurements. (a) Division of the 2D scattering patterns in 4^0 sections and (b) the resulting azimuthal plot which describes the relation between the intensity and the azimuthal angle.*

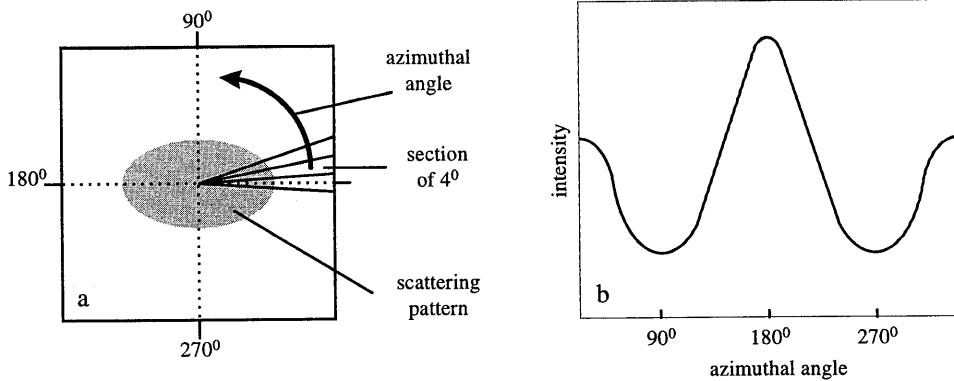The same materials were measured again at the CLRC to confirm the earlier observations at the ESRF, and to collect a complete set of data that can be analysed in terms of absolute intensities. Therefore, the raw data are first normalised by the simultaneously recorded beam intensity of the second ionisation chamber, in order to correct for sample thinning during deformation and the decreasing intensity of the X-ray source. Next, the data are divided by the detector response in order to correct for intrinsic errors in the intensity measurements of the detector used. Finally, the background scattering, which is mainly the result of air, is subtracted. The resulting scattering data are converted to absolute values by multiplying the data by a conversion factor which is derived from the measurements of the PUR reference sample with known absolute intensity[15].

In order to monitor craze formation, cavitation and/or orientation, the intensity distribution parallel and perpendicular to the tensile direction is determined by calculating the invariant, Q, which is defined as:

$$Q = \int s \cdot I(s) \ ds \qquad (4.1)$$

where s is the scattering vector and $I(s)$ the intensity for the oriented samples. The invariant is determined for the two different directions by dividing the patterns in two sections of 90 degrees, parallel, Q_{Π}, and perpendicular, $Q_{\perp}$, to the tensile direction, see Figure 4.3. The invariants calculated are plotted as a function of clamp displacement, see e.g. Figure 4.5b.

In the case of systems which deform via crazing, the craze fibril diameter, D, was calculated using:

$$D = \frac{1}{\pi^3(1-v)} \frac{Q_\perp}{k}$$ (4.2)

where v is the volume fraction fibrils in the craze and $Q_\perp$ is the invariant of the scattering caused by the craze fibrils[16]. The Porod constant, k, was obtained from the Porod analysis by plotting Is^3 versus s^3.
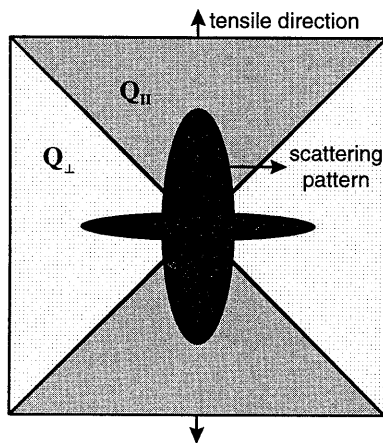
Figure 4.3: *Schematic representation of data analyses as performed for the CLRC measurements. The absolute invariants are calculated separately for both sections of the SAXS pattern, respectively, parallel ($Q_{\parallel}$) and perpendicular ($Q_\perp$) to the tensile direction.*

4.3.2 Analysis of strain data

Considering the adjusted sample geometry and the limited size of the beam, care should be taken in the interpretation of the scattering data in relation to the macroscopic strain or displacement of the stretching device. Therefore, the aim of this study will be to relate the 2D scattering patterns to the actual local strain as viewed by the beam which is calculated by using the intensities measured by the ionisation chambers, see I_0 and I in Figure 4.1b. This will allow for a direct comparison of the local strain data and the X-ray scattering patterns measured.

The strain, ε, of a volume element is defined as:

$$\varepsilon = (\frac{l_t}{l_0} - 1) * 100\%$$ (4.3)

where l_0 and l_t are the lengths of the volume element in the tensile direction at time t=0 (before deformation) and at time t (during deformation), respectively. If introduced voids are excluded, the volume of the deforming material is constant,

$$w_0 \cdot d_0 \cdot l_0 = w_t \cdot d_t \cdot l_t \qquad (4.4)$$

where w and d are the width and thickness of the volume element. By assuming that the contraction in both direction perpendicular to the tensile direction is the same, the local strain equals:

$$\varepsilon_{local} = \left[\left(\frac{d_0}{d_t} \right)^2 - 1 \right] * 100\% \qquad (4.5)$$

In contrast to the length, l, which is drawn out of the beam spot, the thickness, d, can be measured during the complete deformation process. Hence, the local strain can exclusively be calculated from this parameter which can be described by the changes in the absorbed radiation. The absorption equals:

$$I = I_0 \cdot e^{-a \cdot d_t} \qquad (4.6)$$

where a is the adsorption coefficient of the sample which can be determined by using the boundary condition for the thickness prior to deformation, $d_t=d_0$:

$$\frac{I_0}{I} = \frac{(I_0)_{t=0}}{(I)_{t=0}} \qquad (4.7)$$

It can be derived that:

$$\frac{d_0}{d_t} = \frac{\ln(I_0)_{t=0} - \ln(I)_{t=0}}{\ln(I_0) - \ln(I)} \qquad (4.8)$$

Thus, on substituting equation 4.8 in 4.5, the local strain can directly be calculated from the changes in sample thickness during deformation. Note that the occurrence of dilatation processes, like crazing and void formation, are of no relevance since the sample thickness is measured by using the beam intensities, in fact via measuring the absorption directly. Therefore, these calculations can also be used for systems which deform via crazing or rubber cavitation and/or debonding. Hence, the *effective* local thickness, which is obtained via this method, will not necessarily be equal to optical macroscopic sample thickness.

log (intensity)
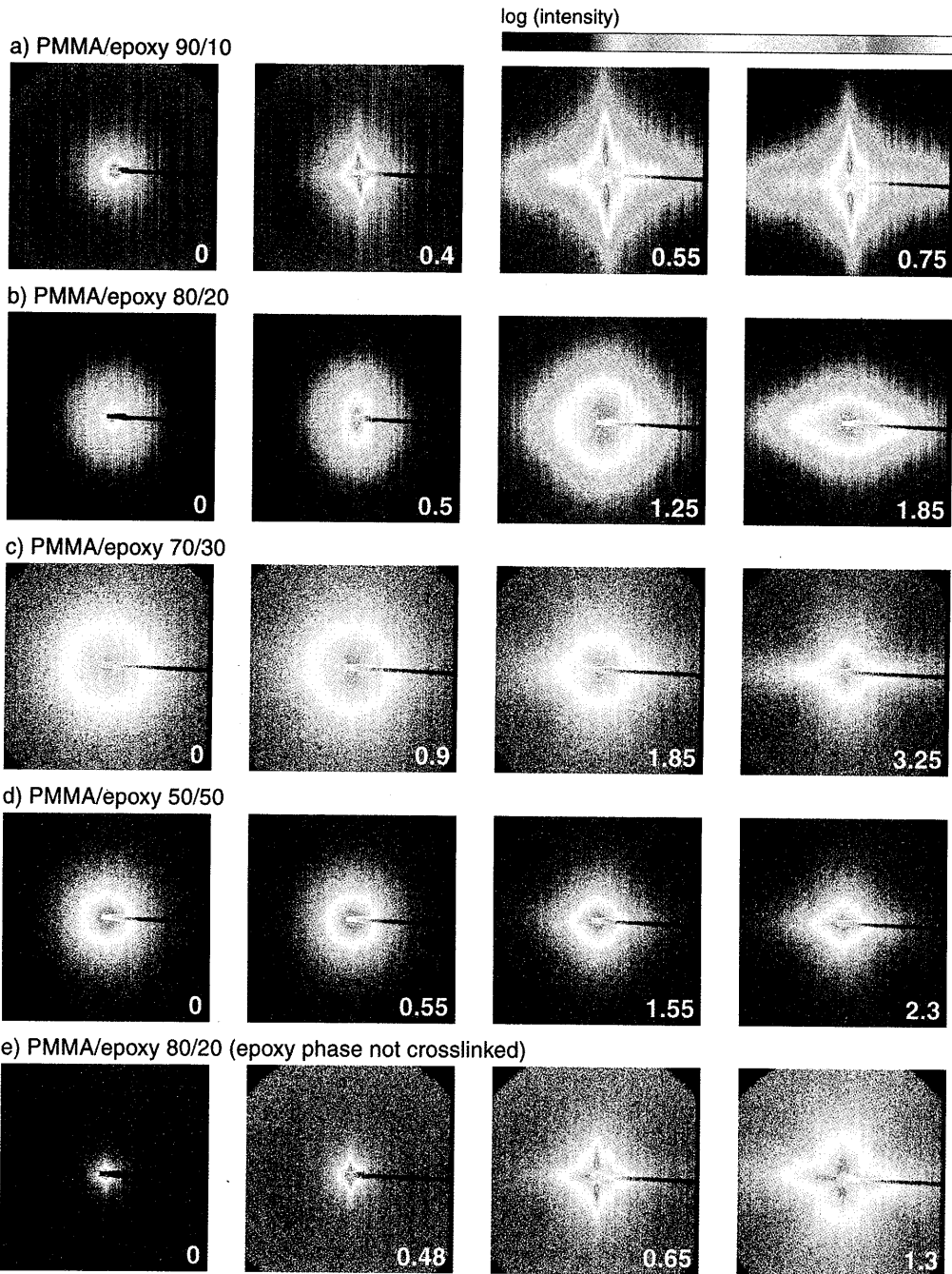
Figure 4.4: *Deformation-SAXS patterns of PMMA/epoxy blends measured at different clamp displacements, x [mm], indicated in the right bottom corner. Experiments performed at the ESRF, ID2-BL4. Tensile direction vertical.*

4.4   Results and Discussion

As discussed in Chapter 3, the PMMA/epoxy blends demonstrate a remarkable synergistic toughness under both tensile and impact conditions. For the blends which contain only 10 wt% rubbery epoxy or less, no separate rubber morphology was found and all samples suffered from brittle failure at limited deformation. The PMMA/epoxy 80/20 blend behaves more ductile upon tensile testing and shows stress-whitening during deformation. In contrast, the blends with 70 - 50 wt% PMMA, which possess the highest tensile toughness, deform via homogeneous contraction over the whole sample without any stress-whitening. As the rubber content is increased even further, the tensile toughness decreases again as a result of the brittle behaviour of the pure epoxy rubber.

Figure 4.5: *SAXS data for the in-situ deformation of PMMA/epoxy 90/10, (a) azimuthal plot (ESRF), (b) absolute invariant perpendicular ($\bullet$) and parallel ($\circ$) to the tensile direction versus the clamp displacement (CLRC), (c) local strain ($\blacksquare$), intensity of the first ($\circ$) and second ($\bullet$) ionisation chamber versus the clamp displacement (CLRC).*

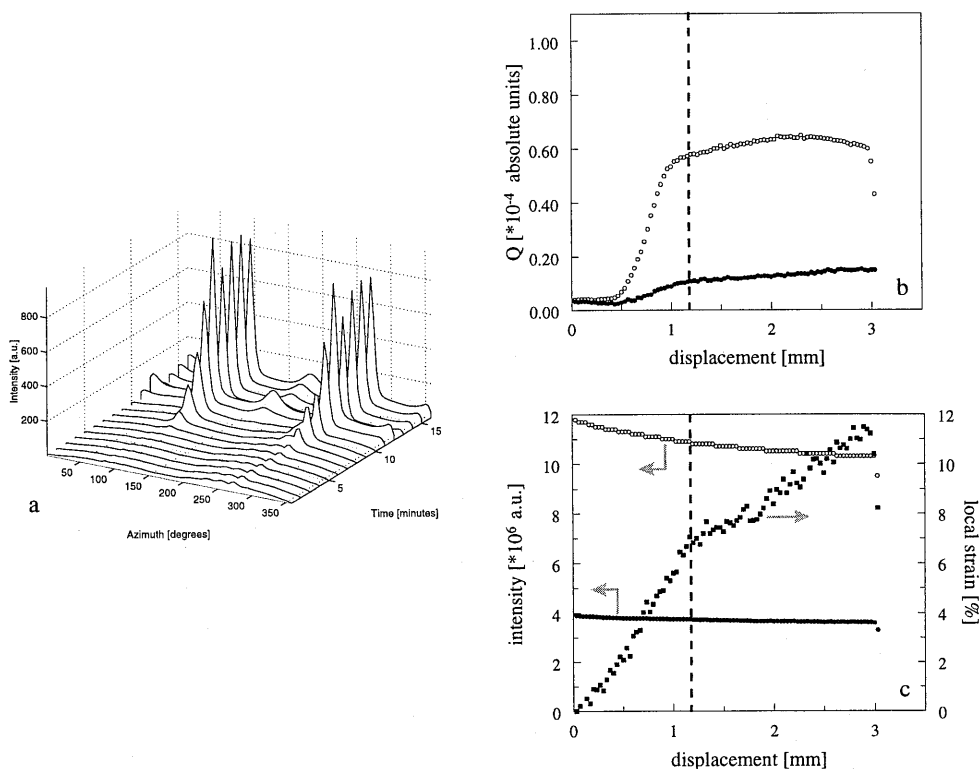Depending on the mode of microscopic deformation, the investigated blends can be divided into three categories, i.e. crazing, cavitation and shear yielding, that will be discussed separately in the following sections. Finally, in an additional section, the influence of crosslinking of the epoxy phase on the microscopic deformation is evaluated.

4.4.1 Microscopic deformation of the brittle systems

Figure 4.4a shows the development of the 2D scattering pattern during tensile deformation of the brittle PMMA/epoxy 90/10 blend. Since this blend is homogeneous, hardly any scattering is observed prior to deformation, displacement x=0 mm. During deformation, intense scattering streaks are developed in the tensile direction, see x=0.4 mm in Figure 4.4a. Upon further drawing, an additional but less intense scattering streak develops perpendicular to the tensile direction, see x=0.55 and x=0.75 mm. As discussed in Chapter 1, the cross-like pattern obtained can be ascribed to the scattering of crazes[16,17]. The intensity of the streak in tensile direction is clearly stronger compared to the scattering resulting from the craze fibrils which is also obvious from the azimuthal plot in Figure 4.5a. The peaks at 90^0 and 270^0, which correspond to the tensile direction, are much more intense compared to the one at 180^0 which results from the craze fibril scattering. Of course, the same trend is observed for the invariants, parallel and perpendicular to the tensile direction, which are plotted as a function of the clamp displacement in Figure 4.5b.

Figure 4.5c shows the relation between the clamp displacement and actual local strain in the beam calculated from the intensities measured by the ionisation chambers using equations 4.5 and 4.8. Initially between 0 - 0.5 mm displacement, the local strain increases with the clamp displacement (Figure 4.5c) without the occurrence of any scattering (Figure 4.5b). The absence of scattering in this region suggests that the local strain measured is the result of sample thinning. The development of scattering beyond a displacement of 0.5 mm, which corresponds to a local strain of ~2.5 %, is associated to the onset of craze formation. The local strain measured during the complete experiment can be divided roughly in two regions with different slopes, see the dashed line in Figure 4.5c. This indicates a difference in local strain rate which appears to be higher for the initial stage. During the deformation at higher strain rate, a strong increase in the invariants is observed between a displacement of 0.5 - 1.2 mm. This can be explained by the nucleation and growth of crazes.

In contrast, in the second region, i.e. between 1.2 and 3.0 mm displacement which corresponds to a lower local strain rate, hardly any changes in the invariants are observed. The constant invariants suggest that the scattering intensity from the crazing process does not vary within the scattering region measured experimentally. This indicates that no new crazes are formed. Nevertheless, the local strain still increases which can simply be explained by sample

thinning and/or by the growth of already formed crazes. However, the scattering from the changes in these crazes cannot be measured within the experimental scattering region.

The difference in local strain rate between the two regions discussed, can be explained by the localisation of deformation in the sample. Apparently, after the crazes are formed within the first region, most of the deformation occurs mainly outside the beam spot which results in a reduced local strain rate for the second region.

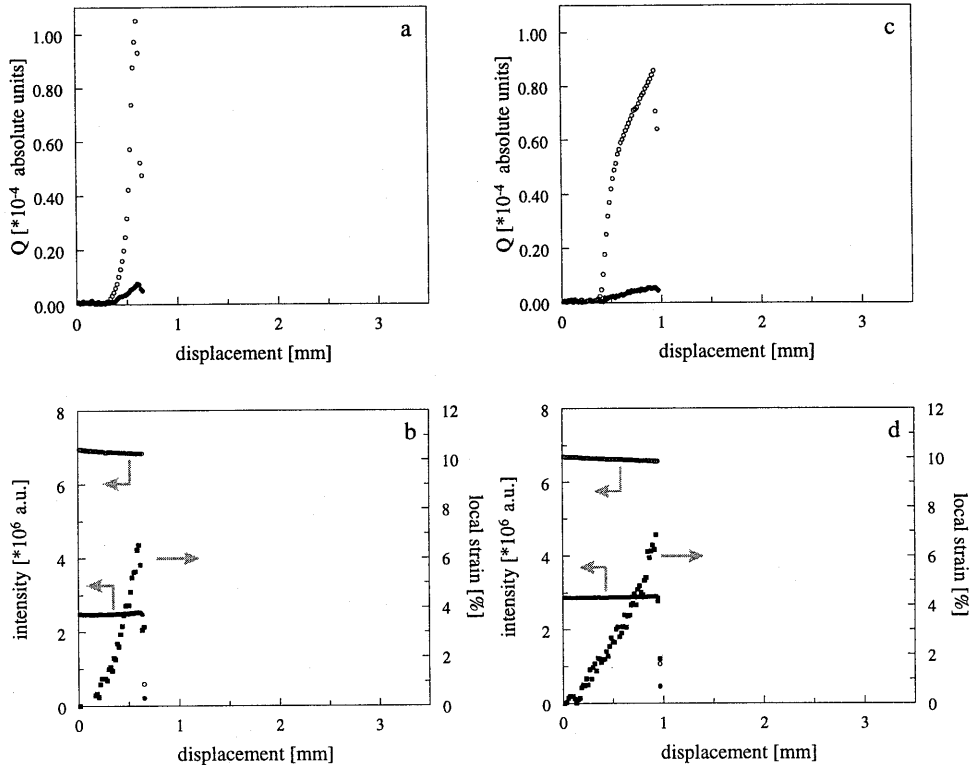**Figure 4.6:** *(a) The absolute invariant perpendicular (●) and parallel (○) to the tensile direction versus the clamp displacement for cast-PMMA (CLRC), (b) local strain (■), intensity of the first (○) and second (●) ionisation chamber versus the clamp displacement for cast-PMMA (CLRC). Comparable graphs for the invariant and local strain data of a PMMA extrusion-grade are respectively shown in (c) and (d).*

For comparison, the invariant and strain data for neat PMMA, both cast and extrusion grade, are depicted in Figure 4.6 with the same values for the displacement axis. The differences in invariants and local strain between the two are limited. Although the displacement might suggest a higher strain for cast-PMMA, the local strain at break is almost the same, compare Figures 4.6b and d. The absolute values of the invariant resulting from the craze fibril scattering are even lower compared to the PMMA/epoxy 90/10 system which indicates a lower craze fibril density, compare Figures 4.5b, 4.6a and c. Although the 90/10 blend is homogeneous and does not possess any craze initiating rubber particles, the tendency for crazing appears to be stronger in comparison to neat PMMA. Moreover, the crazes formed are relatively stable resulting in a higher clamp displacement at fracture. The local strain at break of neat PMMA corresponds with the local strain at the end of region one for the 90/10 blend which is related to the nucleation and growth of crazes. However, in the case of neat PMMA, fracture occurs immediately after the nucleation and growth of the crazes while the stability of the crazes in the 90/10 blend results in a larger deformation volume and, subsequently, in an improvement of the local strain at break from approximately 7 to 12%.

4.4.2 Ductile blends deforming via cavitation

Of all PMMA/epoxy blends, the ductile 80/20 blend is the only one which shows stress whitening during tensile deformation. The mode of microscopic deformation is clearly different from the 90/10 blend as can immediately be concluded from the development of the scattering patterns in Figure 4.4b. Initially, again hardly any morphological scattering is observed. At x=0.5 mm some additional scattering is found in the tensile direction, accompanied by some orientation as can be concluded from the slightly elliptical scattering pattern. At x=1.25, a more symmetric pattern can be observed as the scattering perpendicular to the tensile direction is enhanced. This is, finally, followed by an extensive orientation which results in the strong elliptical scattering pattern as found for x=1.85.

The azimuthal plot for this blend is also very different from those of the brittle crazing systems discussed above, see Figure 4.7a. As observed for the formation of crazes, also in this case some enhanced scattering in the tensile direction is observed. For the 80/20 blend, however, this is followed by a overall increase in intensity indicating the development of electron density fluctuations. The following decrease of the peaks at 90^0 and 270^0, and the subsequent increase at 180^0, indicates the redistribution of the scattered intensity from the parallel to the perpendicular tensile direction as expected from the development of the elliptical scattering pattern. The most plausible explanation in terms of the development of microscopic deformation phenomena for the observed scattering patterns is schematically represented in Figure 4.8. First some crack like voids, or maybe even a limited amount of crazes, are formed causing the additional scattering in tensile direction. Next, the formation of

numerous voids causes the increase in overall intensity. As the voids will relieve the triaxial stress state in the blend, shear yielding is enhanced[18,19] which allows further deformation and, consequently, orientation of the voids in the tensile direction. The changes in the principal axis of the orienting voids results in the development of the ellipsoidal scattering pattern and thus in a redistribution of the intensity.
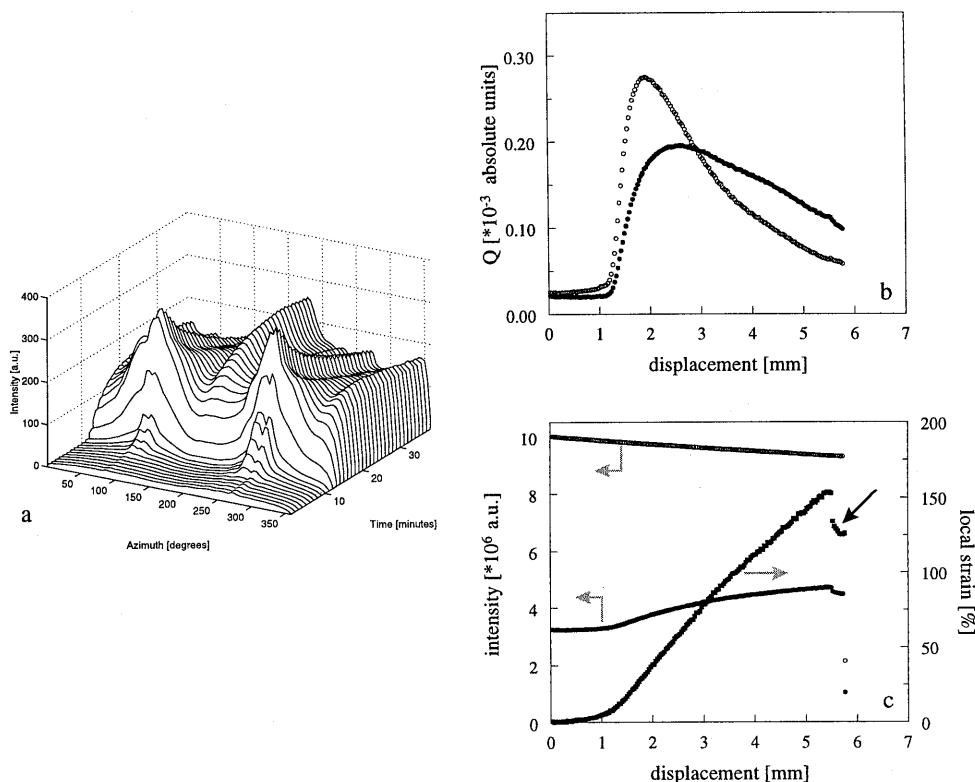
Figure 4.7: *SAXS data for the in-situ deformation of PMMA/epoxy 80/20, (a) azimuthal plot (ESRF), (b) absolute invariant perpendicular (●) and parallel (○) to the tensile direction versus the clamp displacement (CLRC), (c) local strain (■), intensity of the first (○) and second (●) ionisation chamber versus clamp displacement (CLRC).*

Figure 4.7b shows the development and distribution of the absolute invariant values in the directions relative to the tensile direction. The relative difference between the invariants is less compared to the brittle systems which deform via crazing. Both invariants clearly show a maximum which is the result of the decreasing amount of scattering units in the beam as the samples thickness decreases upon further drawing. The decreasing absorption caused by this

thinning process does not contribute to the observed maxima since the scattering data have been normalised to the second ionisation chamber. Still, the ongoing orientation of the voids upon drawing is evident from the crossing over of the invariants.

<div align="center">cavitation   shear yielding   orientation</div>

Figure 4.8: *Schematic representation of the development of cavitation induced shear yielding in PMMA/epoxy 80/20 as derived from the in-situ SAXS-deformation experiments.*
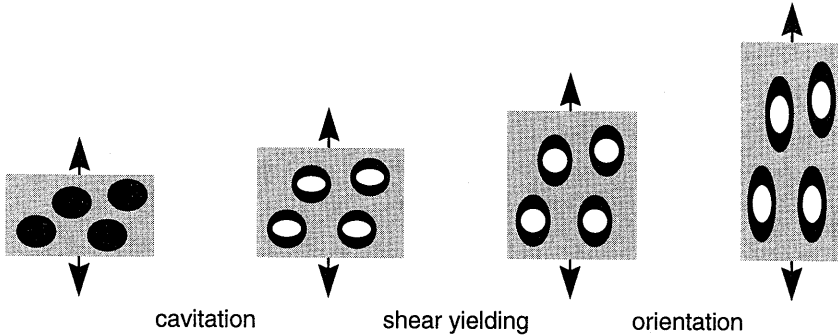
The absolute invariant values are several times larger in comparison to the 90/10 blend which indicates the occurrence of much more dilatation processes during deformation. However, this is accompanied by a much larger local strain of 150%, see Figure 4.7c, which is even higher than the strain calculated from the fracture surfaces in the macroscopic tests, see Figure 3.10b. This difference is a result of the fact that the local strain is calculated via the intrinsic thickness measured by the ionisation chambers which excludes the voids formed during deformation. As can be observed in both Figures 4.7b and c, the deformation in the beam is only initiated after a clamp displacement of 1 mm. The local strain rate beyond a displacement of 1 mm is relatively constant and only slowly decreases towards the end of the experiment. The strength of the proposed local strain calculation method is demonstrated by the last measuring points, indicated by the arrow, which show a sudden drop in the local strain while the values of the invariants are retained. The decrease can be explained by the initiation of a macroscopic crack outside the beam spot which partially relieves the elastic strain and, subsequently, causes thickening of the sample inside the beam. Release of the elastic strain is also the reason for the minor changes observed in the invariant values.

4.4.3 Ductile blends deforming without cavitation

The PMMA/epoxy blends containing 30 to 60 wt% epoxy behave ductile during tensile deformation without any stress whitening. In contrast to the blends discussed above, the scattering patterns of the PMMA/epoxy 70/30 do not show any dramatic changes as a result of the occurrence of dilatation processes, see Figure 4.4c. The changes observed in the scattering

patterns are caused by the orientation of the rubber morphology. As for the previously discussed blends, first (x=0.9 mm) some additional scattering is concentrated in the tensile direction which is followed by the intensity development in the perpendicular direction (x=1.85 mm). Upon further drawing the intensity concentrates parallel and perpendicular to the tensile direction. As confirmed by the azimuthal plot, Figure 4.9a, and the invariants, Figure 4.9b, the overall intensity decreases towards the end of the drawing process. This can again be explained by sample thinning which results in a decreasing amount of scattering units in the beam.
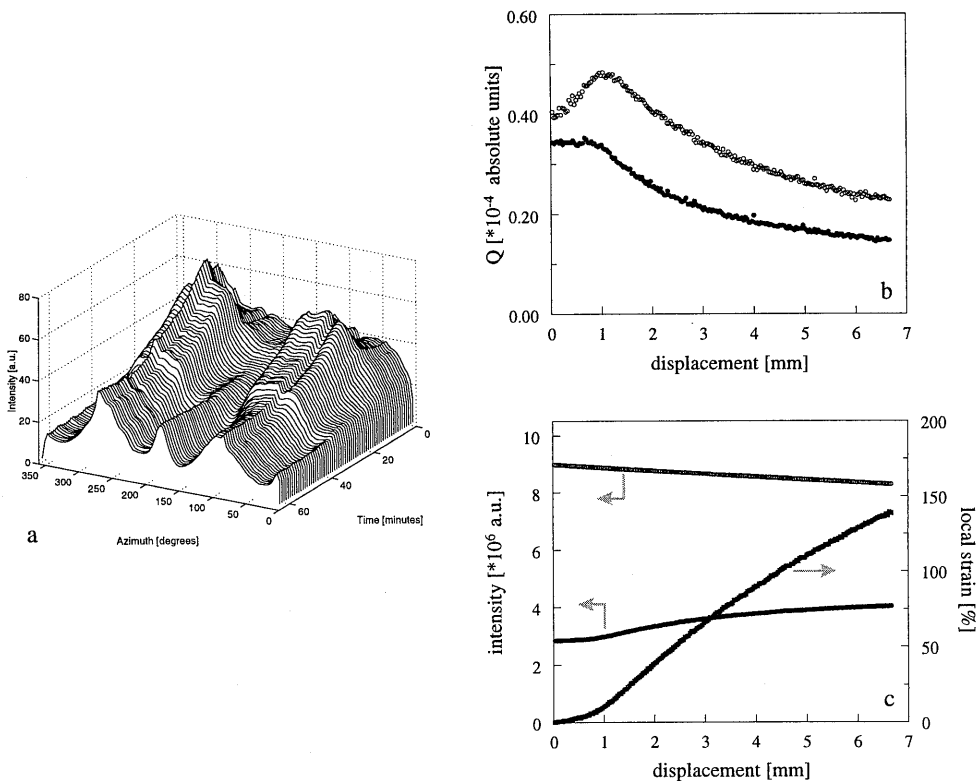

Figure 4.9: *SAXS data for the in-situ deformation of PMMA/epoxy 70/30, (a) azimuthal plot (ESRF), (b) absolute invariant perpendicular (●) and parallel (○) to the tensile direction versus the clamp displacement (CLRC), (c) local strain (■), intensity of the first (○) and second (●) ionisation chamber versus clamp displacement (CLRC).*

Nevertheless, initially at 1 mm displacement, a slight maximum is observed in both the intensity, Figure 4.9a, and invariant in tensile direction, Figure 4.9b, which indicates the occurrence of cavitation during deformation of the 70/30 blend. However, from comparison of the absolute invariant values with those of the 80/20 blend it can be concluded that the amount of cavitation is very limited, compare Figures 4.7b and 4.9b. For PMMA/epoxy blends with an even higher rubber content, cavitation does not occur at all as can be concluded from both the scattering patterns, Figure 4.4d, and the azimuthal plot, Figure 4.10, of the 50/50 blend. Generally, both the 70/30 and the 50/50 blend deform via shear yielding without the necessity of preceding cavitation.

From here it is evident that the scattering patterns observed for these blends should be attributed to the orientation of the rubber morphology. Comparison of the absolute invariants of the PMMA/epoxy 90/10 and 70/30 blends confirms that the scattering is indeed caused by the electron density difference between the PMMA and epoxy phase. The initial invariant values of the 70/30 blend is roughly ten times higher than the 90/10 blend which is considered to be homogeneous and thus does not possess any separate rubber phase at all. Consequently, the limited scattering observed for the blends possessing more than 10 wt% epoxy has to be the result of the electron density difference between the rubber and PMMA phase. Therefore, the changes in the scattering patterns during drawing are the result of morphological orientation.

The local strain plotted in Figure 4.9c is comparable to that of the 80/20 blend, Figure 4.7c. During the first stage of the clamp displacement hardly any plastic deformation is observed. Next, the local strain starts to increase at a strain rate which slowly levels off upon further drawing. Although the drawing process was terminated before fracture had occurred, the maximum strain observed again approached 150% which is in agreement with the values obtained in the macroscopic tensile test, see Chapter 3. In contrast to the 80/20 blend, no sudden changes at the end of the deformation process are observed as result of the premature ending of the test prior to fracture.
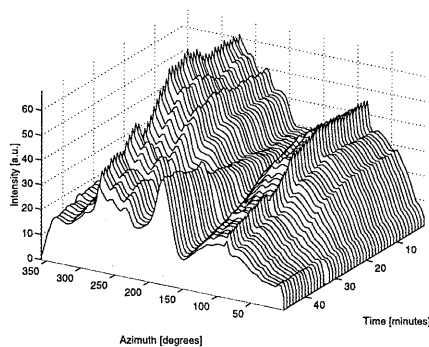

Figure 4.10: *Azimuthal plot for the in-situ deformation of PMMA/epoxy 50/50 (ESRF).*

4.4.4 The influence of the rubber phase

For comparison, the deformation behaviour of a PMMA/epoxy 80/20 blend for which the epoxy is not crosslinked during polymerisation, has been investigated. Instead of using a diamine as curing agent, a similar mono-functional amine (3-isopropoxy propylamine) is used in a stoichiometric amount. Since this results in chain extension, chemically-induced phase separation still occurs during the simultaneous polymerisation of the MMA and epoxy, however, without crosslinking of the epoxy phase.

Figure 4.4e shows the development of the scattering patterns during tensile deformation of this blend. As evident, the mode of microscopic deformation is completely different from the 80/20 blend with a crosslinked epoxy phase, compare Figures 4.4b and e. In Figure 4.4e, first a strong scattering streak is observed in the tensile direction, x=0.48, followed by the development of a second streak perpendicular to the tensile direction, x=0.65. As discussed, the mode of microscopic deformation for these type of typical scattering patterns can be identified as crazing. In spite of the fact that this suggests a brittle macroscopic mechanical behaviour, very stable crazes appear to be formed which allows for the development of an unique craze SAXS pattern, x=1.3. However, the incoming of scattered intensity between the principal axis, may suggest the occurrence of some cavitation during the later stage of the drawing process.

Table 4.2: *The craze fibril diameter of the crazing systems, calculated via the Porod analysis.*

Material	craze fibril diameter [nm]	standard deviation [nm]
PMMA/epoxy 90/10	6.6	0.6
Extrusion PMMA VO52	6.8	0.7
Cast-PMMA	7.6	1.1
PMMA/epoxy 80/20 epoxy phase is NOT crosslinked	5.1	0.08

The remarkable feature observed in Figure 4.11 is the strong intensity of the craze fibril scattering which even approaches that of the streak in the tensile direction. The most probable explanation for this phenomenon is the local plasticising of crazes during deformation[20,21]. This results in the formation of many crazes with a large concentration of extremely stable craze fibrils. As a craze tip proceeds it intersects with the low molecular weight epoxy droplets which plasticise the borders of the craze and, subsequently, enhance its development and stability. According to the few studies reported concerning craze plasticising, the craze fibril diameter is expected to increase in comparison to unplasticised systems. However, the fibril diameter of the crazing systems discussed, PMMA and PMMA/epoxy 90/10, is

approximately 7 nm and appears to decrease to 5 nm for the PMMA/epoxy 80/20 blend with uncrosslinked epoxy, see Table 4.2. The reason for this difference is rather unclear but clearly demonstrates the ability of low molecular weight rubbers or solvents to influence the craze morphology. Additionally, the experiments show that the epoxy phase should be crosslinked to a maximum extent in order to avoid crazing.
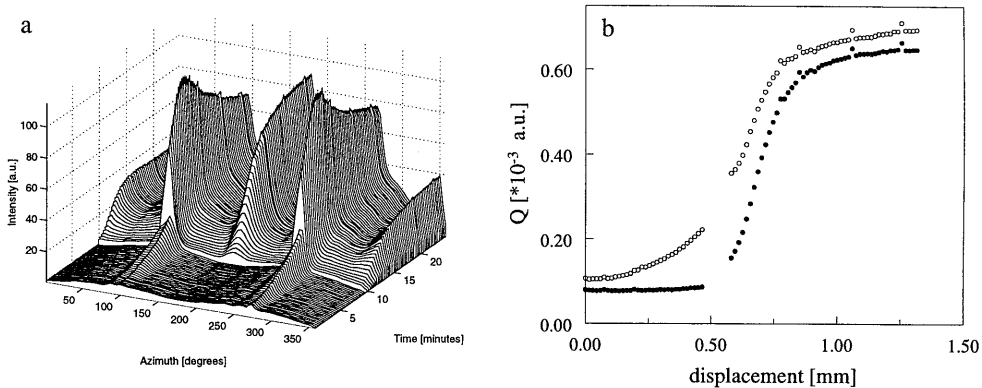

Figure 4.11: *SAXS data for the in-situ deformation of PMMA/epoxy 80/20 for which the epoxy phase is not crosslinked (ESRF), (a) azimuthal plot (b) relative invariant perpendicular (●) and parallel (○) to the tensile direction versus the clamp displacement.*

4.5 Conclusions

The macroscopic synergistic toughening effect observed for the PMMA/epoxy blends is, depending on the rubber content, accompanied by several different types of microscopic deformation mechanisms. The homogeneous and brittle 90/10 blend deforms via the formation of crazes which appear to be much more stable in comparison to those in neat PMMA. Blends with a higher rubber content are macroscopically more ductile and all deform via shear yielding. In case of the 80/20 blend, shear yielding is promoted by the preceding cavitation process which relieves the triaxial stress state and explains the macroscopically observed stress-whitening[18,19]. In contrast, at even higher rubber fractions, cavitation, and the resulting macroscopic stress-whitening, does not occur and shear yielding is the most important deformation process. The scattering patterns observed are mainly the result of morphological orientation caused by the electron density differences between the rubber and PMMA phase.

The importance of a crosslinked epoxy phase is clearly demonstrated by the 80/20 blend for which the epoxy phase has not been crosslinked during polymerisation. The mode of microscopic deformation changes from cavitation induced shear yielding to crazing. The unusual strong fibril scattering observed, compare Figures 4.4e and 4.11, indicates the development of extremely stable craze fibrils which are most probably the result of the local plasticising of craze by the non-crosslinked low molecular weight epoxy rubber.

The proposed calculation of the local strain is successfully used to explain the relation between the scattering patterns and the extent of deformation in the beam spot. The calculated strains are in accordance with the results of the macroscopic mechanical tensile tests. For the 90/10 blend it is revealed that crazing is not initiated for a strain less than 2.5% and that the local strain rate decreases after the initiation and growth of the crazes. The sensitivity of the calculation procedure is demonstrated by the experiment involving the 80/20 blend where sample thickening was detected prior to fracture as a result of macroscopic crack initiation outside the beam spot.

Generally, the simultaneous SAXS-deformation experiments are a powerful method to study the different deformation mechanisms and their development upon drawing. Since the 80/20 blend deforms via cavitation, it offers the possibility to study the influence of sub-micron voids on the mechanical behaviour of brittle amorphous polymers. This will be the subject of the following chapter.

4.6   References

(1)   Bucknall, C.B. *Toughened Plastics*, Applied Science Publishers LTD: London, **1977**.

(2)   Bubeck, R.A.; Buckley, D.J.; Kramer; Brown, H.R. *J. Mater. Sci.* **1991**, *26*, 6249.

(3)   Buckley, D.J., Jr *Ph.D. thesis*, Cornell University, **1993**.

(4)   He, C.; Donald, A.M.; Butler, M.F.; Diat, O. *Polymer* **1998**, *39*, 659.

(5)   He, C.; Donald, A.M.; Butler, M.F. *Macromolecules* **1998**, *31*, 158.

(6)   Lovell, P.A.; Ryan, A.J.; Sherratt, M.N.; Young, R.J. *Polym. Mat. Sc. Eng.* **1994**, *70*, 155.

(7)   Ijichi, Y.; Kojima, T.; Suzuki, Y.; Nishio, T.; Kakugo, M. *Macromolecules* **1993**, *26*, 4, 829.

(8)   Okamoto, Y.; Miyagi, H.; Uno, T.; Amemiya, Y. *Polym. Engin. Sci.* **1993**, *33*, 1608.

(9)   Butler, M.F.; Donald, A.M.; Ryan, A.J. *Polymer* **1997**, *38*, 5521.

(10)   Butler, M.F.; Donald, A.M.; Ryan, A.J. *Polymer* **1997**, *39*, 781.

(11)   Butler, M.F.; Donald, A.M.; Bras W.; Mant, G.R.; Derbyshire, G.E.; Ryan, A.J. *Macromolecules* **1995**, *28*, 6383.

(12)   Hughes, D.J.; Mahendrasinngam, A.; Oatway, W.B.; Heeley, E.L.; Martin, C.; Fuller, W. *Polymer* **1997**, *38*, 6427.

(13)   Sanden van der, M.C.M.; Meijer, H.E.H.; Lemstra, P.J. *Polymer* **1993**, *34*, 10, 2148.

(14)   Plummer, C.J.G.; Béguelin, Ph.; Kausch, H.H. *Polymer* **1996**, *37*, 1, 7.

(15)   Kratky, O.; Pilz, I.; Schmitz, P.J. *J. Coll. Interf. Sc.* **1966**, *21*, 24.

(16)   Paredes, E.; Fischer, E.W. *Macromol. Chem.* **1979**, *180*, 2707.

(17)   Brown, H.R.; Kramer, E.J. *J. Macromol. Sci. - Phys.* **1981**, *B19*, 487.

(18)   Pearson, R.A.; Yee, A.F. *J. Mater. Sci.* **1991**, 26, 3828.

(19)   Bagheri, R.; Pearson, R.A. *Polymer* **1996**, *37*, 20, 4529.

(20)   Gebizlioglu, O.S.; Beckham, H.W.; Argon, A.S.; Cohen, R.E.; Brown, H.R. *Macromolecules* **1990**, 23, 3968.

(21)   Argon, A.S.; Cohen, R.E.; Gebizlioglu, O.S.; Brown, H.R.; Kramer, E.J. *Macromolecules* **1990**, 23, 3975.
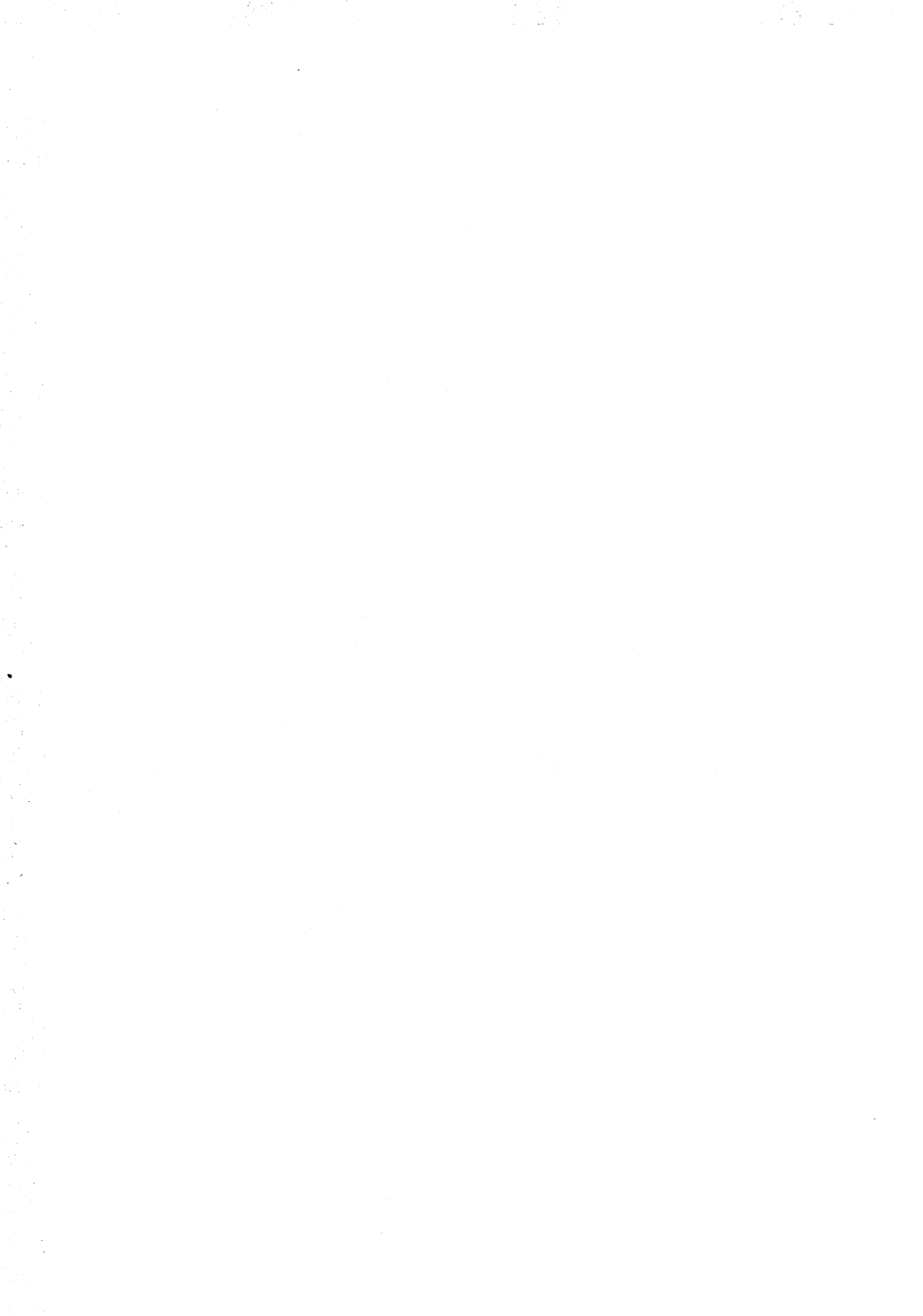
Chapter 5

The influence of strain rate on the microscopic deformation mechanism

5.1 Introduction

The absorption of a sudden impact is often one of the most important material properties and in polymer blends both composition and morphology are designed to achieve a maximum toughness at high deformation rates[1,2]. In order to generate high deformation rates, usually notched samples are used in impact tests. Nevertheless, the accuracy and reproducibility of tensile tests are generally higher and, therefore, often preferred in more fundamental studies. However, due to differences in notch sensitivity, an improved tensile toughness does not always result in an enhanced impact strength. For polycarbonate for example, the Izod impact strength can change by one order of magnitude for test specimens with sharp and blunt notches[3].

A similar effect has been observed in Chapter 3 for the toughness of the PMMA/epoxy blends with the sub-micron morphologies. For slow speed tensile tests, the toughness is already significantly enhanced at a limited epoxy content while the toughness measured under notched impact conditions remains unaffected. SAXS measurements during uniaxial tension revealed that the improved tensile toughness is accompanied by a transition in mode of microscopic deformation from crazing to shear yielding, see Chapter 4.

By using the high intensity of a synchrotron source, time resolved SAXS experiments may be very suitable to study the strain rate dependence of microscopic deformation mechanisms in these blends. Earlier, a few synchrotron-deformation studies have been performed under impact conditions which demonstrated the possibility to follow the development of

microscopic deformation at time resolutions less than one hundredth of a second[4-6]. In this chapter the influence of strain rate on the mode of microscopic deformation in the epoxy-rubber modified PMMA is studied, focusing on the 80/20 blend. As concluded in the former chapter for slow speed tensile tests, this blend deforms via cavitation induced shear yielding. As a result, this particular system can be used to study the influence of sub-micron voids on the mechanical performance of brittle amorphous polymers.

5.2 Experimental

5.2.1 Materials

The PMMA rubber blends were prepared via chemically-induced phase separation during the simultaneous polymerisation of methylmethacrylate (MMA) and an aliphatic epoxy resin (SHELL Epikote 877), see Chapter 3. The size of the dispersed epoxy rubber phase was suppressed by controlling the system viscosity during phase separation, see Chapter 2. In this study one blend composition was considered: PMMA/epoxy 80/20, using the 90/10 composition as a reference.

5.2.2 Techniques

The small angle X-ray (SAXS) experiments were performed at station 2.1 of the synchrotron facility at the CLRC (Daresbury Laboratories, Warrington, United Kingdom). The experimental set-up used has been described in more detail in Chapter 4.

The samples were stretched using a Rheometrics Minimat miniature tensile machine which was tilted 45^0 from the vertical direction in order to avoid experimental errors as result of the rectangular beam spot. The tensile experiments were performed at different deformation rates varying between 0.01 to 25 mm/min using both notched and unnotched samples. Fresh notches were introduced using a scalping knife prior to testing.

The data were converted into absolute intensities in order to allow for a proper comparison of the scattering data collected at different strain rates. Calibration was performed using a polyurethane sample with known absorption coefficients[7]. The total beam intensity in front of and behind the sample was recorded by two ionisation chambers during the complete drawing process.

5.2.3. Data analysis

The way of analysing the scattering and strain data has also been discussed in more detail in Chapter 4. From the scattering data, the invariants parallel, Q_{II}, and perpendicular, $Q_\perp$, to tensile direction are determined in order to visualise the development and extent of orientation during drawing. The absorption data collected by the ionisation chambers are used to calculate the local strain in the beam spot.

5.3 Results and Discussion

5.3.1 Macroscopic properties

The macroscopic properties of the PMMA/epoxy system are summarised in Figure 5.1. The tensile toughness is significantly improved at epoxy contents of 20 wt% and more, and the maximum value is found at 30-40 wt%. In contrast, under notched impact conditions, the toughness remains unimproved up to 30 wt% rubber while the maximum is shifted to a rubber content of 60-70 wt%. The ductility of the PMMA/epoxy 80/20 blend, which showed cavitation during tensile testing, is completely lost at higher deformation rates. In order to explain this in terms of microscopic deformation, in this chapter the strain rate dependence of the cavitation process will be studied. The development of the voids is monitored at different strain rates using both unnotched and notched samples. Notches are applied to increase the local deformation rate.
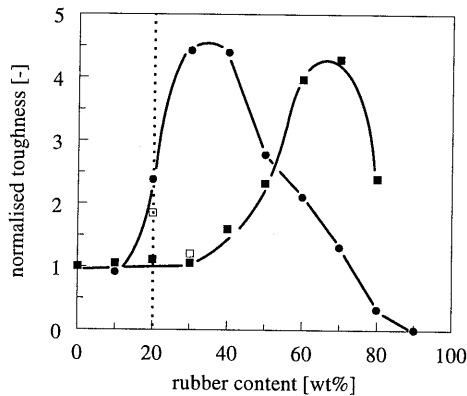
Figure 5.1: *The tensile (●) and impact (■) toughness of the PMMA/epoxy blends normalised to neat PMMA versus the rubber content. Two blends, i.e. 80/20 and 70/30, have been predeformed in tension prior to impact testing (□).*

5.3.2 Unnotched samples

In Figures[i] 5.2a and b the scattering patterns prior to fracture are shown for two unnotched samples, deformed at respectively 0.1 and 25 mm/min. It is evident from these patterns that the deformation for both strain rates is mainly accompanied by cavitation on a microscopic level. The formation of the voids and the development of the resulting scattering patterns have been discussed in the previous chapter. Summarising, cavitation relieves the triaxial stress-state upon drawing which promotes the occurrence of shear yielding. This results in high local

---

[i] SAXS patterns of Figure 5.2 are depicted at page 79.

strains[ii] of more than 150% which leads to orientation of the formed voids in the tensile direction. The observed elliptically shaped scattering patterns are attributed to these highly oriented voids. Apparently, the mode of microscopic deformation does not change with increasing strain rate, in the range investigated. Next, the results at different intermediate strain rates will be discussed in more detail.

0.1 mm/min. As can be observed in Figure 5.3a the invariants in both principal directions show a sudden increase at a displacement of approximately 1 mm. The strong scattering is the result of a sudden enhancement in the electron density difference caused by the onset of void formation. Initially, the scattering in the tensile direction is higher than in the perpendicular direction. This indicates the formation of crack-like shaped voids or the introduction of some crazes which both cause relatively more scattering in the tensile direction[8,9]. The voids thus formed get elongated during further drawing which results into a redistribution of the scattered intensity over both principal directions. Eventually, the perpendicular invariant starts to exceed the parallel invariant at higher draw ratios as expected from the development of the observed elliptical shaped scattering pattern. The overall decrease of the invariants is caused by the decreasing amount of scattering units in the beam due to sample thinning at higher strains.
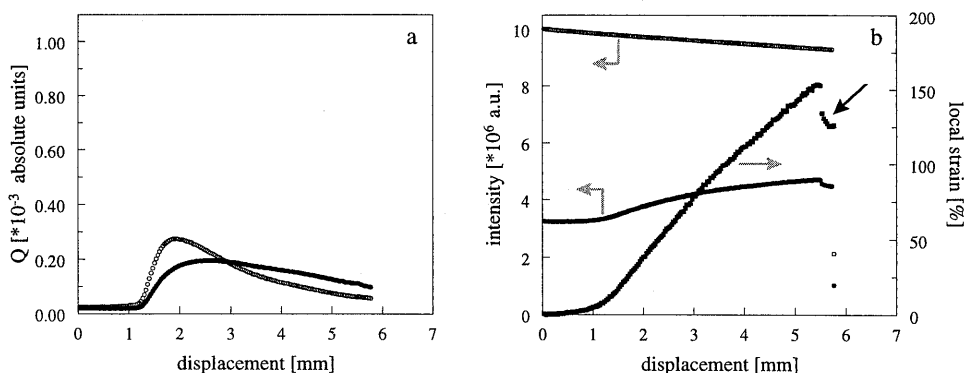
Figure 5.3: *SAXS data for the in-situ deformation of unnotched PMMA/epoxy 80/20 at a displacement rate of 0.1 mm/min, (a) absolute invariant perpendicular (●) and parallel (○) to the tensile direction versus the clamp displacement, (b) local strain (■), intensity of the first (○) and second (●) ionisation chamber versus clamp displacement.*

[ii] The local strain is defined as the strain measured in the local region of the sample exposed by the X-ray beam. For the detailed calculation procedure see Chapter 4.

As expected, the onset of both the local strain and scattering occurs simultaneously and is observed at a displacement of approximately 1 mm, compare Figures 5.3a and b. As a result of the sample geometry, the exact strain rate cannot be controlled but can be estimated from the slope of the local strain versus the clamp displacement which is equivalent to the deformation time. Although the clamp displacement rate is constant (0.1 mm/min), the local strain rate appears to decrease slowly towards the end of the tensile test. The sudden decrease in local strain, indicated by the arrow in Figure 5.3b, is explained by a crack initiation outside the beam spot which allows a partial relieve of the elastic strain. Due to the resulting increase in the sample thickness, local absorption of radiation is enhanced.

1 mm/min. Figure 5.4 shows the results at a displacement rate of 1 mm/min. By increasing the deformation rate by one order of magnitude, a similar development of both invariants is observed, compare Figures 5.3a and 5.4a. Again the introduction of voids causes a sudden increase in scattering intensity. The volume of voids for both strain rates appears to be identical since the value of the invariants is approximately the same. However, increasing the strain rate decreases the relative difference between the invariants for both directions which indicates the formation of more isotropic voids. Less crack-like voids and/or crazes seem to be formed as can be concluded from the relatively decreased amount of scattering in the tensile direction. Due to the void elongation at higher strains, the perpendicular invariant starts again to exceed the parallel invariant.

The local strain is also hardly affected by the increasing strain rate, compare Figures 5.3b and 5.4b. The strain development is similar and at a higher deformation rate the drop in local strain due to crack initiation prior to fracture is again clearly visible, see the arrow in Figure 5.4b. As expected, the slope of the local strain curve is steeper in Figure 5.4b which indicates that the local strain rate increases with the displacement rate of the clamps.
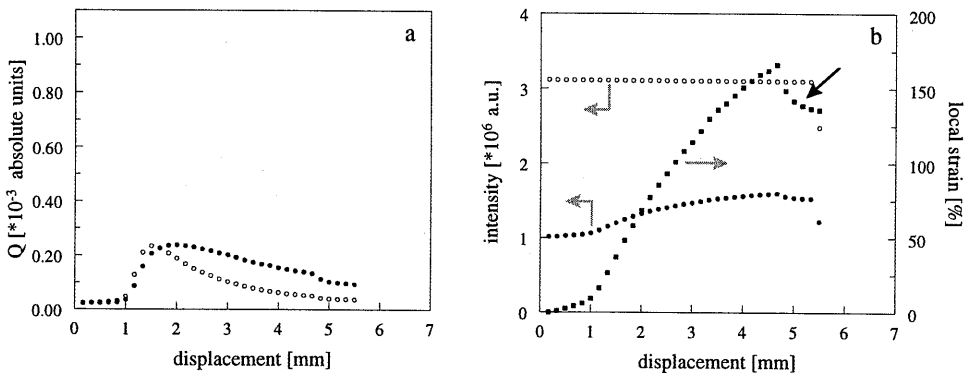

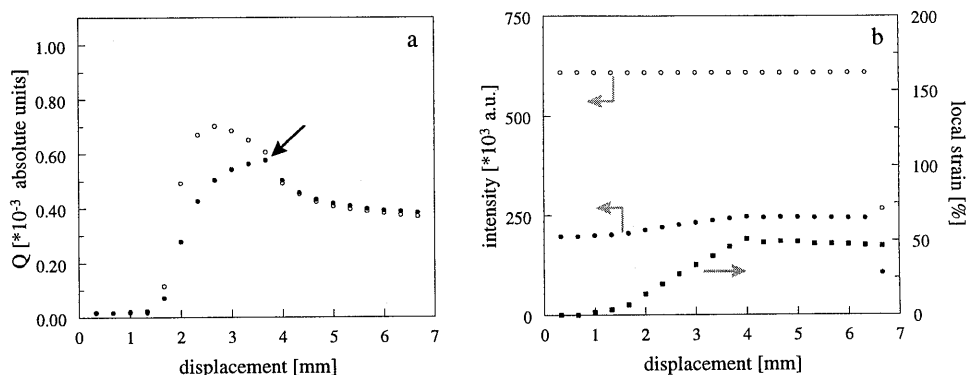**Figure 5.4:** *As Figure 5.3, for a displacement rate of 1 mm/min.*

Figure 5.5: *As Figure 5.3, for a displacement rate of 10 mm/min.*

10 mm/min. By increasing the deformation rate to 10 mm/min, the quantitative values of the invariants increase by a factor of three, compare Figures 5.4a and 5.5a. This suggests an increasing amount of voids and/or void volume. The initial difference between the invariants for both principal directions suddenly disappears at a displacement of almost 4 mm. The value of the invarants become equal as a result of an abrupt change in the perpendicular invariant as indicated by the arrow in Figure 5.5a.

Unlike the measurements at lower deformation rates, Figures 5.3b and 5.4b, here the local strain shows a sudden change at a displacement of 4 mm and becomes constant for the remaining deformation, Figure 5.5b. Moreover, for this particular experiment the increase in deformation rate to 10 mm/min does not result in the expected enhancement of the local strain rate, as can be concluded from the limited slope of the curve, compare Figures 5.3b, 5.4b and 5.5b. In conclusion, the data collected at this strain rate should be carefully interpreted since the invariant and local strain data suggest a rather inhomogeneous deformation behaviour of the material in the beam spot.

25 mm/min. Unlike the experiments performed at a displacement rate of 10 mm/min, Figure 5.6 suggests a homogeneous local deformation at 25 mm/min. Figure 5.6a shows a very strong and abrupt increase of the invariants at a displacement of 2 mm. The reason is most likely again the occurrence of cavitation which introduces a large difference in electron density. The amount of cavitation clearly increases with increasing strain rate as can be concluded from the comparison of the absolute invariants with those of the experiments discussed above. The maxima in the invariants are again the result of sample thinning. From a displacement of 5 mm onward, both invariants become equal as result of a similar electron density fluctuation along the principal directions. This indicates that on average the voids are less oriented along the tensile direction, in contrast to the observations at lower deformation rates, see for an

example Figure 5.3a. This is confirmed by the decrease in the aspect ratio of the elliptical shaped scattering pattern at higher deformation rates, compare Figures 5.2a and b.

The development in local strain in Figure 5.6b occurs in the same displacement regime as the observed changes in scattering intensity, compare Figures 5.6a and b. The maximum slope of the curve is relatively steep which is evidence for a high local strain rate. Moreover, the strain at break is extremely high, more than 200%, and exceeds that of the tests performed at lower strain rates. In contrast to the lower deformation rates, no fracture is detected within the same displacement region. Moreover, beyond 5 mm no increase in local strain is observed, indicating that the deformation occurs outside the region exposed by the incident X-ray beam.

From the development in invariants and local strain measured at different deformation rates, a few general conclusions can be drawn. The absolute values of the invariants suggest that cavitation is enhanced at higher strain rates. At limited rates, deformation starts with cavitation which is followed by a strong orientation in the tensile direction of the voids formed. This explains the development of the elliptical scattering pattern and the resulting differences in scattering intensity between both directions. In contrast, higher rates seem to promote the nucleation of additional voids instead of the orientation of voids which are formed during the early stage of the cavitation process. This is concluded from the fact that the absolute values of the invariants are enhanced with increasing strain rates while the difference between both principal scattering directions are suppressed.
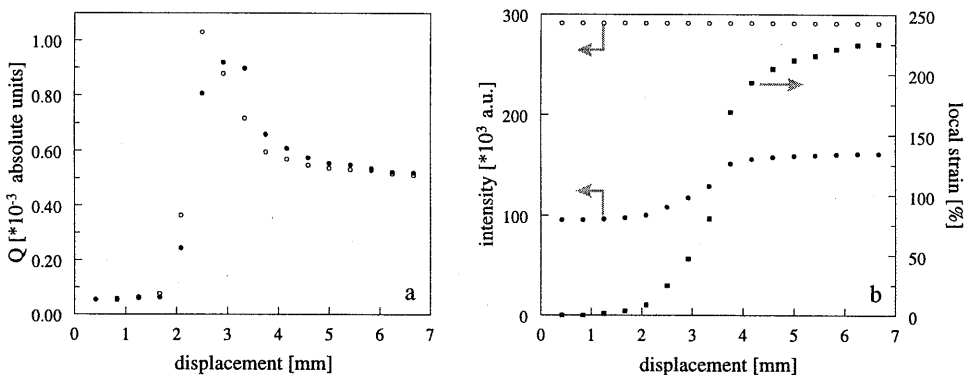
Figure 5.6: *As Figure 5.3, for a displacement rate of 25 mm/min.*

5.3.3 Notched samples

For the experiments discussed above, no transition in mode of microscopic deformation is observed at higher strain rates. Nevertheless, the macroscopic mechanical behaviour of the PMMA/epoxy 80/20 blend changes to brittle for impact conditions. Since 25 mm/min is the maximum displacement rate of the stretching device used, notches are introduced in the test

samples. They will generate an additional increase in the local deformation rate behind the notch.

PMMA/epoxy 80/20. Figures 5.2c and d show the scattering patterns of the deformed zone behind the notch in the PMMA/epoxy 80/20 blend. A displacement rate of 0.01 mm/min (Figure 5.2c) does not result in a transition in deformation behaviour in comparison to the unnotched samples. The strong scattering pattern is again caused by the formation of voids. However, the aspect ratio of elliptical shape is decreased which suggests a limited elongation of these voids upon further drawing. Moreover, the combination of the elliptical SAXS pattern and the enhanced scattering in the tensile direction should be the result of inhomogeneous deformation in the region exposed by beam spot. This is not surprising considering the limited size of the deformation zone behind a notch and the experimental set-up, i.e. the orientation of the beam relative to the sample coordinates. As a result of the inhomogeneous deformation, the invariant in the tensile direction in Figure 5.7a remains higher than the perpendicular invariant during the complete drawing process. The maximum observed is again caused by sample thinning due to shear yielding which is promoted by the introduction of the voids. In spite of the differences observed, the mode of microscopic deformation in a notched sample at limited strain rate is identical to that in a unaxial tensile test without notch, i.e. cavitation induced shear yielding.
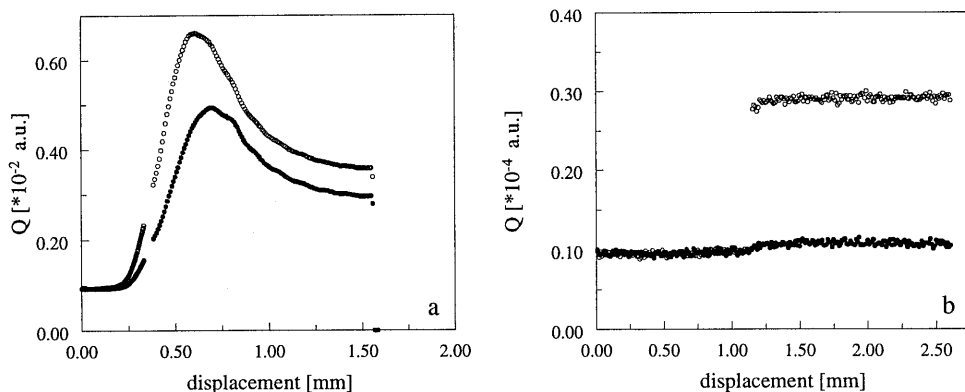
Figure 5.7:   *Invariant perpendicular (●) and parallel (○) to the tensile direction versus the clamp displacement for the in-situ deformation of a notched PMMA/epoxy 80/20 blend at a displacement rate of (a) 0.01 mm/min and (b) 25 mm/min.*

Increasing the displacement rate to 25 mm/min in notched samples causes a dramatic change in scattering pattern, see Figure 5.2d. The void scattering is replaced by only one single but strong streak in the tensile direction, without the occurrence of any scattering in the

perpendicular direction. Moreover, the corresponding perpendicular invariant in Figure 5.7b remains constant in the course of time during the complete deformation process. The scattering of the streak gives rise to a sudden stepwise increase for the invariant in the tensile direction. However, a measuring resolution of 25 ms appears to be insufficient to collect data points during its development. The most plausible explanation for the observed streak is the introduction of crazes as the electron density difference between the craze-bulk and polymer matrix is known to give rise to a very strong scattering in the tensile direction[8,9]. However, in contrast to these results, the scattering of craze fibrils in the perpendicular direction is usually also observed and can be used to determine the total amount of strain related to the crazing process[4,5]. The absence of this scattering suggests the formation of only a small amount of craze volume and/or crazes with a limited fibril content as result of the elevated local strain rate.

PMMA/epoxy 90/10. The occurrence of crazing and the resulting scattering pattern for the PMMA/epoxy 80/20 blend is verified by applying the same test conditions for a 90/10 blend. This blend is brittle and exhibits crazing even at limited strain rates without notching, see Chapter 4. The craze scattering patterns during slow speed tensile testing include the expected fibril scattering in the perpendicular direction which was used to calculate the craze-fibril diameter. More extreme testing conditions result again in only a single scattering streak in the tensile direction as was observed for the PMMA/epoxy 80/20 blend, see Figures 5.2d and e. Consequently, the mode of deformation does not appear to change for the 90/10 blend with increasing the strain rate since the scattering patterns observed at both slow and high speed testing are attributed to crazing. However, the type, size and/or amount of the crazes involved appears to be influenced by the strain rate considering the differences in the craze scattering patterns. Since for the PMMA/epoxy 90/10 blend crazing is expected, the similarity between the scattering patterns of the 90/10 and 80/20 blend further confirms the occurrence of crazing for the latter blend at higher strain rates. Consequently, it can be concluded that the mode of microscopic deformation for the PMMA/epoxy 80/20 blend transforms from cavitation induced shear yielding to crazing by shifting the testing condition from tensile to impact.

5.3.4 Macroscopic versus microscopic deformation

As discussed, the maximum macroscopic toughness of the PMMA/epoxy blends shifts to higher epoxy concentrations by changing the test conditions from tensile to impact. For the PMMA/epoxy 80/20 blend the impact toughness is equal to that of neat PMMA while the tensile toughness is significantly improved. The in-situ SAXS-deformation experiments demonstrate that this is accompanied by a transition in mode of microscopic deformation. In Figure 5.8 the macroscopic performance and the relating microscopic deformation of the

PMMA/epoxy 80/20 blend are summarised. During slow speed tensile testing, cavitation will relieve the triaxial stress state which, subsequently, promotes shear yielding upon further drawing[10,11]. This will enhance the ductility of the blend and thus its tensile toughness, see Figure 5.8a. Since cavitation apparently cannot, or hardly, occur during impact deformation, crazing rather than shear yielding occurs which causes a brittle behaviour and, therefore, a limited impact toughness, see Figure 5.8b. However, the influence of void formation on the impact behaviour can easily be studied by a combination of tensile and impact testing. First, dumbbell shaped samples are predeformed at a limited strain rate in order to induce cavitation in the stress concentration zone, see Figure 5.8c. During the predeformation process, the yield stress is first passed and, subsequently, followed by an additional deformation of a few percent. Next, the samples are shaped into Izod impact bars for which the notch is machined in the precavitated zone. The impact toughness of the PMMA/epoxy 80/20 blends increases substantially by following this precavitation procedure, see the open square in Figure 5.1. In conclusion, cavitation promotes shear yielding also under impact conditions and thus improves the impact strength. This is confirmed by similar predeformation experiments for the PMMA/epoxy 70/30 blend. As expected, the impact toughness is hardly improved since cavitation does not occur during predeformation of this blend, see Chapter 4. The limited toughness enhancement observed in Figure 5.1 is most probably the result of orientation.
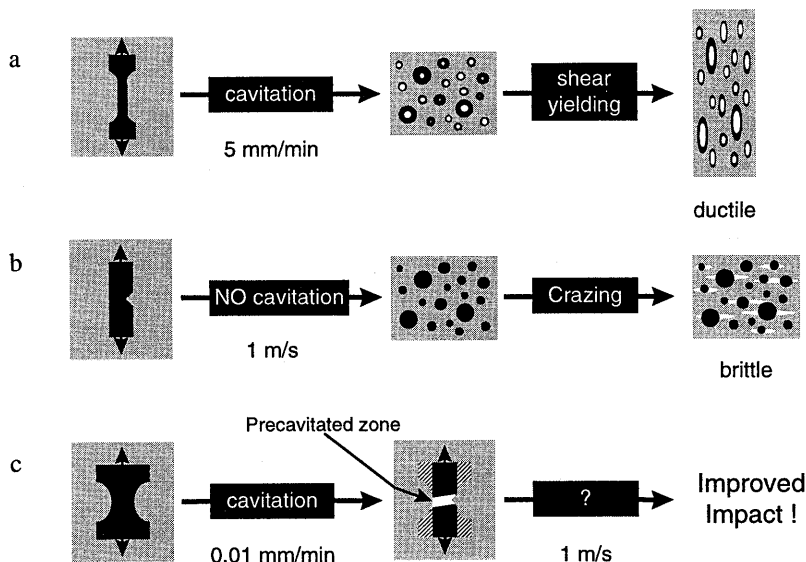

Figure 5.8: *Schematic representation of the relation between the mechanical test, the mode of microscopic deformation determined via the in-situ SAXS measurements and the macroscopic toughness of the PMMA/epoxy 80/20 blend, (a) tensile, (b) impact deformation and (c) a combined test in which a sample is predeformed in tensile prior to impact testing.*

The resistance against cavitation is known to increase with decreasing particle size[12-14]. Hence, this is expected to be of importance especially in case of the sub-micron to nano-sized morphologies of the PMMA/epoxy 80/20 blend. However, this does not explain the apparent strain rate dependence of the cavitation process. An alternative reason can be found in the strain rate dependence of the rubber modulus[12,15,16]. At very high rates the modulus of the dispersed rubber phase may approach that of a glass which will promote its resistance against cavitation[15]. As a result, cavitation and thus shear yielding is suppressed during impact deformation which explains the brittle failure found.

5.4 Conclusions

The improved toughness of a PMMA/epoxy 80/20 blend during tensile deformation is lost under impact conditions. In order to explain this finding, the changes in microscopic deformation of this blend are studied by means of real-time SAXS-deformation experiments.

During uniaxial tensile testing at limited strain rate, shear yielding is promoted by the occurrence of cavitation which causes a ductile macroscopic behaviour. At higher deformation rates the volume of voids formed increases while the degree of orientation of these voids in the tensile direction after formation decreases. Apparently, the nucleation of new voids is enhanced by a higher rate while deformation at limited rate more predominantly occurs via the orientation of voids which are formed in an early stage of the drawing process.

By the introduction of a notch, the strain rate is enhanced which results in a transition from cavitation induced shear yielding to crazing. This is in accordance with the macroscopic mechanical behaviour of the blend which becomes brittle under impact conditions.

The relation between the strain rate and the degree of the cavitation of the PMMA/epoxy 80/20 seems to possess an optimum. First, the tendency for cavitation is enhanced by the higher strain rate which would suggest an additional toughness improvement at macroscopic level. However, at even higher rates void formation can no longer occur causing brittle failure. Apparently, cavitation is a prerequisite for this blend to behave ductile at a macroscopic level. This is confirmed by the enhanced impact strength of the PMMA/epoxy 80/20 system which is precavitated during slow speed tensile deformation prior to impact testing.

Generally, the toughness of brittle amorphous polymers can be improved by a transition in mode of microscopic deformation from crazing to shear yielding. In order to achieve this, one should aim for a smaller but more readily cavitating dispersed rubber phase.

5.5 References

(1) Bucknall, C.B. *Toughened Plastics*, Applied Science Publishers LTD: London, **1977**.

(2) Kinloch, A.J.; Young, R.J. *Fracture Behaviour of Polymers*, Elsevier Applied Science Publishers LTD: London, **1983**.

(3) Plati, E.; Williams, J.G. *Polym. Eng. Sci.* **1975**, *8*, 941.

(4) Bubeck, R.A.; Buckley, D.J.; Kramer; Brown, H.R. *J. Mater. Sci.* **1991**, *26*, 6249.

(5) Buckley, D.J., Jr *Ph.D. thesis*, Cornell University, **1993**.

(6) Hughes, D.J.; Mahendrasinngam, A.; Oatway, W.B.; Heeley, E.L.; Martin, C.; Fuller, W. *Polymer* **1997**, *38*, 6427.

(7) Kratky, O.; Pilz, I.; Schmitz, P.J. *J. Coll. Interf. Sc.* **1966**, *21*, 24.

(8) Paredes, E.; Fischer, E.W. *Macromol. Chem.* **1979**, *180*, 2707.

(9) Brown, H.R.; Kramer, E.J. *J. Macromol. Sci. - Phys.* **1981**, *B19*, 487.

(10) Pearson, R.A.; Yee, A.F. *J. Mater. Sci.* **1991**, 26, 3828.

(11) Bagheri, R.; Pearson, R.A. *Polymer* **1996**, 37, 20, 4529.

(12) Lazzeri, A.; Bucknall, C.B. *Polymer* **1995**, 36, 15, 2895.

(13) Cho, K.; Gent, A.N. *J. Mater. Sci.* **1988**, 26, 141.

(14) Dompas, D.; Groenincks, G. *Polymer* **1994**, *35*, 22, 4743.

(15) Smit, R.J.M. *Ph.D. thesis*, Eindhoven University of Technology, **1998**.

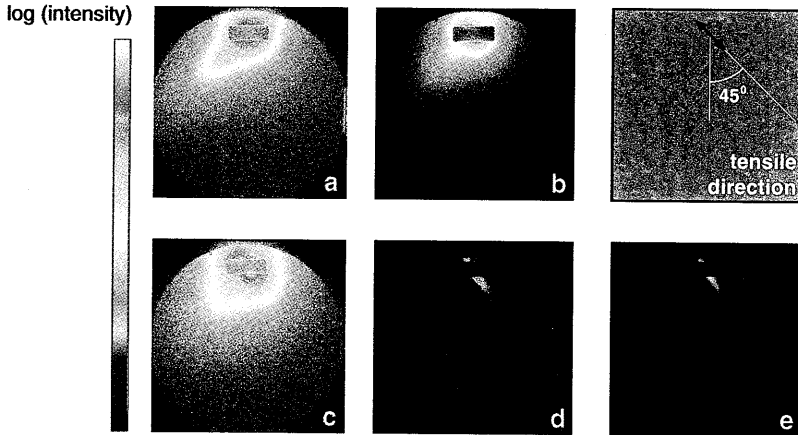(16) Smit, R.J.M.; Meijer, H.E.H.; Brekelmans, W.A.M.; Govaert, L.E. *J. Mater. Sci.* **1998**, submitted.

log (intensity)

Figure 5.2: *Small angle X-ray scattering patterns of the PMMA/epoxy 80/20 blend prior to fracture, deformed at (a) 0.1 mm/min and (b) 25 mm/min. Scattering patterns for notched samples of the same blend stretched at (c) 0.01 mm/min and (d) 25 mm/min. (e) The pattern measured for a notched PMMA/epoxy 90/10 sample tested at 25 mm/min. The tensile direction is tilted 45^0. Experiments performed at CLRC, Station 2.1.*

a) Semi-IPN
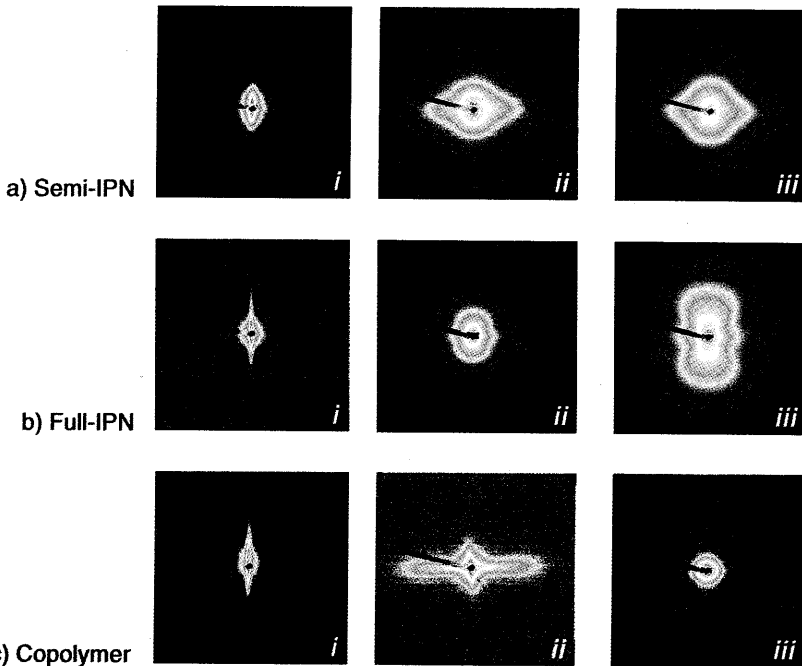
b) Full-IPN

c) Copolymer

Figure 6.8: *SAXS patterns prior to fracture of PMMA/epoxy systems: (a) semi-IPN, (b) full-IPN, (c) copolymer, for different compositions: (i) 90/10, (ii) 80/20, (iii) 70/30. Tensile direction vertical. Experiments performed at ESRF, ID2-BL4.*

Chapter 6

Influence of interphase mixing on the mechanical properties

6.1 Introduction

In the previous chapters the approach towards toughening of brittle amorphous polymers and the relation with the mode of microscopic deformation has been discussed extensively. The chemical blending procedure introduced in Chapter 2, clearly demonstrated that the system viscosity during phase separation can be used to control the size of the final morphology. In Chapter 3, this approach was successfully adopted for the simultaneous polymerisation of methylmethacrylate and epoxy resin yielding transparent toughened rubber-modified PMMA.

Major disadvantage of the application of chemically-induced phase separation is the limited degree of demixing which may influence the mechanical properties of the final blend. This has also been recognised for interpenetrating polymer networks (IPNs) which are synthesised conform a comparable simultaneous polymerisation strategy[1,2]. Instead of a high viscosity, morphology coarsening during phase separation is mainly suppressed by crosslinking of the networks involved which physically restrict complete demixing. For certain IPNs with nano-sized morphologies unique mechanical properties have been found from which the origin is not understood and that cannot be explained by conventional toughening approaches such as the initiation of multiple crazes or shear bands[3-6]. Hardly any attention has been paid to the question how the morphology and/or partial demixing influences the mode of microscopic deformation[7].

In this chapter the influence of interphase mixing, i.e. incomplete demixing resulting in a broad interface in which the composition gradually changes from one phase to the other, on

the mechanical properties is studied in order to elucidate the mechanisms of the enhanced toughness that is observed for the PMMA/epoxy system. Regarding the combination of a thermoplastic and thermosetting network, this blend can be considered as a semi-IPN[1]. Demixing is suppressed by either crosslinking of the PMMA phase or copolymerisation of the PMMA and epoxy networks. This yields, respectively, a full-IPN and a kind of copolymer. The differences in mechanical behaviour on both macroscopic and microscopic level are determined in order to reveal the influence of interphase mixing in comparison to the obvious influence of the sub-micron morphology.

6.2 Experimental

6.2.1 Materials

The epoxy resin used is a diglycidyl ether of polypropylene oxide (DGEPPO, SHELL Epikote 877) supplied by CFZ (Chemische Fabriek Zaltbommel, Zaltbommel, The Netherlands). The curing agent, Jeffamine D230 supplied by Huntsman (Zaventem, Belgium), is a diamine which also possesses a polypropylene oxide (PPO) backbone.

In the free-radical polymerisation several monomers were used: methylmethacrylate (MMA, Aldrich), diethylene glycol dimethacrylate (DEGDMA, Aldrich) and glycidylmethacrylate (GMA, Aldrich). All monomers were purified prior to use. The polymerisation was performed over a broad temperature range which required the application of three initiators with different reactivity: 2,2'-azobis(4-methoxy-2,4-dimethylvaleronitrile) (V-70 initiator supplied by WAKO Chemicals, Neuss, Germany), 2,2-azobis(isobutyronitrile) (Perkadox AIBN, AKZO-NOBEL) and *tert*-butyl-peroxybenzoate (Aldrich). The 10 hour half-life time decomposition temperature in toluene of these initiators increases, respectively, from 30, 64 to 103 °C.

6.2.2 Blend preparation

The polymerisation of MMA and epoxy was performed simultaneously and was similar to the procedure described in Chapter 3. A homogeneous solution of MMA, epoxy, curing agent and the three mentioned free-radical initiators was prepared for several MMA-epoxy weight ratios. After purging the solution with nitrogen gas for several minutes, the polymerisation was performed in a closed cast mould. Immediately after the addition of the most reactive initiator, V-70, the polymerisation of MMA was initiated. The solution was left at room temperature for 24 hours. Subsequently, the moulds were placed in an oven with a programmed temperature profile: 20 hours at, subsequently, 30 °C, 50 °C, 70 °C, and 90 °C, followed by two post curing steps at 110 °C for 3 hours and 120 °C for 2 hours. Afterwards, the moulds were kept in the oven which was allowed to cool slowly to room temperature.

The blends obtained consist of a thermoplastic PMMA matrix with a dispersed epoxy rubber phase, see Chapter 3. Considering the simultaneous polymerisation route and the character of the phases, these blends can be classified as semi-IPNs. The same route was followed to prepare full-IPNs and

copolymers based on the constituents mentioned above. The recipe involved the addition of respectively DEGDMA (6.5 wt% based on MMA) as a crosslinking agent for the PMMA phase, or GMA (12.2 wt% based on Epikote 877) which participates in both the MMA free-radical and the epoxy step polymerisation.

6.2.3 Analysis

Dynamic mechanical thermal analysis (DMTA) was performed for all blends prepared. A Polymer Laboratories (now: Rheometrics Scientific) Dynamic Mechanical Thermal Analyser MkII was used in the bending mode with a frequency of 1 Hz, a strain of 40 μm and a heating rate of 2 °C/min.

Transmission (TEM, Jeol 2000 FX) electron microscopy was used to investigate the morphology of the blends. The samples were microtomed below their glass transition temperature using a Reichert-Jung Ultracut E. Contrast was enhanced by staining the epoxy phase using RuO_4 vapour for 10 min.

6.2.4 Mechanical properties

Tensile tests were performed at room temperature using a Zwick 1445 tensile machine. Dog-bone shaped tensile bars with a gauge length of 38 mm were machined from the polymerised plaques and tested at a strain rate of $1.3*10^{-3}$ s^{-1}. An Instron Extensometer 2630-107 was used to collect accurate displacement data to determine the blend moduli.

Impact tensile tests (1 m/s) were performed using a Zwick Rel SB 3122 tensile machine. The test specimens were prepared according to the ASTM D-256 protocol. However, in this case the machined notches were sharpened prior to testing using a fresh razor blade. The impact energy was calculated by the integration of the measured force-displacement curve divided by the fracture surface area.

6.2.5 Microscopic deformation

The microscopic deformation mechanism during tensile deformation is studied by time-resolved small angle X-ray experiments using the synchrotron radiation facility at the ESRF (European Synchrotron Radiation Facilities, Grenoble, France). The measurements were performed at beamline ID2-BL4 using a X-ray wavelength of 1 angstrom and a detector-to-sample distance of 10 meters. The size of the beam was 0.2x0.5 mm^2. For all three systems, samples of the 90/10, 80/20 and 70/30 composition were deformed in uniaxial tension using a Rheometrix Minimat miniature tensile machine at a displacement rate of 0.1 mm/min. The scattering patterns were collected using a 2D-CCD detector. The patterns were used for the qualitative identification of the mode of microscopic deformation.

6.3   Results and Discussion

The morphology and mechanical properties of the in-situ polymerised PMMA/epoxy semi-IPNs have already been discussed in Chapter 3. Sub-micron or nano-sized morphologies have been obtained by controlling the coarsening process after chemically-induced phase separation using the system viscosity. This requires an initially homogeneous solution and, therefore, a

certain compatibility between the constituents. The enhanced viscosity and compatibility suppresses the degree of demixing in the final blend and, as a consequence, completely demixed blends possessing the required morphology do not result from this route. Hence, this complicates the desired distinction between the influence of interphase mixing and morphology on the mechanical properties.

Therefore, the only possibility left to study the influence of limited molecular demixing, is to explore some routes which tend to result in the opposite direction. Using DEGDMA, demixing can be suppressed even more by crosslinking the PMMA phase which results in a full-interpenetrating polymer network (full-IPN) consisting of two interwoven thermosetting networks. Alternatively, the degree of demixing can be suppressed by the addition of GMA which participates in both the free-radical MMA and the epoxy step-growth polymerisation[8]. In this case, a copolymer is synthesised since the PMMA and epoxy networks are chemically bonded.
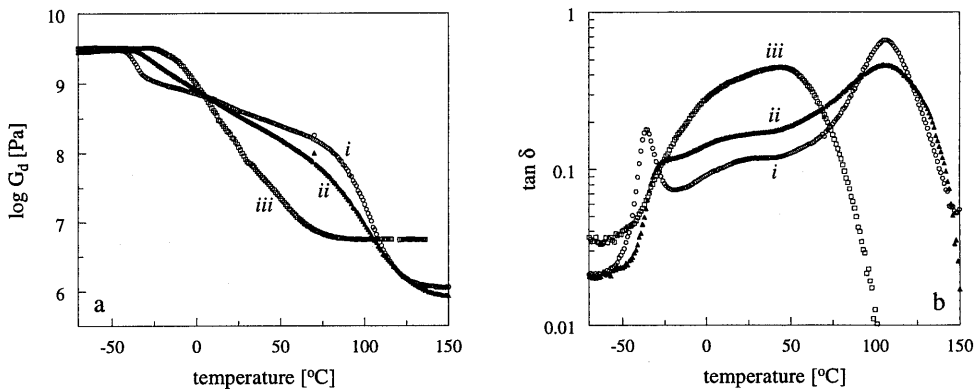

Figure 6.1: *DMTA measurements of in-situ polymerised PMMA/epoxy 50/50 blends, (a) dynamic modulus (log G_d) and (b) loss angle (tan δ): (i) semi-IPN, (ii) full-IPN, (iii) GMA-copolymer.*

6.3.1 DMTA measurements

The influences on demixing are studied by DMTA measurements, as shown for the PMMA/epoxy 50/50 blends in Figure 6.1. For the semi-IPN clearly two peaks and thus two separate phases are obtained. By crosslinking the PMMA phase, the degree of demixing is decreased, as can be concluded from the suppression of the rubber transition at ~-35 °C, and the enhanced broadening of the PMMA transition. For the GMA-copolymer both networks indeed seem to be chemically bonded without the presence of any phase separation. For tan δ, one very broad peak is observed bridging the temperature range from the epoxy T_g (~-35 °C) to the T_g of the PMMA phase (~115 °C). The dynamic modulus G_d does not show any

transitions but slowly falls off in the same temperature range. This suggests the presence of one single phase, despite the fact that this behaviour is clearly different from a completely statistical random copolymer. For these copolymers one single sharp peak is observed at a glass transition temperature determined by the ratio of the constituents. In contrast, the actual DMTA measurement suggests a more quasi-homogeneous GMA-copolymer possessing a broad spectrum of compositions which include all intermediate ratios between neat PMMA and epoxy. As expected, the effects observed in DMTA are less pronounced for blends in which one of both phases is present in excess, see e.g. the PMMA/epoxy 80/20 blend in Figure 6.2. The differences resulting from demixing can, however, still be observed and may thus affect the mechanical behaviour.
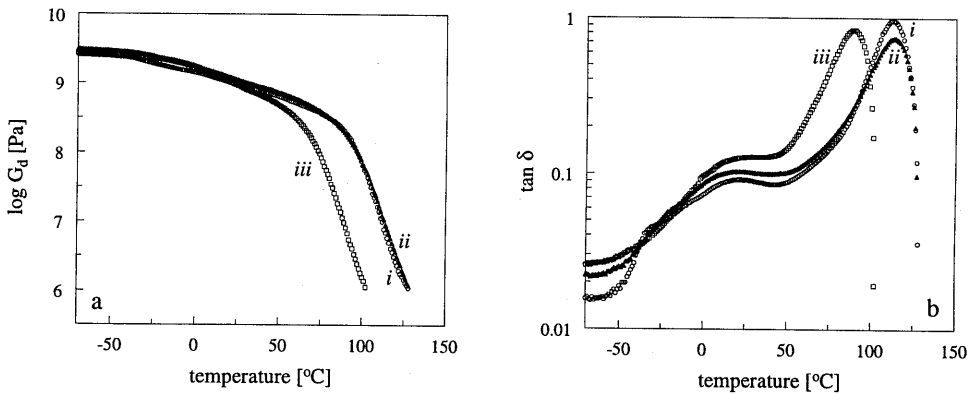

Figure 6.2:   *DMTA measurements of in-situ polymerised PMMA/epoxy 80/20 blends, (a) dynamic modulus (log G_d) and (b) loss angle (tan δ). (i) semi-IPN, (ii) full-IPN, (iii) GMA-copolymer.*

Table 6.1:   *Optical appearance of the PMMA/epoxy blends.*

PMMA/epoxy	90/10	80/20	70/30	60/40	50/50	40/60	30/70	20/80	10/90
Semi-IPN	transparent				hazy	white			trans.
Full-IPN	transparent					hazy		white	trans.
Copolymer	transparent								

6.3.2 Morphology

The trends in demixing observed in the DMTA measurements are confirmed by the morphology studies, see Figure 6.3, and the optical appearance of the blends, see Table 6.1. For the GMA-copolymer, all compositions are transparent while some of the full- and semi-IPNs are white due to a relatively coarse two phase morphology. The composition at which the blends become hazy, increases from 50 wt% epoxy for the semi-IPN to 60-70 wt% for the full-IPN. Apparently, the size of the morphology decreases as the PMMA phase is crosslinked or even chemically bonded to the epoxy phase which is confirmed by the TEM micrographs in Figure 6.3.
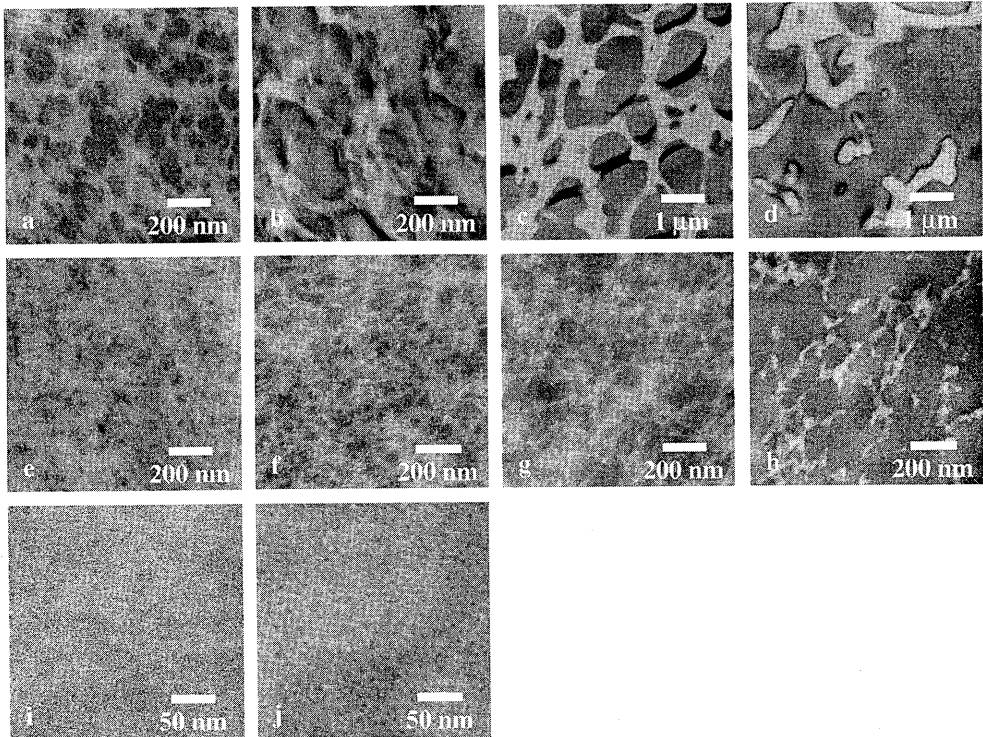

Figure 6.3: *Transmission electron micrographs of the PMMA/epoxy systems: semi-IPNs, (a) 50/50, (b) 40/60, (c) 30/70, (d) 20/80, (e)-(h) same compositions for the full-IPNs, copolymer (i) 50/50, and (j) 20/80.*

6.3.3 Tensile behaviour

Surprisingly, the macroscopic strain at break seems to be hardly affected by the huge differences in demixing or morphology, see Figure 6.4. All three blends show a comparable synergistic effect with a high strain at break for the intermediate epoxy concentrations. The only real difference is observed for the GMA-copolymer at epoxy concentrations of 30 wt% or

more. Here, a decreased strain at break is observed which is most likely the result of the high crosslink-density.

For a low epoxy content the differences in the "so-called" *local* strain at break are also limited. Here the *local* strain at break is defined by the ratio between the cross-sectional area before and after fracture and supplies some information about the relative amount of plastic deformation compared to elastic deformation and thus the contribution of the rubber phase. The GMA-copolymer systems appear to be almost completely elastic for blends containing 50 wt% epoxy or more. In comparison, the semi- and full-IPNs deform much more plastically, also at intermediate epoxy concentrations. Compared to the semi-IPN, the local strain at break of the full-IPN is smaller which is most probably the result of crosslinking in combination with an enhanced elasticity (reflected by a high reversible deformation) as result of a decreased demixing.
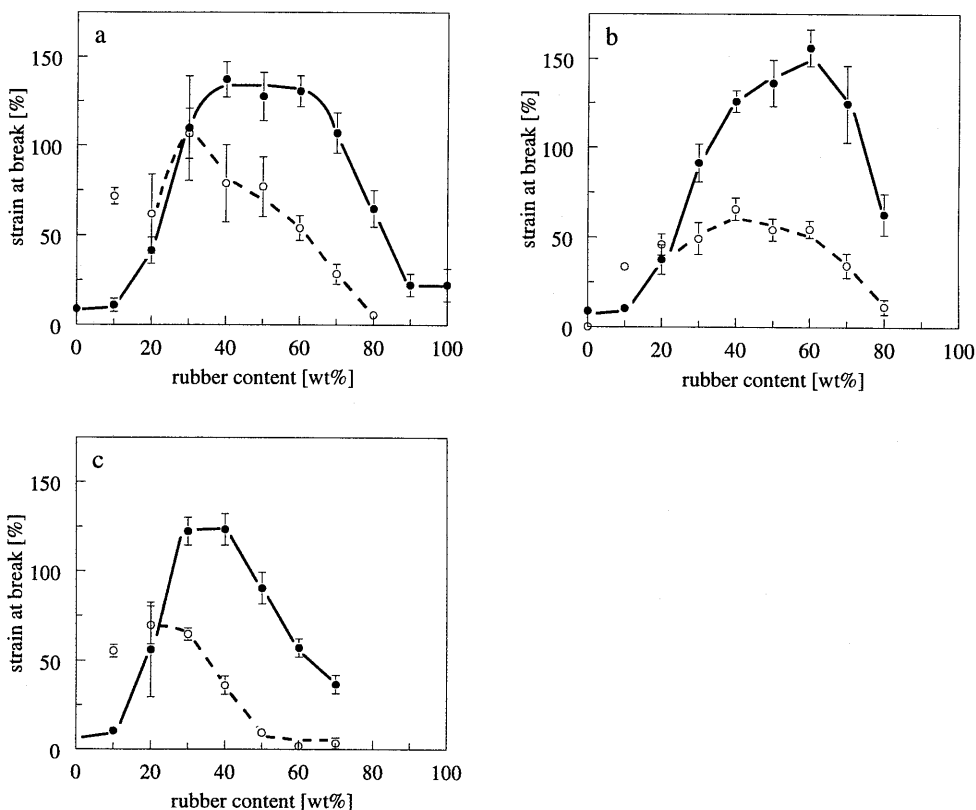

Figure 6.4: *Macroscopic (●) and local (○) strain at break of the PMMA/epoxy systems, (a) semi-IPN, (b) full-IPN, (c) GMA-copolymer.*
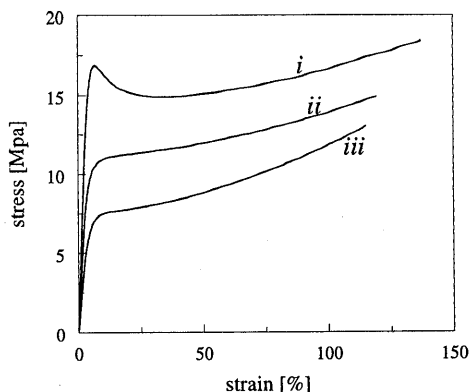
Figure 6.5: *Stress-strain curves for the three PMMA/epoxy 60/40 blend, (i) semi-IPN, (ii) full-IPN and (iii) GMA-copolymer.*

Apart from the (minor) differences described above, the strain at break data, although spectacular for PMMA, suggest a rather uniform overall deformation behaviour for all three systems. However, the more detailed stress-strain behaviour of the 60/40 compositions in Figure 6.5 clearly shows that there is a considerable influence of demixing. The semi-IPNs demonstrate a clear yield stress followed by pronounced strain softening known from the tensile and compression behaviour of blends consisting of rubber particles in thermoplastic matrices. For both the full-IPN and the copolymer, however, the yield stress is suppressed and the strain softening is completely disappeared. This clearly shows that decreasing the degree of demixing enhances the influence of the epoxy rubber phase. As can be expected, this effect is less pronounced for systems with a higher PMMA content which all demonstrate a stress-strain behaviour with a clear yield stress followed by strain softening and, subsequently, hardening. However, the values of the yield stress and modulus for the full-IPNs and the GMA-copolymers are somewhat smaller compared to the blend-like semi-IPNs, see Figure 6.6.

6.3.4 Tensile and impact toughness

In slow speed tensile testing, modulus, yield stress and strain at break can be combined to a definition of tensile toughness, through the absorbed energy during tensile deformation till fracture, represented by the area under the stress-strain curve. For low epoxy contents (< 20 wt%) limited differences are observed, see Figure 6.7a. For higher epoxy contents, the tensile toughness of the semi-IPNs is clearly larger as a result of the higher strain at break in combination with the higher yield stress and modulus. The rapidly decreasing toughness of the GMA-copolymer is explained by the almost totally elastic behaviour of this system.
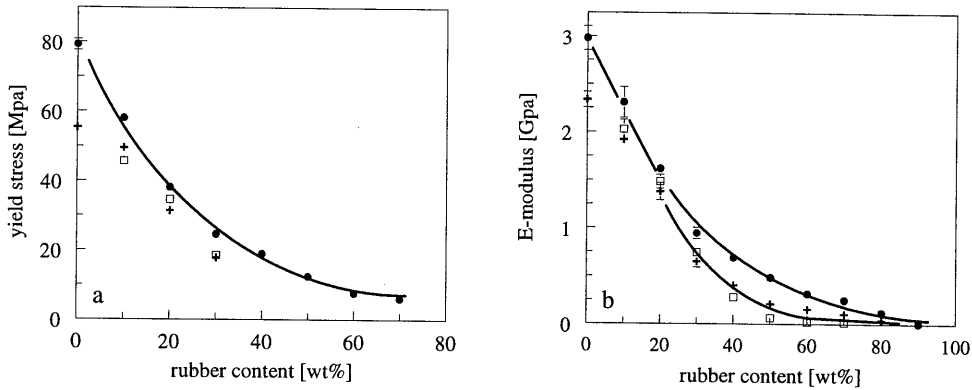
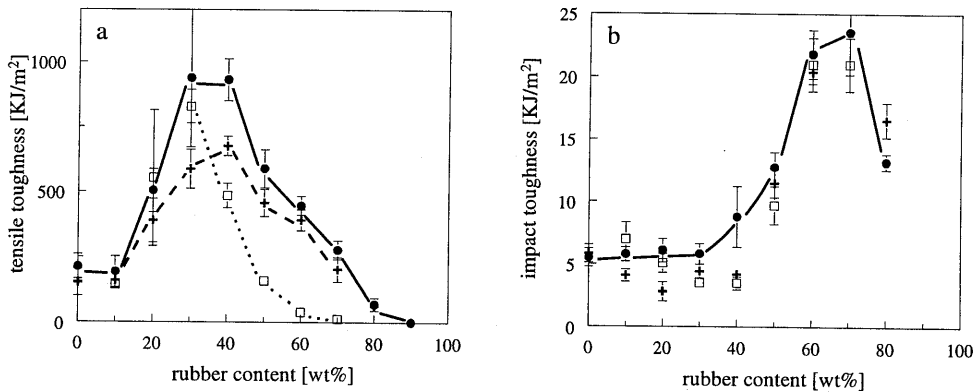**Figure 6.6:** *(a) Yield stress and (b) modulus of (●) semi-IPN, (□) full-IPN and (+) GMA-copolymer.*

Figure 6.7: *(a) Tensile and (b) impact toughness of (●) semi-IPN, (□) full-IPN and (+) GMA-copolymer.*

Under notched impact conditions a comparable trend in toughness can be expected. However, the rubber content at which the maximum toughness is now observed, clearly shifts to higher values (compare Figures 6.7a and b). Apparently, the strain rate dependence of toughness is not really affected by the degree of interphase mixing since its absolute value is rather system independent. The full-IPN and GMA-copolymer demonstrate a somewhat remarkable trend for epoxy concentrations less than 50 wt%. In contrast to the concentration independent behaviour of the semi-IPNs, the toughness appears to decrease with an increasing rubber content. This is most likely again the result of the more elastic behaviour of the systems with a higher rubber content and the absence of a separate rubber phase which results in an enhanced notch sensitivity, see Chapters 3 and 5. In Chapter 5 it was demonstrated that precavitating the PMMA/epoxy 80/20 blend in tension prior to impact testing, resulted in a significant

enhancement of the impact toughness, even at low epoxy concentrations. In general, the toughness of the blends is mainly determined by these kind of microscopic deformation phenomena which may be influenced by the degree of interphase mixing as will be discussed in more detail in the following section.

6.3.5 Mode of microscopic deformation

Despite the limited difference in macroscopic mechanical behaviour, the deformation on a microscopic level may still be affected by the degree of demixing. As in Chapters 4 and 5, time-resolved SAXS is used to monitor the mode of microscopic deformation. The resulting scattering patterns prior to fracture as shown in Figure 6.8[i] are used for the qualitative identification of the microscopic deformation.

Semi-IPNs. The mode of microscopic deformation of the semi-IPNs, as shown in Figure 6.8a, has extensively been discussed in Chapter 4. For the 90/10 blend, the strong scattering streaks in the tensile direction in combination with the weaker scattering perpendicular to that, have been explained by the introduction of crazes, see pattern *i*. During the early stage of the drawing process of the 80/20 blend voids are formed as result of rubber cavitation. The elliptical scattering pattern in a later stage, see *ii* in Figure 6.8, is caused by the elongation of these voids in the tensile direction. Deformation of this blend occurs via shear yielding which explains the enhanced tensile toughness on macroscopic level. Finally, the 70/30 blend also deforms via shear yielding, however, without the formation of voids. The observed scattering pattern is caused by the orientation of the rubber morphology upon drawing, see *iii* in Figure 6.8a.

Full-IPNs. The scattering patterns for the full-IPNs are shown in Figure 6.8b. The brittle 90/10 system again deforms via crazing as can be concluded from the strong scattering streaks in the tensile direction. No relevant scattering is observed in the perpendicular direction which suggests the absence of craze fibrils or the formation of crazes with a limited amount of fibrils.

For the 80/20 full-IPN, deformation does not result in the elliptically shaped scattering pattern as observed for the semi-IPN which indicates the absence of voids being elongated in the tensile direction. Moreover, cavitation seems to be suppressed as can be concluded from the limited changes in the scattered intensity during drawing, not shown here. This is confirmed by the macroscopic tensile tests which, in contrast to the semi-IPN, do not show any stress-whitening. Instead, some additional scattering in the tensile direction is found. Although not fully understood, this may be the result of the initiation of a limited amount of crazes or crack-

---

[i] SAXS patterns of Figure 6.8 are depicted at page 79.

like voids as also discussed in Chapter 4. The combination with the weak scattering at the equator results in a pattern rather similar to that of the 70/30 semi-IPN which was explained in terms of morphological orientation. For the 80/20 full-IPN, the equator scattering is, however, considerably less which may be the result of the crosslinked PMMA phase suppressing the morphological orientation.

The resulting scattering pattern of the 70/30 full-IPN as shown in *iii* Figure 6.8b has not been observed earlier and a possible explanation for the scattering pattern will be given below. The scattering perpendicular to the tensile direction is again similar to that of the 70/30 semi-IPN and may again be caused by the orientation of the morphology. This, however, cannot explain the additional scattering in the tensile direction. A possible alternative reason is the localisation of deformation which results in zones in the order of tens of nanometers possessing a different electron density. This may result in the scattering pattern observed if these zones are asymmetrically shaped and positioned in such a way that their average distance is smaller in the tensile direction.

Copolymer. As can be concluded from the first scattering pattern in Figure 6.8c, the 90/10 composition of the copolymer also deforms via crazing. As observed for the full-IPN with the same composition, the scattering streak in the tensile direction is sharper in comparison to the 90/10 semi-IPN. Moreover, the pattern does not show any scattering resulting from possible craze fibrils.

In contrast, tensile deformation of the 80/20 copolymer system results in the typical cross-shaped craze scattering pattern including the scattering in the perpendicular direction which is relatively strong in comparison to the 90/10 semi-IPN. Considering the crosslinked character of the system and the craze pattern of the 90/10 composition, the development of crazes with a high fibril content may be rather unexpected. The sharp streaks in the tensile direction, however, do suggest that this system indeed deforms via crazing. Remarkably, the scattering angle in perpendicular direction is considerably larger in comparison to the craze scattering patterns discussed earlier. For crazes in polycarbonate at elevated temperatures[9] comparable scattering patterns have been observed where the large scattering angle is ascribed to the relatively thicker craze fibrils in comparison to polystyrene and poly(methyl methacrylate). A second possible explanation may be a wide distribution of inter-fibril distances. In conclusion, the results suggest that deformation of the 80/20 copolymer system is mainly accompanied by crazing.

The scattering pattern of the 70/30 copolymer system does not show any evidence of dilatation processes and/or orientation. Apparently, deformation of the thermosetting network occurs rather homogeneously without the introduction of any electron density differences. Hence, shear yielding is the only mode of microscopic deformation involved.

6.3.6 Macroscopic versus microscopic deformation

According to the results presented in Section 6.3.3, the macroscopic properties are hardly influenced by the degree of demixing. The mode of microscopic deformation, however, clearly changes for the different systems within the composition range studied. The brittle blends containing 10wt% epoxy resin, all deform via crazing while for the 80/20 composition significant differences are observed. Although the macroscopic toughness is the same, the semi-IPN 80/20 is the only system which clearly shows cavitation while the copolymer system again deforms by craze formation. Apparently, the toughness enhancement in the latter case is the result of multiple crazing. After all, this may not be surprising since cavitation is not very likely to occur in the homogeneous system. Finally, the enhanced tensile toughness of the 70/30 systems is in all cases accompanied by the occurrence of shear yielding without any dilatation processes. However, the differences in both morphology and network give rise to changing scattering patterns.

In conclusion, the mode of microscopic deformation is clearly influenced by the degree of interphase mixing but, in this case, does not result in dramatic differences in the macroscopic toughness. These set of experiments, however, clearly demonstrate that the microscopic deformation should be considered in order to draw any solid conclusions concerning the relation between the morphology and the resulting macroscopic properties.

6.4 Conclusions

In this chapter it has been demonstrated that the degree of phase separation in the PMMA/epoxy semi-IPN systems can be reduced by crosslinking the PMMA phase, which results in the formation of full-IPNs, or by the partial copolymerisation of both phases. A comparable synergistic toughening effect is observed for all three systems under both tensile and impact conditions. Generally, the difference in mechanical behaviour between the three systems is limited. For the intermediate compositions, however, the tensile toughness of the semi-IPNs is clearly higher which is most likely the result of an enhanced degree of demixing. It remains, however, difficult to distinguish unambiguously between the separate effects of interphase mixing and morphology on the mechanical behaviour. Compared to the pure copolymer with its broad spectrum in compositions all with their own T_g, a more brittle behaviour could have been expected for the full- and semi-IPNs since the contribution of the "brittle" PMMA phase is more pronounced. These blends demonstrate, however, a toughness equal or even higher than that of the copolymer system and for this reason interphase mixing alone cannot be responsible for the toughness improvement. This may be explained by nano-

sized morphology which causes a transition in mode of microscopic deformation from crazing to shear yielding, see Chapter 1.

Considering the influence of precavatition on the impact toughness of the PMMA/epoxy blends, as discussed in the previous chapter, the differences in toughness are mainly determined by the mode of microscopic deformation. Despite the influence of the interphase mixing on the microscopic deformation, the macroscopic toughness is found to be rather system independent.

6.5   References

(1)   Klempner, D.; Sperling, L.H.; Utracki, L.A. *Advanced Chemistry Series*, American Chemical Society: Washington DC, **1994**, *239*.

(2)   Kim, S.C.; Sperling, L.H. *IPNs around the world*; John Wiley & Sons: Chichester, **1997**.

(3)   Chou, Y.C.; Lee, L.J. *Polym. Eng. Sci.* **1995**, *35*, 12, 976.

(4)   Han, X.; Chen, B.; Guo, F. In *IPNs around the world*; Kim, S.C., Sperling, L.H.; John Wiley & Sons: Chichester, **1997**, 241.

(5)   Hourston, D.J.; Schäffer, F.U. *Polymer* **1996**, *37*, 16, 3521.

(6)   Barret, L.W.; Sperling, L.H.; Gilmer, J.W.; Mylonakis, S.G. In *Advances in Chemistry Series*; Klempner, D.; Sperling, L.H.; Utracki, L.A.; American Chemical Society: Washington DC, **1994**, *239*, 489.

(7)   Jang, B.Z.; Pater, R.H.; Soucek, M.D.; Hinkley, J.A. *J. Polym. Sci., Part B: Polym. Phys. Ed.* **1992**, *30*, 643.

(8)   Scarito, P.R.; Sperling, L.H. *Polym. Eng. Sci.* **1979**, *36*, 4, 297.

(9)   Bark, M.; Cunis, S.; Fink, M.; Gehrke, R.; Heise, B.; Karl, A.; von Krosigk, G.; Lode, U.; Pomper, T.; Wilke W. *Tagungsband "Polymerwerkstoffe '96"* **1996**, 350.

Chapter 7

Conclusions and Recommendations

7.1 Conclusions

7.1.1 Blending

Chemical blending routes involving chemically-induced phase separation are explored to prepare sub-micron and/or nano-sized rubber morphologies in a thermoplastic polymer matrix. In Chapter 2 it has been demonstrated for the PPE-PS/epoxy system that an accurate control over the system viscosity during phase separation can be used to tailor the size of the dispersed epoxy phase. Phase separation in a highly viscous environment suppresses the morphology coarsening process which, subsequently, results in the desired sub-micron or even nano-sized epoxy particles. For the application of reactive solvents this requires a curing strategy in which the reaction temperature is equal to the glass transition temperature of the initial solution; $T_{cure}=T_g$.

In Chapter 3, this approach has successfully been applied in the rubber modification of brittle amorphous polymers, PS and PMMA. The T_g-curing strategy, however, cannot be applied for the simultaneous polymerisation of MMA and epoxy but also in this case, an enhancement of the viscosity has been used to control the morphology coarsening process.

Incomplete demixing of the phases involved appears to be the major drawback of the application of phase separation during blending. In the case of the systems discussed in this thesis (PPE-PS/epoxy, PMMA/epoxy), the interphase mixing is caused by the combination of a rather high compatibility between phases and the large interfacial area as result of the limited size of the morphology. As described in Chapter 3, the compatibility is needed since curing in a highly viscous system requires a certain miscibility at relatively low temperatures

in order to prevent premature thermally-induced phase separation which cannot be controlled. Moreover, curing below T_g restricts the formation of separate phases which results in a kind of interpenetrating polymer network (IPN). Figure 7.1a schematically represents the resulting systems after phase separation in an highly viscous environment in which, besides both neat phases, all intermediate compositions are present as an interphase. Hence, demixing will also for the PMMA/epoxy blends not result in two completely separated phases, see Figure 7b, as is aimed for in order to produce an ideal model system to study the influence of nano-sized rubber particles on the mechanical properties of brittle amorphous polymers.

In conclusion, the required sub-micron and/or nano-sized rubber morphologies can be prepared but the developed blending procedure does not result in *the* ideal model system.
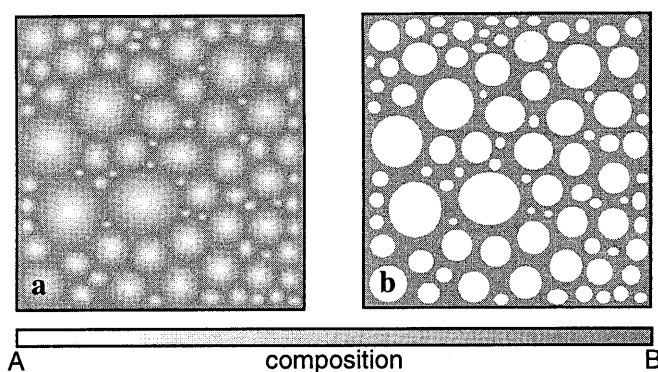

Figure 7.1: *Schematic representation of (a) the morphology resulting from chemically-induced phase separation in a highly viscous environment resulting in a high degree of interphase mixing and (b) the ideal, completely separated two phase morphology. The white phase (A, e.g. epoxy) and the grey phase (B, e.g. PMMA), respectively, represent the completely phase separated dispersed phase and thermoplastic matrix.*

7.1.2 Mechanical behaviour of PMMA/epoxy blends

The toughness of the transparent rubber modified PMMA blends prepared via chemically-induced phase separation appears to be strain rate dependent. For a limited epoxy content (<40 wt%) the enhanced tensile toughness is lost under impact conditions. The importance of understanding the cause of a certain macroscopic behaviour in terms of mode of microscopic deformation and its relation to the rubber morphology has been demonstrated in Chapter 4. Time-resolved SAXS-deformation experiments showed that the enhanced tensile toughness results from the transition from crazing to shear yielding. For the PMMA/epoxy 80/20 blend the importance of void formation is proven to be a requirement for the occurrence of shear

yielding. At higher deformation rates, however, cavitation can no longer occur which results in crazing and thus a brittle response, see Chapter 5.

The time-resolved SAXS measurements do not allow for a direct relation between the elongation of the sample and measured scattering patterns as result of the limited size of the beam-spot. The scattering data should be related to the extent of deformation in the local zone exposed by the beam. In this study the *local* strain has, therefore, been determined by monitoring the beam intensity in front of and behind the sample during the complete deformation experiment. This does allow for a reliable comparison of the local deformation and the scattering data.

In order to distinguish between the influence of the rubber morphology and the limited degree of demixing between the PMMA and epoxy phase, the properties of a full-IPN and copolymer system based on the same constituents have been studied. Especially for the systems with a high PMMA fraction, no large differences in toughness are found while the mode of microscopic deformation is clearly influenced. Cavitation induced shear yielding only occurs in semi-IPN 80/20 system which appears to shift to (multiple) crazing for the homogeneous copolymer with the same composition. Despite the incomplete demixing, resulting in a morphology as depicted in Figure 7.1a, the presence of the small dispersed rubber phase appears to be essential for the formation of voids. Generally, the set of experiments presented in Chapter 6 concerning the different IPN-like systems, clearly demonstrates the importance of studying the mode of microscopic deformation in order to draw any solid conclusions about the relationship between morphology, demixing and macroscopic mechanical behaviour.

In conclusion, the toughness of the brittle amorphous polymer PMMA has been improved by the introduction of the aimed sub-micron epoxy-rubber phase. The contribution of demixing and morphology, however, cannot completely be separated but the enhanced performance is certainly not only caused by interphase mixing. Hence, the rubber morphology plays a key-role in the toughness improvement.

7.1.3 Toughening of polymers using the concept of critical ligament thickness

Earlier several other systems already suggested the existence of a critical ligament material thickness determining the mechanical behaviour of heterogeneous polymeric systems. For semi-crystalline polymers, the concept of interparticle distance was introduced by Wu et al. for nylon-6[1,2]. Muratoglu et al. showed that this is the result of an enhanced matrix plasticity caused by the specific crystal morphology between two particles[3,4]. Van der Sanden et al. generalised the critical thickness concept for amorphous polymer systems and claimed a toughness enhancement in PS as result of a transition from crazing to shear yielding[5,6]. Moreover, Gloaguen et al. observed an enhanced plasticity in PMMA during compression tests at a critical interparticle distance of 60 nm[7]. Finally, enhanced mechanical properties are

also found in other systems based on brittle amorphous polymers possessing a nano-sized rubber morphology, e.g. IPNs and block-copolymers.

The aim of this thesis was to develop a ductile heterogeneous system based on brittle amorphous polymers. In order to combine a ductile mechanical behaviour (i.e. small ligament thickness) with a minimum loss in modulus and strength the size of the rubber morphology in the PMMA/epoxy model system has almost been decreased to nano-scale. The toughness is already improved at an epoxy content of 20 wt% and is indeed the result of the anticipated transition in mode of microscopic deformation from crazing to shear yielding. It is, however, demonstrated that, especially for the sub-micron rubber morphologies, a detailed understanding of the deformation on microscopic level is of crucial importance in order to explain the relation between the macroscopic properties and aspects like rubber morphology, strain rate and degree of interphase mixing.

7.2 Recommendations

7.2.1 Intrinsic mechanical behaviour of thin ligaments

The most straightforward explanation for the suppression of the crazing process upon decreasing the morphology size is probably the limited local thickness which becomes to small to allow for the formation of a craze. Alternatively, also the intrinsic behaviour of the polymer network may change as result an enhanced molecular mobility in the thin ligaments. In several studies, a glass transition temperature depression has been observed for PMMA and PS films which possess a thickness in the order of 30-100 nm[8-11]. However, only the measurements on free films[8] should be considered since the glass transition temperature appears to be dependent on the substrate used. A T_g-depression is expected to influence the intrinsic mechanical behaviour of the polymer since an enhanced mobility may change the relative contributions of yield stress, strain softening and strain hardening. This may result in a toughness improvement whereas the system may suffer from an undesired decrease in yield stress.

Consequently, additional understanding of physical and mechanical properties of thin polymer ligaments will be of crucial importance since this may explain the fundamental reason for the enhanced toughness. Furthermore, this may also answer the question if the introduction of thin ligaments can ever result in a useful construction material (so without loss in modulus and yield stress).

Recently, some investigations have been initiated to determine the effect of layer thickness on the mobility by means of solid-state NMR. Mulder et al. observed a mobile PMMA-fraction in PMMA-PS multi-layer tapes with a layer-thickness of approximately ~70 nm[12]. This has been

confirmed in our laboratories where a similar effect has also been detected in both PMMA and PS spheres possessing a size in the order of ~30 nm[13]. These results demonstrate that the physical properties of thin polymer ligaments should be taken into account during the development of the tough heterogeneous polymer systems.

7.2.2 Improvement of the impact toughness

The reason for the loss of the enhanced toughness of the PMMA/epoxy 80/20 system by increasing the deformation rate has been explained by the strain rate dependence of the rubber modulus. At high deformation rates the modulus of the rubber phase is expected to approach that of a glass which no longer allows for the occurrence of cavitation and thus a ductile shear yielding response. The straightforward method to avoid this problem is the application of a rubber phase which possesses an even lower glass temperature. As demonstrated by Smit, however, the dispersed phase does not necessarily have to possess a rubbery character. The maximum toughness is expected for an easily cavitating modifier which, subsequently, supports the strain hardening process at a higher strain[14,15]. The importance of cavitation is clearly demonstrated by the results in this thesis while delocalisation is enhanced by the stronger strain hardening behaviour.
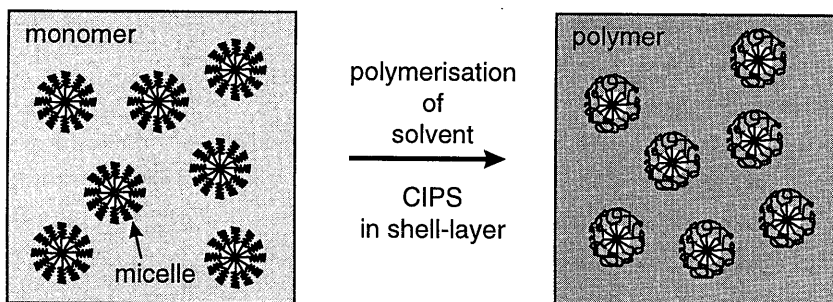

Figure 7.2: *Schematic representation of diblock-copolymer micelles in a reactive solvent which after polymerisation results an easily cavitating nano-sized morphology.*

A possible route to prepare a system which meets these requirements may be the application of diblock-copolymer micelles[16,17]. These molecular structures should be formed in a reactive solvent like styrene and/or acrylate, which after polymerisation forms the brittle amorphous matrix. With respect to the solvent, the blocks should consist of an incompatible and a compatible block, see Figure 7.2. The shell-block can be a rubber or another easy-deforming soft polymer which will phase separate upon polymerisation of the solvent resulting in a strong matrix adhesion. By decreasing the molecular weight of the core-block, which can even be a glass, the size of the dispersed phase can be suppressed and its resistance against

cavitation can be minimised. Finally, the additional application of for instance electron-beam irradiation[18] can be used to destroy the core-polymer which will suppress the resistance against void formation even further. Moreover, the shell can be crosslinked in the same treatment resulting in an increased modulus and thus an enhanced strain hardening. Of course, this last step requires an accurate selection of the block-copolymer used. Major problem to overcome in the application of micelles is the tendency of block-copolymers to form lamellar or co-continuous morphologies at higher concentrations. These type of structures may, however, lead to tough heterogeneous polymer systems which do not suffer from the interphase mixing as discussed for the PMMA/epoxy blends.

7.3 References

(1) Wu, S. *Polymer* **1985**, 26, 1855.

(2) Wu, S. *Polym. Eng. Sci.* **1988**, 35, 549.

(3) Muratoglu, O.K.; Argon, A.S.; Cohen, R.E.; Weinberg, M. *Polymer* **1995**, *36*, 5, 921.

(4) Muratoglu, O.K.; Argon, A.S.; Cohen, R.E. *Polymer* **1995**, *36*, 11, 2143.

(5) Sanden van der, M.C.M. *Ph.D. thesis*, Eindhoven University of Technology, **1993**.

(6) Sanden van der, M.C.M.; Meijer, H.E.H.; Lemstra, P.J. *Polymer* **1993**, *34*, 10, 2148.

(7) Gloaguen, J.M.; Heim, P.; Gaillard, P.; Lefebvre, J.M. *Polymer* **1992**, 33, 4741.

(8) Forrest, J.A.; Dalnoki-Veress, K.; Dutcher, J.R.; Rowat, A.C.; Stevens, J.R. *Mat. Res. Soc. Symp. Proc.* **1996**, 407, 131.

(9) Wallace, W.E.; Zanten van, J.H.; Wu, W.L. *Phys. Rev. E* **1995**, 52, 52.

(10) Forrest, J.A.; Dalnoki-Veress, K.; Stevens, J.R.; Dutcher, J.R. *Phys Rev. Lett.* **1996**, 77, 2002.

(11) Keddie, J.L.; Jones, R.A.L.; Cory, R.A. *Europhys. Lett.* **1994**, 27, 59.

(12) Mulder, F.M. et al., in preparation.

(13) Casteren van, I.A. *Masters thesis*, Eindhoven University of Technology, **1998**.

(14) Smit, R.J.M.; Meijer, H.E.H.; Brekelmans, W.A.M.; Govaert, L.E. *J. Mater. Sci.* **1998**, submitted.

(15) Smit, R.J.M. *Ph.D. thesis*, Eindhoven University of Technology, **1998**.

(16) Hillmyer, M.A.; Lipic, P.M.; Hajduk, D.A.; Almdal, K.; Bates, B.S. *J. Am. Chem. Soc.* **1997**, 119, 2749.

(17) Hillmyer, M.A.; Bates, B.S.; Almdal, K.; Mortensen, K.; Ryan, A.J., Fairclough J.P.A. *Science* **1996**, 271, 976.

(18) Van Gisbergen, J.G.M. *Ph.D. thesis*, Eindhoven University of Technology, **1991**.

Samenvatting

Polystyreen (PS) en poly(metyl methacrylaat) (PMMA) zijn typische voorbeelden van brosse amorfe polymeren. Op grond van de netwerkdichtheid wordt echter verwacht dat beide polymeren ductieler zijn dan polycarbonaat (PC) dat taai is. De verstrekgraad van PS en PMMA blijkt op microscopische schaal inderdaad hoger te zijn dan die van PC terwijl er op macroscopische niveau reeds breuk optreedt bij een geringe deformatie. Dit is een direct gevolg van een extreme mate van rek-lokalisatie tijdens deformatie resulterend in crazes: spanningsdragende microscheurtjes die vroegtijdig uitgroeien tot fatale breuk.

De doelstelling van het onderzoek in dit proefschrift is het ontwikkelen van een taai heterogeen polymeersysteem uitgaande van brosse amorfe polymeren. Dit wordt gerealiseerd via de sturing van de morfologie die de ontwikkeling van crazes op microscopisch niveau moet voorkomen en shear-yielding bevordert: het gebruikelijke deformatiemechanisme in taaie polymeren. Ten einde dit taai gedrag te combineren met een minimaal verlies in stijfheid en vloeispanning wordt de benodigde fractie rubber geminimaliseerd door de grootte van de morfologie te reduceren tot submicron- of nanoschaal.

Deze morfologie-grootte kan niet worden gerealiseerd door het dispergeren van incompatibele polymeren met behulp conventionele verwerkingstechnieken zoals extruderen en compounderen. Daarom wordt gebruik gemaakt van "chemisch blenden", waarbij de rubbermorfologie het gevolg is van reactie-geïnduceerde fasenscheiding. De gewenste submicron structuren kunnen worden gerealiseerd door de polymerisatiecondities dusdanig te sturen dat er fasenscheiding optreedt in een hoog visceus systeem, wat coalescentie van de zich vormende disperse rubber-fase onderdrukt.

Deze blendmethodiek is toegepast om, met behulp van een alifatisch epoxyhars (die resulteert in een rubber na uitharden) taai, transparant, rubber-gemodificeerd PMMA te synthetiseren. In uniaxiale deformatie wordt voor de PMMA/epoxy blends inderdaad een sterk verhoogde taaiheid gemeten voor een rubberconcentratie van 20 gewichts% en meer. Tijdens slagvastheidstesten gaat deze toegenomen ductiliteit echter volledig verloren en moet minimaal 40 gewichts% epoxy-rubber worden toegepast om enige verbetering te realiseren. Het mechanische gedrag van de PMMA-rubber blends blijkt dus sterk afhankelijk te zijn van de deformatiesnelheid.

De macroscopische mechanische eigenschappen worden bepaald door het microscopische deformatiemechanisme wat kan worden beïnvloed door de specifieke rubbermorfologie. De hoge stralingsintensiteit van de synchrotron is gebruikt om met behulp van in-situ small-angle X-ray scattering (SAXS) experimenten tijdens mechanisch testen de deformatie op microscopisch niveau zichtbaar te maken. Het brosse karakter van de PMMA blend met 10 gewichts% epoxy-rubber blijkt het gevolg van crazing terwijl het taaier materiaalgedrag voor hogere rubberfracties het gevolg is van shear-yielding. In het geval van de PMMA/epoxy 80/20 blend wordt dit vooraf gegaan door rubber-cavitatie waardoor het shear-yielding proces wordt versterkt. Tijdens deformatie bij hogere snelheden (impact) kan er echter geen cavitatie meer optreden wat opnieuw resulteert in crazing en als gevolg daarvan een brosse respons geeft tijdens de slagvastheidtesten. Het belang van cavitatie wordt geïllustreerd door het systeem voorafgaande aan de slagvastheidstest te caviteren in een langzame trekproef. Dit resulteert in een verhoogde taaiheid tijdens impactcondities.

Tot slot is ook de invloed van de mate van fasenscheiding op de mechanische eigenschappen van de PMMA/epoxy blends onderzocht. Naast de morfologie kan immers ook de aanwezigheid van epoxyhars opgelost in de PMMA-matrix het uiteindelijke gedrag van de blend beïnvloeden. Onafhankelijk van de deformatiesnelheid blijkt dit effect op macroscopische niveau echter zeer gering, met name in het geval van een lage rubberfractie. Het microscopische deformatiemechanisme is echter wel aan verandering onderhevig als gevolg van een beperkte ontmenging.

Inzicht in het microscopische deformatiegedrag blijkt van essentieel belang ten einde betrouwbare conclusies te kunnen verbinden aan de invloed van de rubbermorfologie, de deformatiesnelheid en de mate van ontmenging op de macroscopische mechanische eigenschappen van de PMMA/epoxy blends. Concluderend blijkt dat de introductie van een submicron rubbermorfologie resulteert in een taai heterogeen polymeersysteem op basis van brosse amorfe polymeren welke inderdaad het gevolg is van de beoogde transitie in het microscopisch deformatiegedrag van crazing naar shear yielding.

Acknowledgements

Curriculum Vitae

The author of this thesis was born in Helmond, the Netherlands, on April 7th 1970. After finishing secondary school (VWO, Carolus Borromeus College, Helmond) in 1988, he studied Chemical Engineering at the Eindhoven University of Technology. After completion of his Masters thesis entitled "Toughening of polystyrene via controlled plastisication" in the group of Prof. P.J. Lemstra, he obtained his Masters' Degree in 1993.

In the following year, he started the PhD-study described in this thesis in the same group. The research was performed under supervision of Prof. H.E.H. Meijer (Materials Technology, Department of Mechanical Engineering, Eindhoven University of Technology). During this period the author completed all six modules of the course "Register Polymeerkundige" (RPK, "Registered Polymer Technologist") organised by "Polymeertechnologie Nederland" (PTN, Dutch Polymer Society) which covers all aspects in the field of polymer technology.

From October 1998, the author will join General Electric Plastics (GEP) in Bergen op Zoom, The Netherlands.

Stellingen

behorend bij het proefschrift

Toughening of Glassy Amorphous Polymers
via Chemically-induced Phase Separation

van

B.J.P. Jansen

1. De morfologie-grootte van blends die worden bereid met behulp van reactie-geïnduceerde fasenscheiding kan sterk worden gereduceerd door de viscositeit van het reagerend medium te verhogen.
   ➣ *Dit proefschrift, hoofdstukken 2 en 3.*

2. Door het in-situ meten van de absorptie in simultane X-ray verstrooiings-experimenten tijdens deformatie, kan het gemeten verstrooiingspatroon op verantwoorde wijze worden gerelateerd aan de rek.
   ➣ *Dit proefschrift, hoofdstuk 4.*

3. Het nucleatie- en groeiproces van gaten tijdens mechanische deformatie lijkt een sterke overeenkomst te vertonen met kristallisatie. Een hogere deformatiesnelheid resulteert in een groter aantal, minder georiënteerde gaten terwijl voor kristallisatie geldt dat een hogere afkoelsnelheid leidt tot een groter aantal maar kleinere kristallen.
   ➣ *Dit proefschrift, hoofdstuk 5.*
   ➣ *Turnbull, D., Fischer, J.C., J. Chem. Phys. 1949, 17, 71.*

4. De methodiek voor het aanbrengen van precracks in testmonsters om de resistentie van polymeren tegen scheurgroei te bepalen blijkt in sommige gevallen dermate afhankelijk van de gevolgde experimentele procedure dat er getwijfeld kan worden aan het praktisch belang van de resulterende fracture toughness waarde, K_{Ic}.
   ➣ *Jansen B.J.P., Tamminga K.Y., Meijer H.E.H., Lemstra P.J., Polymer 1998, submitted.*
   ➣ *Pearson, R.A., private communications 1997.*

5.   Gezien de fenomenen zoals crazing en stress-whitening, die optreden tijdens de deformatie van brosse polymeren, en de resulterende X-ray verstrooiingspatronen kan met recht worden gesteld: *taai is saai.*

6.   Het gebruik van de gedeeltelijke oplosbaarheid van monomeer in de waterfase om het Trommsdorff-effect tijdens de suspensie-polymerisatie van methylmethacrylaat te beschrijven strookt niet met de algemene gedachtegang dat deze polymerisatie kan worden aangemerkt als een mini-bulk polymerisatie.
      ➢ *Kalfas, G., Ray W.H.*, Ind. Eng. Chem. Res. *1993, 32, 1822.*

7.   De tegenstellingen tussen Oost- en West-Europa worden geïllustreerd door het verschil in streven naar eenheid.

8.   Gezien de toenemende invloed van economische aspecten op het onderzoek aan de Nederlandse universiteiten kan niet worden verwacht dat de Nederlandse wetenschap nog in staat zal zijn probleemstellingen zoals die van Fermat te bewijzen.
      ➢ Elsevier *1998*, 31, *69.*

9.   Het is achteraf maar zeer de vraag of de vermeende *toeval* van Ronaldo voor de door Brazilië verloren WK-finale daadwerkelijk op *toeval* berust.

10.   In tegenstelling tot wat verwacht zou mogen worden, heeft het gebruik van stimulerende middelen niet *positief* bijgedragen tot het aantal wielrenners dat de Tour de France '98 tot een goed einde heeft gebracht.

11.   Het aantal files op de wegen zou sterk verminderen als de Nederlandse Spoorwegen wat minder bussen zouden inzetten.